



# Western Engineering

**MSE 4499 — Mechatronic Design Project**

---

## **CubeSat Ground Station**

by

Jianhui Li, Tushar Mahajan, Paavan Raj, and Annie Wu

**Final Report**

Faculty Advisor: Dr. Sabarinathan and Dr. Cross

Date Submitted: February 14, 2019

Total Word Count: 7488

## **Executive Summary**

Western University's is designing a CubeSat satellite to be launched in 2021. An important component in accurately tracking the satellite is the ground station, which must be able to communicate in both S-band and UHF frequency bands. To accurately track the satellite, the ground station must be able to physically align the antenna with the satellite, monitor and predict the future positioning, and correct antenna direction. This overall scope of this project is to design a fully functioning ground station that will be able to track an object already orbiting in space with easily accessible data.

The concept generation process was split up into three components: the base, the actuation system, and antenna placement. The selected concept consisted of a truss base with an outer, protective box, a main hollow pole that would house the azimuth, with a platform that holds the elevation motor, with a coupler to connect to the antenna's arm. Throughout the fabrication and electrical component selection process, this design was iterated multiple times.

A detailed concept selection process was followed for selection of the main shaft shape, bearings, retaining rings, materials of machined components, gearbox, motors, encoders, GPS module, and power supply. These choices were validated through various engineering tools such as decision matrices, go/no-go screenings, and finite element analysis. Prior to ordering materials, the design was validated by the University Machine Services. In terms of software design, the overall system architecture and is based on the Robotic Operating System that will run on the Raspberry Pi, which will interface with Arduino to control the devices.

The main components of the prototype was completed in time for the mechatronics showcase and was tested throughout the week leading up to it as well as afterwards, through unit testing of individual components and testing of the overall ground station through tracking the Sun, Moon, and International Space Station, whose data is readily available online.

Moving forward, there are some aspects of the prototype that need to be changed for the ground station to be in its final state. First, the wood was rather cheap and deformed, so it was difficult to get the ground station to be level, which the azimuth subsystem required. Also, there were some tolerance issues with the 3D printed gearbox and though it does work, some of the components should be resin printed for a more perfect fit. As well, there was not enough time to create the outer box for the base even though weatherproofed wood was purchased.

The purpose of this report is to provide necessary background information and context for the project, outline the choices made throughout the design process and the supporting engineering analyses, provide all details with regards to testing and prototyping, and make any recommendations for the future. It is the definitive record of all the work conducted over the course of the design project.

## Table of Contents

Executive Summary .....	ii
Table of Contents .....	iii
List of Figures .....	iii
List of Tables .....	viii
Problem Statement .....	1
Background Information .....	1
Project Scope, Objectives, and Constraints.....	2
Concept Generation, Evaluation, and Selection.....	3
Ideation and Selection Process for Main Subsystems.....	3
Mechanical Design.....	6
Main Shaft Evaluation and Selection.....	6
Bearing Evaluation and Selection .....	8
Retaining Rings Evaluation and Selection .....	10
Machined Components Evaluation and Selection .....	12
Gearbox Evaluation and Selection .....	12
Electrical Design.....	13
Wind Considerations.....	13
Torque of Elevation Motor .....	14
Motor Selection .....	17
Encoder Evaluation and Selection .....	18
GPS Module Evaluation and Selection .....	19
Power Supply Evaluation and Selection .....	19
Controller Evaluation and Selection .....	20
Engineering Analysis .....	21
Gearbox.....	21
Bearing Holder .....	25

Refinement of Design.....	26
Concept Iterations .....	26
Software Design.....	32
System Architecture.....	32
User Interface.....	33
Data Flow .....	33
Stepper Motor Control Simulation .....	34
Prototype Development .....	35
Prototype Description.....	35
Prototype Construction.....	35
Prototype Cost.....	39
Validation Protocols and Results .....	41
Conclusion .....	50
Future Work and Recommendations .....	51
Mechanical Recommendations .....	51
Electrical Recommendations .....	51
Software Recommendations.....	51
References .....	52
Appendices.....	54

## List of Figures

Figure 1: FEA Analysis showing displacement for a round tube with three points of contact .....	7
Figure 2: FEA Analysis showing displacement for a square tube with two points of contact .....	7
Figure 3: Model of Parabolic Dish Antenna with 0.6m Diameter.....	15
Figure 4: Required Elevation Motor Torque Over Varying Angles .....	16
Figure 5: Maximum Von Mises Stress in The Output Ring Gear .....	22
Figure 6: Maximum Displacement in The Output Ring Gear .....	23
Figure 7: Maximum Von Mises Stress in The Input Connector.....	23
Figure 8: Stress in gear due to worst case scenario loading.....	25
Figure 9: Bearing Holder Factor of Safety .....	26
Figure 10: Concept truss base .....	27
Figure 11: Modified base .....	27
Figure 12: Concept azimuth subassembly.....	28
Figure 13: Modified azimuth subassembly .....	28
Figure 14: Concept elevation subassembly.....	28
Figure 15: Modified elevation subassembly.....	29
Figure 16: Final design.....	29
Figure 17: The base subsystem.....	30
Figure 18: Azimuth subsystem.....	31
Figure 19: Elevation subsystem .....	31
Figure 20: System architecture diagram .....	32
Figure 21: User interface diagram.....	33
Figure 22: Data flow diagram .....	34

Figure 23: Final prototype.....	39
Figure 24: Software communication set up .....	43
Figure 25: Data for two stepper motors .....	43
Figure 26: GPS coordinate data.....	44
Figure 27: Node communication .....	44
Figure 28: Result from GPS module compared to Google Map coordinates .....	44
Figure 29: Results from moon tracking code.....	45
Figure 30: Online moon data.....	45
Figure 31: Results from ISS prediction code .....	45
Figure 32: Actual ISS location .....	46
Figure 33: Off-center crescent moon .....	49
Figure 34: Off-center full moon.....	49

## List of Tables

Table 1: Project objectives and constraints .....	2
Table 2: Decision matrix of base design specifications .....	3
Table 3: Evaluation of base design options with respect to Table 2 above .....	4
Table 4: Decision matrix of actuation system design specifications.....	5
Table 5: Evaluation of actuation system design options with respect to Table 4 above.....	5
Table 6: Go/no-go screening for antennae placement options .....	6
Table 7: Ball bearings.....	8
Table 8: Thrust bearing specifications .....	9
Table 9: Retaining ring specifications .....	11
Table 10: 3D printing filament specifications .....	13
Table 11: Decision matrix of motor specifications .....	17
Table 12: Results of evaluation of motors.....	17
Table 13: Comparison of motor options.....	18
Table 14: Comparison of encoder options.....	18
Table 15: Comparison of GPS module options .....	19
Table 16: Comparison of power supply options .....	20
Table 17: Comparison of controller options .....	21
Table 18: Costs of materials from electronics shop.....	40
Table 19: Costs of materials from University Machine Services .....	40
Table 20: Costs of materials from miscellaneous shops .....	41
Table 21: Costs of general project resources .....	41
Table 22: Validation for each mechanical/electrical component .....	42
Table 23: Validation for integration of mechanical/electrical components .....	42

Table 24: Validation for entire system tracking the Moon on Sunday, March 31 <sup>st</sup> at 10 am .....	46
Table 25: Validation for entire system tracking the Moon on Sunday, March 31 <sup>st</sup> at 12 pm .....	47
Table 26: Validation for entire system tracking the Sun on Sunday, March 31 <sup>st</sup> at 3 pm .....	47
Table 27: Validation for entire system tracking the ISS on Monday, April 1 <sup>st</sup> at 1:30 pm .....	48
Table 28: Validation for entire system tracking the Sun on Monday, April 8 <sup>th</sup> at 2:00 pm .....	48

## **Problem Statement**

Western University's CubeSat Project is designing two parallel CubeSat satellite systems, with different communication frequency bands, that will undergo a trade-off, launching only one of them in 2021. They lack an accessible system on the ground that can provide real-time communication with the satellite, monitor and predict the movement of the satellite, and correct antenna direction based on its trajectory. This ground system must be robust to either communication schemes.

The problem statement is to design and build a functional satellite tracking ground station with high alignment accuracy between the CubeSat in orbit and the ground station, to achieve better communication and data transfer.

## **Background Information**

A CubeSat is a miniature satellite intended for low earth orbit (LEO), with each unit measuring some multiple of 10x10x10 cm and weighing less than 1.33 kg [1]. Western's two CubeSat designs will communicate in different frequency bands – UHF and S-band, requiring two separate Yagi and parabolic dish antennae. The parabolic antenna will need to rotate between 15 to 165 degrees and operate around 2 GHz and a Yagi needs a 30-degree field operating around 300 MHz [2].

Simplified General Perturbations (SGP) models are used to model the orbit of LEO objects. The two-line element set is a data format that encodes the orbital elements of a satellite at a given point in time. The two-line elements that are created from the SGP orbit determination can be used to model an adequately accurate propagation of the CubeSats motion [3].

Though ground stations have been a well-known aspect of satellite use, there has been a burst of do-it-yourself ground stations in recent years, constructed from various off the shelf, commercial components. Innovation Solutions in Space is a company with a variety of ground stations designed specifically for small satellites in LEO. They have one ground station that has both Yagi and parabolic antennae and can track satellites using a steerable antenna system that can be remotely controlled through the internet, with speeds up to 6°/sec [4]. This ground station is unique in how it can function in both S-band and UHF band frequencies; however, lacks the ability to be fully autonomous and is meant to track multiple satellites at once, lacking detailed information for any specific satellite. GOMSpace's AS2000 ground station also supports both S-band and UHF but has a fixed height and needs to be mounted high above the ground in a flat area [5].

After researching many existing ground stations, they all seem to lack some design elements such as autonomy and portability. Our ground station aims to fill this gap and since it is focused on tracking a single satellite, it will have higher precision and be able to provide

more detailed information. Additionally, we aim to add another level of innovation by including a GPS module so that when the ground station is moved to various locations, the position of the antenna relative to the satellite is considered. When the antenna is moved, the positioning of the antenna needs to be calibrated to adjust for the change in relative position. This can be done by tracking the longitude, latitude, and height above sea level of the antenna using a GPS. The calibration involves tracking the sun and adjusting the antenna's elevation and azimuth to reflect the change in location [6]. The control loop that calibrates the antenna depending on the strength of the signal received will fine tune the calibration.

An emerging technology used in commercial ground stations to control the position of the antenna is a rotator controller. This controller changes the current and voltage, forward or reverse rotation, and regulates speed and torque of two motors that drive the antenna. Looking at more affordable alternatives determined that motor drivers can also be used to achieve this task, which simply handles the power to drive the motors while digital control is done by an external microprocessor [7].

### **Project Scope, Objectives, and Constraints**

The overall scope of this project is to design a fully functioning satellite tracking ground station for Western's CubeSat. This project will cover the electrical and mechanical subsystems for motor actuation and sensory data acquisition, a control system for mitigating tracking error, and the orbital prediction algorithm that the ground station will employ to track the satellite's orbit. However, since the satellite will not be launched by the end of the semester, the plan is to accomplish successfully aligning with and tracking an orbiting object in space whose data is readily available, such as the moon or the International Space Station (ISS).

The key objectives and constraints can be seen in Table 1 below. The objectives were outlined by reviewing the background information and determining what current ground stations were lacking, as well as determining what the most important features of the design were to maximize on the given budget. The determined constraints reflect what the ground station had to do to be considered functional.

Table 1: Project objectives and constraints

Objectives	Constraints
<ul style="list-style-type: none"><li>· Transportable</li><li>· Requires low maintenance</li><li>· Manufactured from as many off the shelf components as possible</li></ul>	<ul style="list-style-type: none"><li>· Maintain high alignment accuracy with the satellite</li><li>· Predict orbital trajectory of the satellite</li><li>· Correct antenna direction and orientation</li><li>· Withstand external environmental conditions</li></ul>

Since the sizes of antennae are so diverse and can get up to 1 meter in diameter, the term “transportable” should be clarified to mean that it can fit in the standard short bed truck, which on average measures 6.75 x 8.175 feet.

## Concept Generation, Evaluation, and Selection

### Ideation and Selection Process for Main Subsystems:

Over the course of the design process, many concepts and iterations were examined and fine-tuned to develop the most recent design. To begin, the system was broken down into three main subsystems: the base, the actuation system, and the antenna placement. For the base and actuation system, the main requirements were determined, and their importance was ranked in decision matrices, which have been included below. Since the antenna placement was more straightforward, a go/no-go matrix was used in determining the most favourable concept.

A strong foundation was needed, so the base was the first portion of the design that was optimized. The main requirements for the base were for it to be wide, strong in compression, lightweight for portability, and able to enclose the electronics. The original concepts were a box base, a wide truss, and a quadpod design. The truss structure allowed for the box surface to be supported while also better distributing the large, concentrated load. The box structure was kept as a housing since it would easily protect the inner electronics and systems from the elements.

Table 2: Decision matrix of base design specifications

	Portable	Ease of Assembly	Stability	Rigidity	Robustness	Cost	Implementation	Total	Weight
Portable	1	2	1	0.33	0.5	2	0.5	7.33	0.136
Ease of Assembly	0.5	1	1	0.5	0.5	0.5	1	4	0.074
Stability	1	1	1	0.75	0.5	0.5	0.5	5.25	0.098
Rigidity	3	2	1.33	1	1	1.33	1	10.66	0.198
Robustness	2	2	2	1	1	1.33	0.75	10.08	0.188

Cost	0.5	2	2	0.75	0.75	1	1.33	8.33	0.155
Implementation	2	1	2	1	1.33	0.75	1	8.08	0.150
							Total	53.73	1

Table 3: Evaluation of base design options with respect to Table 2 above

	Quadpod	Wide Truss Base	Box Base
Portable	0	0	0.136
Ease of Assembly	0.074	-0.074	0
Stability	0	0.098	0.098
Rigidity	0.198	0.198	0
Robustness	0	0.188	0
Cost	0	0	0.155
Implementation	0.150	0.150	0.150
Percentage	42.2	56	53.9

The next system that was designed was the actuation system. The initial concepts were to have the motors mounted in the base and use pulleys, use a rotator controller, or use two motors to mimic a rotator. The most recent concept features two stepper motors with coincident axes of rotation, where one motor is mounted in the pole such that its axis is vertical, and the other motor is mounted horizontally on a platform. The reason why the motors are orientated this way is because the two angles that would need to be controlled, the azimuth (horizontal angle) and the altitude (vertical angle) rotate along these axes, making the system easier to model. The altitude motor would be under considerable torque loads, so counterweights were used to mitigate the weight.

Table 4: Decision matrix of actuation system design specifications

	Lightweight	Accuracy	Resolution	Complexity	Cost	Implementation	Total	Weight
Lightweight	1	0.33	0.33	1	0.75	0.5	3.91	0.097
Accuracy	3	1	1	2	1.33	1.33	9.66	0.240
Resolution	3	1	1	1.33	1	0.75	8.08	0.201
Complexity	1	0.5	0.75	1	0.75	1	5	0.124
Cost	1.33	0.75	1	1.33	1	0.75	6.16	0.153
Implementation	2	0.75	1.33	1	1.33	1	7.41	0.184
						Total	40.22	1

Table 5: Evaluation of actuation system design options with respect to Table 4 above

	Single Azimuth and Single Elevation	Rotator Controller	Actuation in Base with Pulleys
Lightweight	0	0.097	0.097
Accuracy	0	0.240	0
Resolution	0	0.201	0
Complexity	0.124	-0.124	-0.124
Cost	0.153	-0.153	0.153
Implementation	0.184	0.184	0
Percentage	46.1	44.5	12.6

The final sub-assembly that was considered was the antenna placement assembly. The original concepts featured simultaneously mounting both a Yagi and parabolic dish; however, only one frequency band would be used. A more efficient, modular design was used to accommodate either individual antenna.

Table 6: Go/no-go screening for antennae placement options

	Balance	Rotational Geometry	Portability	Cost	Implementation	Overall
Parabolic in Centre with Yagi on Side, with Opposing Counterweight	Go	No Go	Go	Go	Go	Go
Parabolic in Centre with Yagi on Each Side	Go	Go	No Go	No Go	No Go	No Go
Parabolic on one Side, Yagi on the Other	No Go	No Go	No Go	Go	Go	No Go
Modular (Antennae Replacement)	Go	Go	Go	Go	Go	Go

With all the subsystems conceptualized and designed, the integration of all three was simple. The main pole would run through the base and be supported by the truss structure. This hollow pole is large enough to house the azimuth motor, just underneath the platform holding the altitude motor. The platform rests on a bearing so it may freely rotate when the azimuth motor spins. The altitude motor is connected to the gearbox, which has an outer ring that functions similarly to a large coupler with an additional antenna attachment, that will work with either antenna.

## **Mechanical Design:**

### ***Main Shaft Evaluation and Selection:***

The pole connecting the base to other assemblies was evaluated using FEA. The original concept utilized a round pole with flanges and contacts at three different heights with the base. This resulted in minimal deflection of the other subassemblies with respect to the base. However, the flanges used to make the connections between the base components and the pole would need to be custom made. To avoid this, a square tube was used, and

connections were made using angle brackets. Using an FEA simulation shows the stressed on the points of contact with the circular tube the square tube (See Figures 1 and 2).

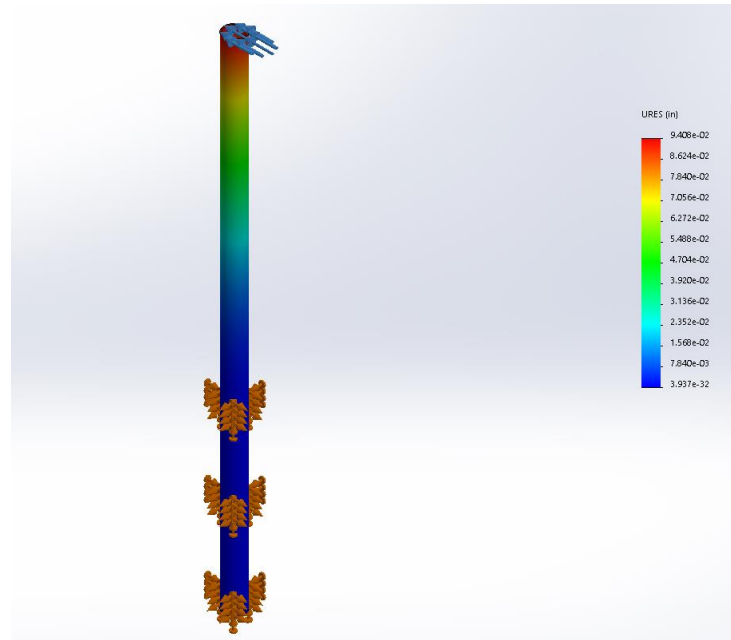


Figure 1: FEA Analysis showing displacement for a round tube with three points of contact.

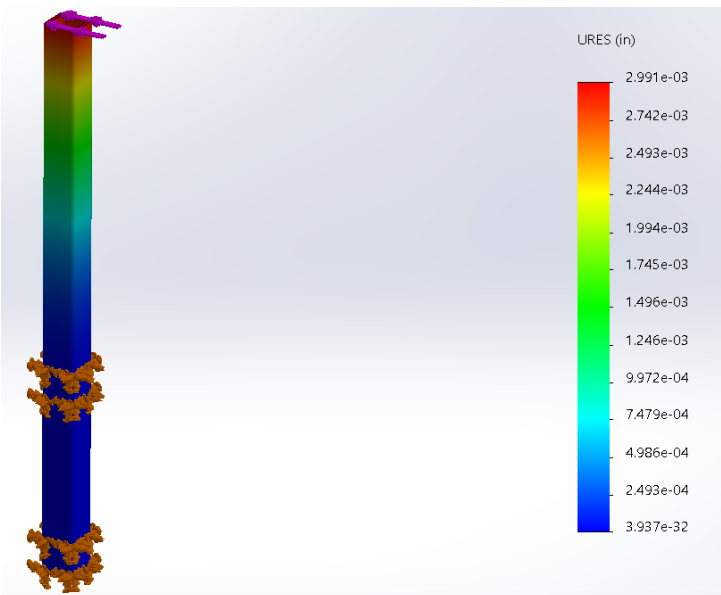


Figure 2: FEA Analysis showing displacement for a square tube with two points of contact.

On both poles, the outer face was split into sections where there was contact with the base in order to fix those sections of the pole, with a force of 150 N applied to the top face. The displacement during extreme weather conditions of the square tube with two points of contact (0.0029 inches) was less than the displacement of the circular tube with three points of contact (0.094 inches). Therefore, a square tube was selected.

***Bearing Evaluation and Selection:***

Initially, face-mount crossed-roller bearings were initially selected as these bearings could replace the need for dual radial bearings and a thrust bearing to eliminate all forces on the shaft welded to the base plate. However, a single bearing of the size required costs \$130+ [8]. This bearing would not be feasible for this project and therefore, 2 radial ball bearings and one thrust bearing was used instead. As these bearings were to be placed in an enclosed area, open radial bearings were selected as there is less internal friction in the bearing than with shielded or sealed bearings allowing for better power transmission. The selected steel ball bearings had a factor of safety of 36 as the load of 13.25 N was divided between two radial bearings with a rated static loading of approximately 480 kilograms combined (static load was selected instead of dynamic load as the rated loading for static loads was approximately half of the rated loading for a dynamic load and, therefore, it was more likely to fail due to a static load).

Table 7: Ball bearings [9]

Bearing Type	Ball
For Load Direction	Radial
Construction	Single Row
Seal Type	Open
Inner Ring Type	Standard
Ball Bearing Type	Standard
Trade No.	R8
For Shaft Type	Round
For Shaft Diameter	1/2"
ID	0.5"
ID Tolerance	-0.0003" to 0"

For Housing ID	1 1/8"
OD	1.125"
OD Tolerance	-0.0004" to 0"
Width	1/4"
Width Tolerance	-0.005" to 0"
Ring Material	Steel
Ball Material	Steel
Cage Material	Steel
Radial Load Capacity, lbs.	
Dynamic	1,100
Static	530
Maximum Speed	25,500 rpm
Lubrication	Required

Table 8: Thrust bearing specifications [10]

System of Measurement	Inch
Bearing Type	Ball
For Load Direction	Thrust
Seal Type	Open
For Shaft Type	Round
Ball Bearing Type	Standard
For Shaft Diameter	1 1/4"
ID	1.253"

ID Tolerance	0" to 0.009"
OD	1 7/8"
OD Tolerance	-0.012" to -0.001"
Thickness	0.437"
Thickness Tolerance	-0.01" to 0.01"
Ball Material	Steel
Cage Material	Nylon Plastic
Washer Material	Steel
Thrust Load Capacity, lbs.	
Dynamic	95
Static	540
Maximum Speed	2,500 rpm
Lubrication	Required
Temperature Range	-40° to 220° F

The thrust bearings required an inner diameter greater than the diameter of the shaft used (0.5 inches) and less than the outer diameter of the round bar used to make the bearing holder (3 inches). Thrust bearings that met these criteria made from steel were significantly more expensive. Therefore, Nylon thrust bearings were used. This bearing offered a dynamic and static load much greater than the required 60 lbs and a maximum speed that was also higher than required (1 rpm required speed).

#### ***Retaining Rings Evaluation and Selection:***

The retaining rings were selected based solely on the diameter of the shaft as the thrust load capacity of all retaining rings were significantly larger than required. Upon refining the options based on the diameter of the shaft on McMaster-Carr's website, black-phosphate 1060-1090 spring steel retaining rings were selected as they were economical compared to the other options available. Furthermore, these retaining rings had close to the highest thrust load capacity for the shaft size. The other options available had features that were not required

from the retaining rings used such as beryllium copper rings that conduct electricity and stainless-steel rings that are harder and thus provided a higher thrust load capacity.

Table 9: Retaining ring specifications [11]

Retaining Ring Type	External
Retaining Ring Style	Standard
System of Measurement	Inch
Material	1060-1090 Spring Steel
Finish	Black Phosphate
For OD	1/2"
For Groove	
Diameter	0.468"
Diameter Tolerance	-0.002" to 0.002"
Width	0.039"
Width Tolerance	0" to 0.003"
Ring	
ID	0.461"
ID Tolerance	-0.005" to 0.002"
Thickness	0.035"
Thickness Tolerance	-0.002" to 0.002"
Min. Hardness	Rockwell C40
Thrust Load Capacity	1,670 lbs.

### ***Machined Components Evaluation and Selection:***

The following are all custom components, and all were fabricated from 4140 steel.

- Bearing Holder
- Bearing Holder Flange
- Bar Topper Flange
- Bar Topper Flange Plates
- Bar Topper Motor Plate
- Motor Coupler
- Motor Holder
- Base for elevation motor
- Motor Plate
- Motor Shaft

4140 is an extremely common low alloy steel, with extremely high yield strength, torsional strength and Youngs Modulus [12]. These are all extremely important as these components carry heavy loads which are discussed in section 2. Furthermore, 4140 has a relatively high strength to cost ratio, is easily machined, and is readily available in the required sizes. Although there are materials that would have been easier to machine, such as aluminum, these materials are much more expensive, so they were disregarded. 4140 has chromium in it to improve corrosion resistance. However, it does not contain as much chromium as stainless steel which is highly corrosion resistant and would be an ideal material for this application. However, stainless steel is not only more expensive than 4140, but also considerably harder to machine because they are tougher, gummier and tend to work harden very rapidly [13]. Furthermore, we were limited by the availability of materials at the UMS in the required time frame, and, therefore, chose the best material available.

### ***Gearbox Evaluation and Selection:***

Initially, gearboxes found on McMaster-Carr were considered for this application. However, these were extremely costly and even a 10:1 gearbox were over \$700 [14]. Therefore, these gearboxes were disregarded as they were not cost effective. Upon further research, a 3D printed 160:1 compound planetary gearbox was found that would require less than \$60 of filament and would be able to handle the required torques [15].

Once this gearbox was selected, the 3D printing filament needed to be selected. The 3D printing filament required needed to be slightly flexible as the ring gears need to be slightly

flexed during assembly in order to ensure proper contact between the gears in the gearbox. Due to this, ABS, even with its higher strength, was not a suitable material. Similarly, Nylon was also too rigid for this application. PLA was the only material with the flexibility and strength for this application. HATCHBOX PLA was selected as it has high dimensional accuracy. The specifications can be seen in Table 10 below.

Table 10: 3D printing filament specifications [16]

Glass Transition Temperature	60 °C
Maximum Temperature: Mechanical	50 °C
Density	1.3 g/cm <sup>3</sup>
Young's Modulus	3.5 GPa
Ultimate Tensile Strength	59 MPa
Yield Strength	70 MPa
Filament Diameter	1.75 mm
Dimensional Accuracy	±0.03mm
Printing Temperature	190 °C – 220 °C

## **Electrical Design:**

### ***Wind Considerations:***

The external force of wind has a large impact on the torque required to actuate the dish, and therefore, the torques of the elevation motor especially. The previous report stated that the maximum wind speed recorded is approximately 80 kph. Of this, the value is correct but the explanation of this value was in fact misreported. All calculations were done using a parabolic dish antenna chosen by a fellow Western CubeSat team, as it is significantly larger and heavier than a Yagi Uda. This chosen antenna was the General Dynamics Series 1111 0.76, 1.0 & 1.2M – C & Ku-Band parabolic dish. The antenna is operational with a wind load of 72 kph [17], therefore 80 kph was used in all the calculations as a higher-order estimate of what the motor needs to be able to handle. Once wind speeds in the location of the antenna reach 72 kph, the ground station should stop all movements. Using the surface drag equation of a body in a fluid [18], the force exerted on the antenna when the face is at 45° to the wind can be found using the following equations:

$$F_{wind} = \frac{1}{2} \rho_{air} v_{wind}^2 A_{dish}$$

$$\rho_{air} = 1.2 \frac{kg}{m^3}$$

$$v_{wind} = 80 \frac{km}{h} = 22.2 \frac{m}{s}$$

$$A_{dish} = 0.622 m^2 \cdot \sin 45^\circ = 0.439.82 m^2 \text{ (antenna tilted slightly upwards)}$$

$$F_{wind} = \frac{1}{2} \times 1.2 \frac{kg}{m^3} \times \left( 22.2 \frac{m}{s} \right)^2 \times 0.439 m^2 = 130.0 N$$

And the torque applied is thus:

$$\tau = Fr = 130.0 N \cdot 0.4 m \cdot \cos 45^\circ = 36.8 N \cdot m$$

#### **Torque of Elevation Motor:**

For the elevation motor, there are many factors that play into minimum required torque that the motor should supply. Assuming a parabolic dish as a basis, the main considerations would be; the effects of wind incident to the antenna, the mass moment of inertia that is produced by the antenna arm, torques caused by friction and the inertial load that the motor experiences from the geometry of the components.

To begin, the effects of wind can impart up to 36.8 Nm of torque onto the motor when the antenna is at an angle of 45°. This will be the principal force that the motor will have to counteract during active operation. Another large moment is caused by the mass of the antenna and the arm that the antenna is attached to. The mass of the antenna is approximated as 16.16 kg, as given by a SolidWorks model (Figure 3 below) of a 0.6 m diameter parabolic antenna. With a straight beam attachment of length 0.40 m and mass 0.967 kg (this is adjustable but taken as a nominal estimate based on dish diameter), and the center of mass of the antenna being 0.06 m away from the attachment point, the location of the mass moment is calculated as follows.

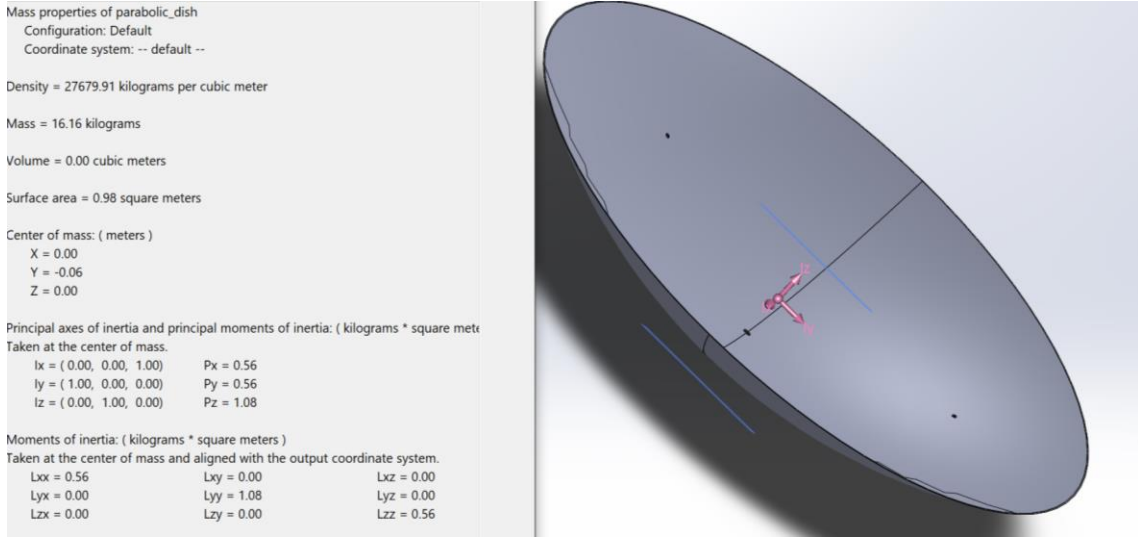


Figure 3: Model of Parabolic Dish Antenna with 0.6m Diameter

$$COM = \frac{0.46m \times 16.16 \text{ kg} + 0.2m \times 0.967 \text{ kg}}{16.16\text{kg} + 0.967\text{kg}}$$

$$COM = 0.445 \text{ m}$$

Using as the distance the point load exerts its force, the mass moment exert by the antenna and the arm is calculated as follows

$$\begin{aligned}\tau_{mass} &= F \times r \cos \theta \\ \tau_{mass} &= (16.16\text{kg} + 0.967\text{kg}) * 9.81 \frac{\text{m}}{\text{s}^2} \times 0.445\text{m} \cdot \cos \theta \\ \tau_{mass} &= 74.76 \cdot \cos \theta \text{ Nm}\end{aligned}$$

where  $\theta$  is the angle of the arm with respect to the horizontal. At horizontal, i.e.  $\theta = 0^\circ$ , the torque the motor has to produce is at its maximum, and when the arm is vertical, no moment is experienced.

The inertial loads experienced by the motor were found to be  $0.56 \text{ kgm}^2$  along the axis parallel to the axis of rotation, from the SolidWorks model, an operational speed of  $0.043 \text{ rad/s}$  (approximately which is  $150^\circ$  over 10 minutes), and a  $0.1 \text{ s}$ , the inertial load of the system can be calculated as follows, from rest:

$$\begin{aligned}\tau_{inertia} &= I\alpha \\ \tau_{inertia} &= I \frac{d\omega}{dt}\end{aligned}$$

$$\tau_{inertia} = (0.56 \text{ kgm}^2) \left[ \frac{(0.043 \frac{\text{rad}}{\text{s}} - 0 \frac{\text{rad}}{\text{s}})}{0.1 \text{ s} - 0 \text{ s}} \right] = 0.2408 \text{ Nm}$$

Using the above equations, the required motor torque over the varying angles of operation, i.e.  $\theta$ , can be plotted as to show the worst-case torque requirements for the motor during various stages of operation.

$$\begin{aligned}\tau_{motor}(\theta) &= \tau_{mass} + \tau_{inertia} + \tau_{wind} \\ \tau_{motor}(\theta) &= 74.76 \cos(\theta) + 0.2408 \text{ Nm} + \frac{1}{2} A_{dish} \rho_{air} v_{wind}^2 r \cdot \cos(\theta) \\ \tau_{motor}(\theta) &= 74.76 \text{ Nm} \cdot \cos(\theta) + 0.2408 \text{ Nm} \\ &\quad + \frac{1}{2} (0.622 \text{ m}^2 \cdot \sin(\theta)) (1.2 \frac{\text{kg}}{\text{m}^3}) (22.2 \frac{\text{m}}{\text{s}})^2 (0.4 \text{ m} \cdot \cos(\theta)) \\ \tau_{motor} &= 74.76 \text{ Nm} \cdot \cos(\theta) + 0.2408 \text{ Nm} + 73.57 \text{ Nm} \cdot \cos(\theta) \cdot \sin(\theta)\end{aligned}$$

Plotting  $\tau(\theta)$  using the above function now gives the graph seen in Figure 4 and assessing the maxima of this plot gives the maximum torque that the motor must be able to provide.

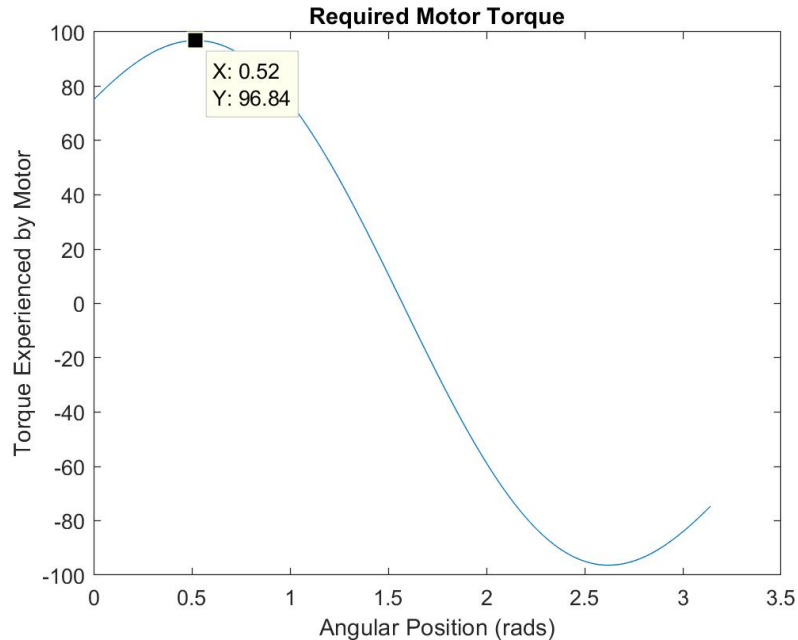


Figure 4: Required Elevation Motor Torque Over Varying Angles

From this plot, the maximum torque value occurs at approximately 0.52 radians (about  $30^\circ$ ), and the required worst case torque at this point is 96.84 Nm, taking into

consideration the portion of the wind perpendicular to the antenna, the effect the angle has on the effective moment arm of the antenna, and the inertial loads.

With the implementation of 3-stage 160:1 gearbox reduction, the effective torque needed by the motor to operate under these worst-case conditions would be 0.605 Nm. A factor of safety of 2, to account for rotor and gearbox inertia and other unconsidered factors would then put the minimum allowable torque to 1.21 Nm.

***Motor Selection:***

In the initial considerations, stepper, DC brushless, and DC brushed motors were considered. The most important specification throughout the selection process was torque, as there were very specific motor torque requirements that needed to be met. Other important specifications were speed and repeatability, as the antennae needs to be able to move to the point at which the satellite is detected and needs to be able to return to the same position each time. Cost is also important as there are strict budget requirements. The decision matrix and result of the evaluation can be seen below.

Table 11: Decision matrix of motor specifications

	Speed	Torque	Repeatability	Cost	Total	Weight
Speed	1	0.5	0.5	2	5	0.246
Torque	2	1	3	2	8	0.394
Repeat	2	0.33	1	1	4.33	0.213
Cost	0.5	0.5	1	1	3	0.147
					20.33	1

Table 12: Results of evaluation of motors

	Stepper Motor	DC Brushless	DC Brushed
0.246	0.246	0.246	0.246
0.394	0.394	0.394	0.394
0.213	0.213	0	0
0	-0.147	-0.147	-0.147
Percentage	85.3	70.6	49.3

The results from the decision matrix suggest the stepper motor as the best option. Stepper motors provide a constant holding torque without the need for the motor to be powered and the torque of a stepper motor at low speeds is greater than a DC motor of the same size [19]. Three different standard NEMA sized stepper motors were considered, and comparisons can be seen in Table 13 below.

Table 13: Comparison of motor options

	Nema 34	Nema 23	Nema 17
Holding Torque	7.07 Nm	3.0 Nm	0.6 Nm
Step Angle	1.8 deg	1.8 deg	1.8 deg
Operating Voltage	-	4.2 V	10 V
Weight	3.13 kg	1.6 kg	0.5 kg
Cost	\$125.92	\$49.86	\$22.09

The NEMA 17 motors were selected because they met the calculated torque requirements for the scenario of both the azimuth and elevation motors, and the difference in cost was extremely helpful to staying within budget. It should be noted that our original calculations were too oversimplified in the future, motors with a higher torque should be used.

#### ***Encoder Evaluation and Selection:***

Since the stepper motor is also a positional transducer itself, it technically needs no source of feedback on the positioning of the gears in the elevation system. However, to ensure accuracy, the following encoders were compared.

Table 14: Comparison of encoder options

	Cui AMT20 Series	Broadcom AR18 Series	HEDM-55xx
Encoder Type	Absolute	Optical	Optical
Resolution	0.08° (12 bits)	1.4° (8 bits)	0.35°
Accuracy	±0.2°	±0.2°	-

Serial Protocol	SPI	SSI 3-Wire	SPI 3-Wire
Maximum Speed	8000 RPM	15000 RPM	30000 RPM

Comparing the three encoders that were considered, the main differences are the resolutions, the maximum speed, and the communications protocols. For the purposes of this project, high angular resolution is important, and operating are much less so. Finally, the communication protocol (SPI) works very well with Arduino as an interface as all Arduino models are equipped with at least one SPI port, making integration simple.

#### ***GPS Module Evaluation and Selection:***

A GPS module was needed to be able to locate the ground station's coordinates, to be used in the calculation of where the orbiting CubeSat is in reference to the ground station. This is used in determining the angle at which the antenna needs to be pointed. There were two main considerations for selection of the GPS – startup time and accuracy. Within startup timing, the cold start is the time it takes for the GPS to get the first fix if it has moved several hundred kilometers. The hot start time is if the receiver has been off for less than an hour of time. The sensitivity of a GPS can be affected by clock errors, ephemeris errors, and atmospheric effects [20]. A few GPS modules were compared as seen below.

Table 15: Comparison of GPS module options

	NEO-6M	NEO-7M	EM-506
Cold Start	27 s	30 s	35 s
Hot Start	1 s	1 s	1 s
Sensitivity	-161 dBm	-161 dBm	-163 dBm
Compatibility	Arduino, RPI	Arduino, RPI	Arduino
Price	\$20-40	\$90	\$40

The GPS module options were extremely similar. The NEO-6M was selected fully based on the slightly better cold start and the significantly better price.

**Power Supply Evaluation and Selection:**

For power, a wall powered supply unit would need to be used as the constant power draw from the ground station and the desire to have low maintenance would mean that a portable power supply such as a battery would not be able feasible someone would need to charge and replace the battery. The choices were narrowed down to either a computer power supply with various power rails, laptop charger with a DC-DC converter to achieve desired voltage requirements or a 150W outdoor power supply.

Table 16: Comparison of power supply options

	EVGA 600	200W Laptop Charger	Outdoor Power Supply
Input Voltage	120 VAC	120 VAC	120 VAC
Output Voltage	12V, 5V, 3.3V	18V	12 V
Output Power	600 W	200 W	150 W
Converter	In-built	Needs External	Needs External
ESA Approval	Approved	Approved	Not Approved
Waterproof	No	No	IP67
Price	\$70	\$60	\$40

For the power supply, the choices each had their pros and cons, with the price being especially close between the choices. The first thing to note is that the EVGA power supply has multiple power rails, which is highly useful since it eliminates the need for an external voltage regulation circuit. Additionally, the rails provided supply a substantial amount of current which can power the electronics of the ground station, with excess power that additional components (such as antenna, mission controls console, etc.) may use in the future should the project require. The laptop power supply works similarly but requiring the converter circuit as well as the having a lower power output means that future additions will need their own power supply unit as there is very little to spare. Finally, the outdoor power supply supplies the least amount of power and lowest single voltage; however, it is designed for purposes very similar to the usage of the power supply unit in our ground station. The major drawback here; however, is that the outdoor supply lacks ESA approval, which means to be used the ground station and additional \$400 must be spent to use it. Summarizing the above,

the selected power supply is the EVGA 600, in conjunction with a heating system to keep it above its 0° operating temperature, as well as an IP67 rated enclosure within the base housing.

***Controller Evaluation and Selection:***

For controlling the individual electronic components, a microcontroller is needed to process the data from the system and provide meaningful outputs that ensure the system behaves as intended. The following microcontrollers were analyzed for effectiveness in providing the desired outputs

Table 17: Comparison of controller options

	Raspberry Pi 3B+	Arduino Uno	PIC Microcontroller
RAM	1 GB	2 KB	256 KB
Flash Memory	-	32 KB	1 MB
IO Pins	40	20	62
Clock Speed	1.4 GHz	16 MHz	180 MHz
Internet Capabilities	Yes	No	No
Cost	\$50	\$25	\$30 (w/o headers)

From the above table, the Raspberry Pi easily outperforms the other two microcontrollers in terms of RAM and clock speed, making it easily the best choice for use in this project because it is able to do many complex calculations in quick succession (such as orbital prediction). One caveat is that the Raspberry Pi is optimized for certain peripherals such as keyboards and LCD displays, and not so much motors and small sensors. To bypass this issue, Arduino Unos will be used in a master-slave configuration with the Pi as they are optimized for running simple tasks in a loop and thus better suited for handling general IO tasks while the Pi is better for handling task management and heavy computations.

## Engineering Analysis

### Gearbox:

Although FEA was conducted, a multitude of factors can affect the final strength of the 3D printed components such as:

- The specific material properties of the filament used as the properties can change between different manufacturers
- Infill Pattern
- Print defects
- Nozzle thickness
- Printing temperature

This, along with the inherent errors in FEA studies, results in high inaccuracies between simulated strength of the part and the actual strength of the part. A study done at the United States Merchant Marine Academy [21] has created a formula for converting the material properties given by the manufacturer of the filament to actual properties of the printed part based on the wall thickness, infill, and the infill pattern. Tests done with the use of this formula show that it allows for a better approximation of the material properties. It is recommended, however, that a factor of safety above 2 should be used in order to account other factors that the strength of the 3D print is dependent on. For a property  $P$ , the material property  $P_m$  can be used to find the design property  $P_d$  as

$$P_d = P_m * K_{FFF} \left( \frac{A_w}{A_x} + \frac{A_i}{A_x} * K_{i,\%} * K_{i,t} \right)$$

Calculations based on this formula can be found in Appendix 1.

A new material was created in Fusion 360 using these adjusted material properties. Due to the complexity of the model, it was not possible to run a dynamic analysis on all of the parts of the gearbox. Therefore, a static analysis was run on the two components, the output ring gear, and the input connector, at the points of maximum load.

The output ring gear has a maximum load when the moment of the antenna and the wind load are at their greatest. The most critical point of failure is the face attached to the pole holding the antenna. Therefore, a force of 210 N (130 N of force from the weight and  $150 * \cos(45)$  from the wind load), was applied. A fixed constraint was applied to the body of the output ring gear. The result of this simulation can be seen in Figure 5. With a maximum stress of 2.481 MPa, the part has a factor of safety of above 19. There is a maximum displacement of 0.02 mm that will not affect the positioning of the antenna as seen in Figure 6.

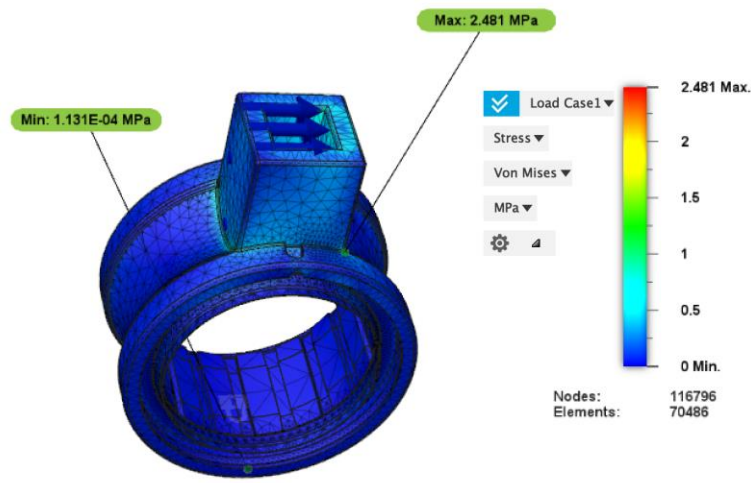


Figure 5: Maximum Von Mises Stress in The Output Ring Gear

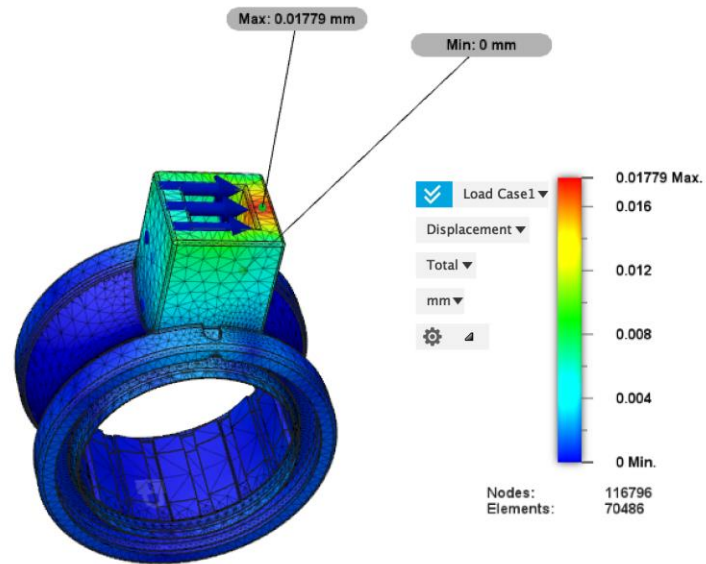


Figure 6: Maximum Displacement in The Output Ring Gear

As before, the most critical point of failure for the input connector occurs when the output gear has the maximum load as when the output torque is the highest, the input torque will also be at a maximum. Although the calculated maximum load was 0.605 Nm between the gears, a torque of 1 Nm was applied to the input connector to account for friction. A fixed constraint was applied to the body of the shaft. The maximum stress in the part was 3.828 MPa as seen in Figure 7, resulting in a factor of safety of approximately 13.

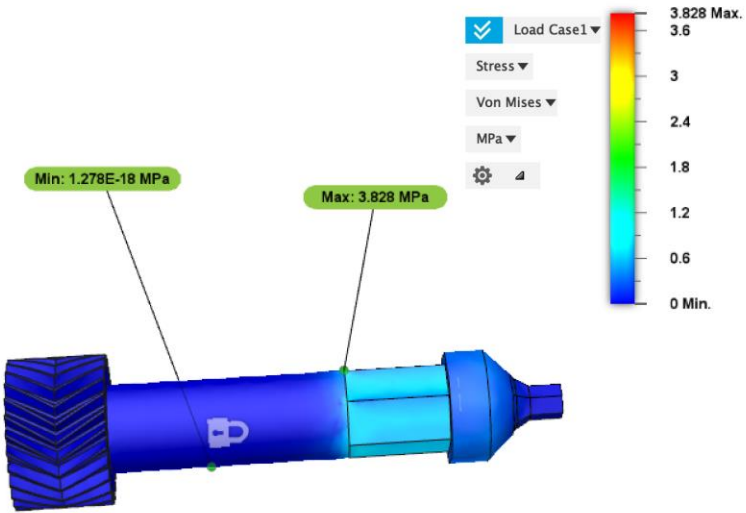


Figure 7: Maximum Von Mises Stress in The Input Connector

The forces on the teeth of the gears were then calculated to ensure that the teeth of the gears would not fail. For this gearbox, 9 planets engage with the sun gear. This means that the total tooth force that each planet gear exerts on the sun gear (and vice versa) has effectively been divided by 9. The sum of sun-planet tooth forces for the nine-planet planetary gear set turns out to be as follows:

$$F_{PS} = \frac{T_i}{9 \times 0.5N_s m \cos\phi}$$

$T_i$ : Input torque.

$N_s$ : Number of teeth on the sun gear

$m$ : module of the gear (reference diameter/number of teeth in the gear. This is the same for all gears in a planetary gearbox)

$\phi$ : pressure angle.

$$F_{PS} = \frac{1 \text{ Nm}}{9 \times 0.5(26)(0.022m/26)\cos(20)} = 34.273 \text{ N}$$

To determine the force applied to a single tooth, it is necessary to determine the number of contact ratio. The contact ratio can be calculated as follows [22]:

$$\rho_c = \frac{\sqrt{r_{o1}^2 - r_{b1}^2} + \sqrt{r_{o2}^2 - r_{b2}^2} - C \sin\phi}{p_b}$$

$r_{o1}$ : radius to the outer circle of gear 1

$r_{o2}$ : radius to the outer circle of gear 2

$r_{b1}$ : base circle radius of gear 1

$r_{b2}$ : base circle radius of gear 2

C: distance between the centers of the two gears

$p_b$ : base pitch ( $p_b = p \cos \phi$ , where  $p$  is the pitch of the gear)

$$\rho_c = \frac{\sqrt{11.52^2 - 4.80^2} + \sqrt{23.35^2 - 14.06^2} - 30.5\sin 20}{2.88\cos 20} = 1.2415$$

Therefore, the force per tooth can be calculated as follows:

$$F = \frac{F_{PS}}{N_p \times \rho_c} = \frac{34.273 \text{ N}}{9 \times 1.2415} = 3.07 \text{ N}$$

A normal force of 3.07N was applied to a single face of a tooth and a static study was run. The results of this study can be seen in Figure 8 below. The maximum stress in the part was 0.1791 MPa resulting in a factor of safety of 200+.

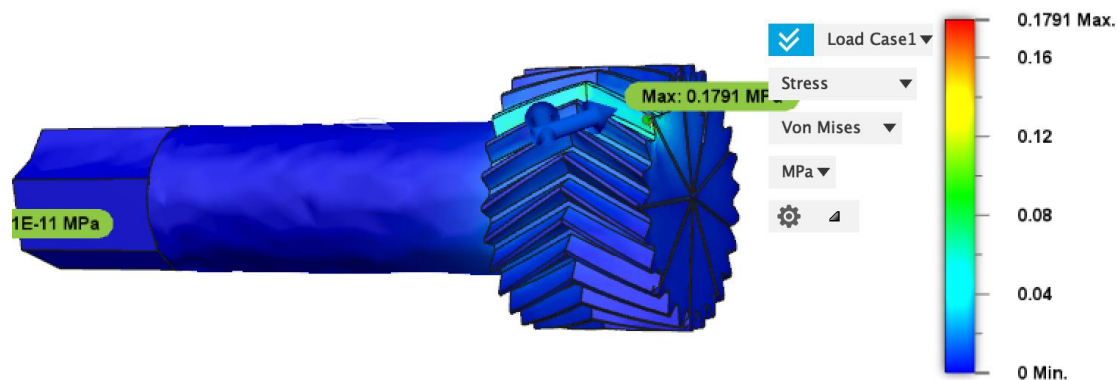


Figure 8: Stress in gear due to worst case scenario loading

Analysis of other components of the gearbox was deemed not necessary as the loads were evenly distributed over large areas for those components, thereby making them highly unlikely to fail. These components include the ring gears and the gearbox holders. The ring gears have a similar loading on their teeth resulting in an extremely high factor of safety. The gearbox holders use the entire outer surface area of the ring gears as well as 15 ridges to transfer load from the gears to the gearbox holder, thereby making them highly unlikely to fail as well.

### **Bearing Holder:**

Another point of failure could be the bearing holder as it holds the weight of the 10-inch-long, 0.5-inch-thick square steel plate as well as the entire elevation subassembly. The location of the bearing holder can be found in Figure 18 in the following section. In order machine the part with the tolerances required to press fit radial bearings, as well as to have sufficient access to the motor coupler, the 2.5-inch-wide steel round bar was machined down to a thickness of 0.25 inches. As the total weight transferred through a thrust bearing to the bearing holder is approximately 40 pounds (the exact value is not known due to the 3D printed components), an FEA analysis was run to determine the factor of safety of this component. The outside bottom 0.125 inches, as well as the bottom of the component, were fixed as these faces will be welded to the rigid body. A force of 110 (50 pounds for the subassembly (rounding up as the exact value was unknown), 40 pounds for the antenna (the heaviest antenna being considered by the communications team), and 20 pounds for the downward component of the wind load) was applied to the face that the thrust bearing will rest on. This FEA analysis resulted in a minimum factor of safety of 332 as seen in Figure 9.

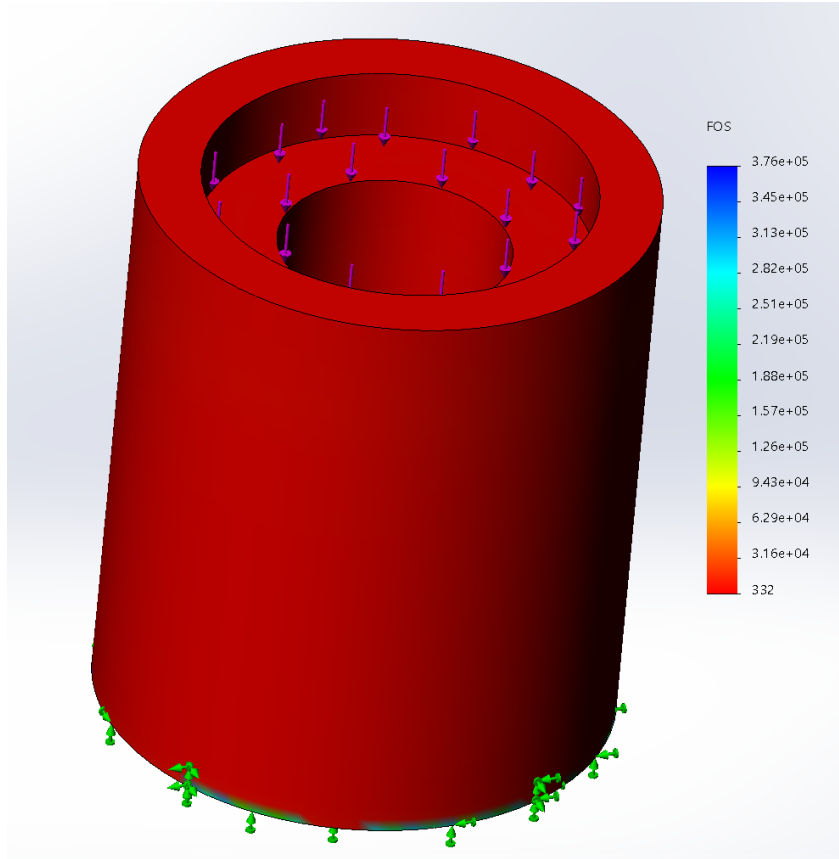


Figure 9: Bearing Holder Factor of Safety

## Refinement of Design

### Concept Iterations:

The chosen concept for the base included a telescoping pole design that allowed the height of the pole antenna to be adjusted as needed and allowed for easier transportation. This design used two circular metal tube whose diameters and tolerances would allow a loose running fit. The pole would be fastened to the base using custom, machined flanges. To reduce the cost and amount of labor, the telescoping poles were replaced with a 2" wide square metal tube. This iteration is easier to mount as angle brackets can be used. These angle brackets are inexpensive and can rigidly secure the square tube to the base. The square metal tubing is also relatively inexpensive so if a longer or shorter pole is required, another pole can be easily obtained.

The base design was further refined, as the selected concept used butt joints for all connections and required trusses to secure the larger tube into place (see Figure 10). The connections using angle brackets between the square tube and the top and bottom horizontal sections of wood have a larger surface area than the connections in the concept originally selected. Therefore, it was found that the additional trusses added between the horizontal sections of wood would be redundant. This was confirmed using an FEA simulation that used three points of contact with the circular tube and two points of contact with the square tube. It was determined that the deflections in the square tube would be lower than the deflections in the circular tube. In order to increase the strength of the base, all butt joints were replaced with finger joints (see Figure 11).

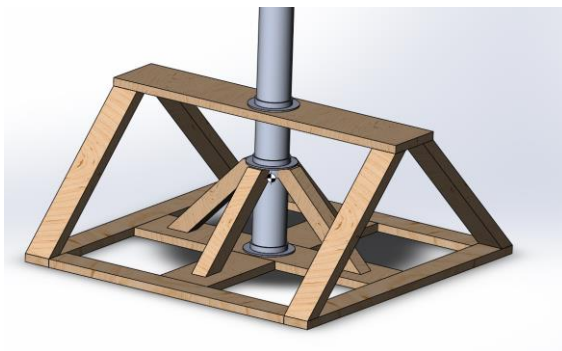


Figure 10: Concept truss base

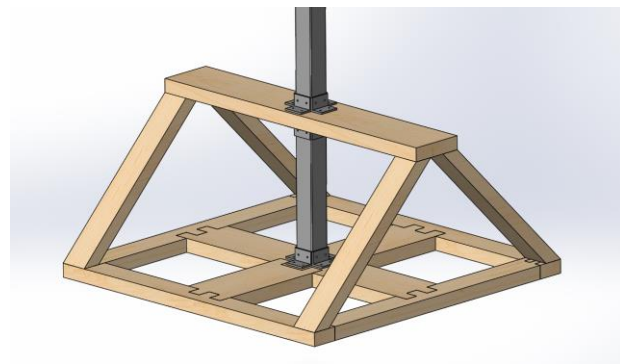


Figure 11: Modified base

The azimuth subassembly design used two machined components. The motor would be fastened to the bottom component and a thrust bearing would be placed on top of the motor, bearing axial loads exerted by the upper component (See Figure 12). However, this design did not consider the radial loads, so two ball bearings were added to the shaft to accommodate that load [23]. The original design made the motor inaccessible without disassembly, as it was fully enclosed. The entire azimuth subassembly was redesigned to better mount the subassembly to the pole and the shaft to the upper component as seen in Figure 13 below. The square tube is connected to the motor using a circular plate that is welded onto a small section of a larger square tube. The motor is directly mounted to this piece. A 4" long metal rod is machined to hold the radial and thrust bearings in place. It is welded to a circular plate and will be fastened to the motor plate. The bearings are press fit into this piece and the shaft is pushed through it. The top plate that holds the elevation subassembly is machined from a 1/4" thick metal plate so that 1/8" of the plate rests on the thrust bearing and is inside the metal rod that holds the bearings. The top plate has a hole drilled into the center where the shaft is welded to it. This design allows the components to be machined easier while reducing axial and radial forces on the shaft.

The elevation subassembly in the selected design used counterweights to reduce the amount of torque needed from the motor. However, this design required three large, custom couplers on the shaft and linear bearings in the top plate (see Figure 14). As this would add considerable expenses to the project, it was replaced with a 3D printed 160:1 planetary gearbox (see Figure 15).

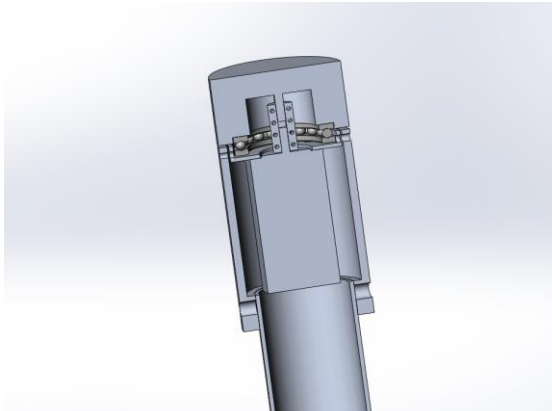


Figure 12: Concept azimuth subassembly

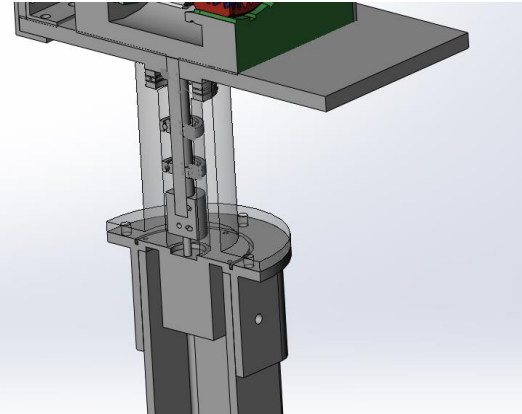


Figure 13: Modified azimuth subassembly

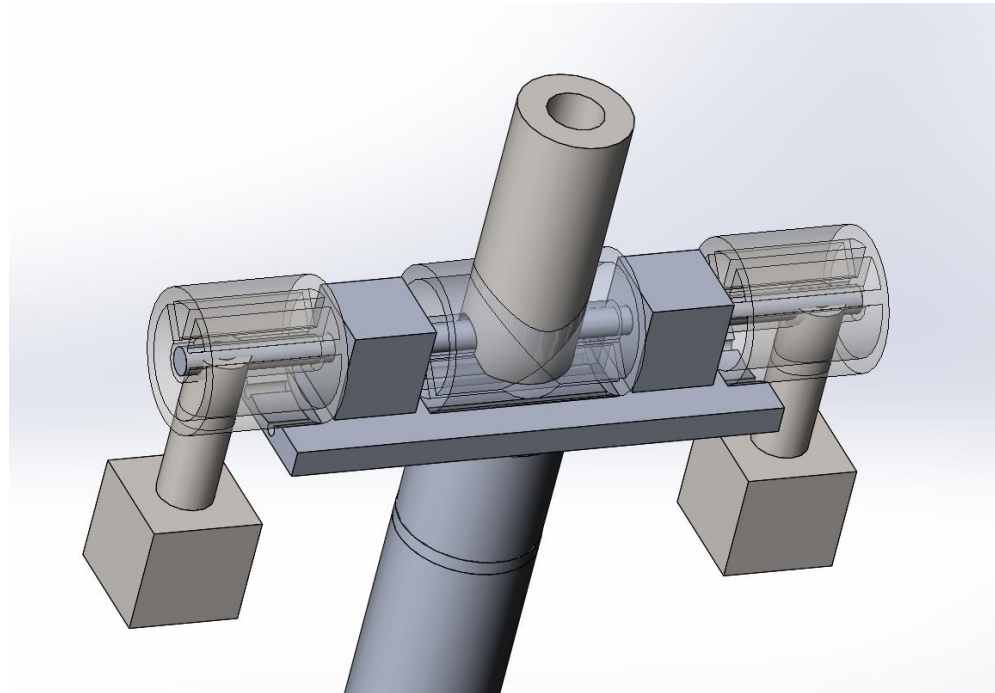


Figure 14: Concept elevation subassembly

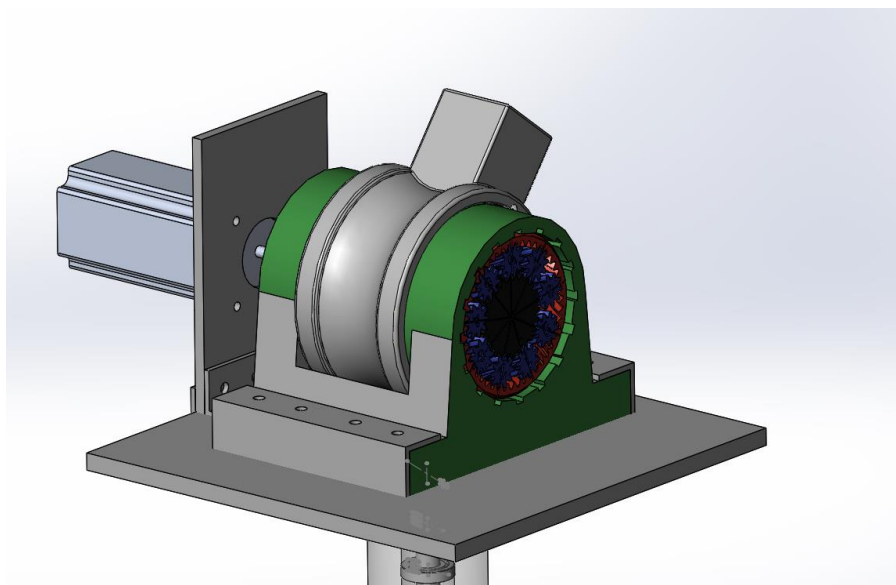


Figure 15: Modified elevation subassembly

The final design using the discussed subassemblies is below:

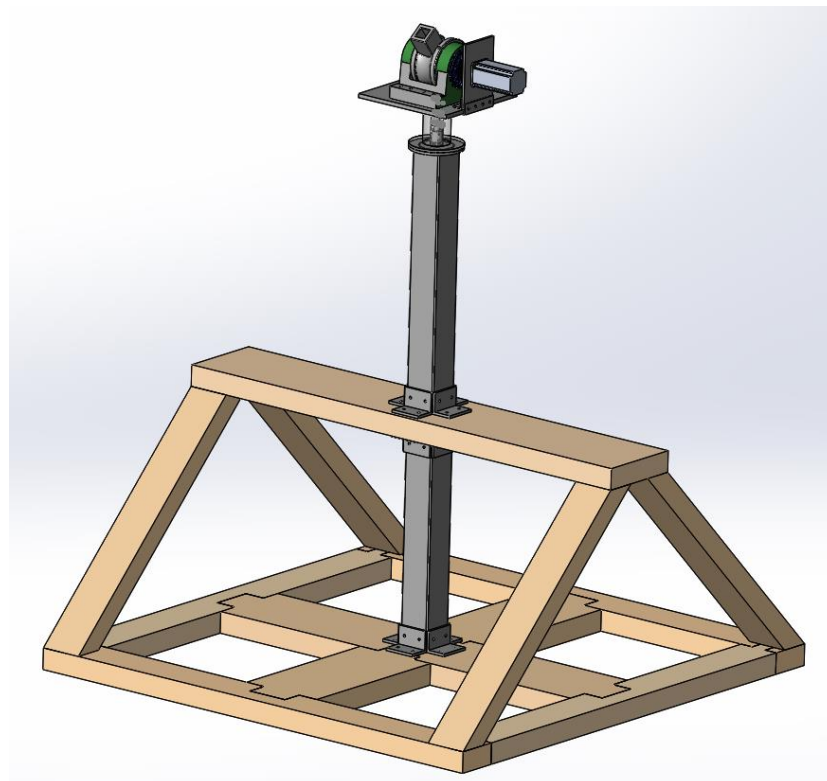
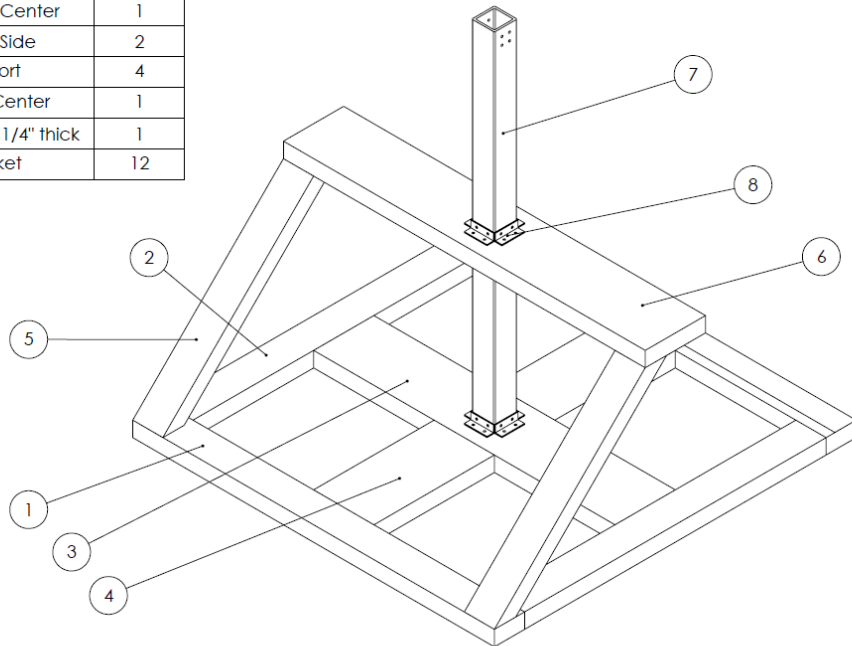


Figure 16: Final design

The selected concept's design with all the mechanical components and some of the selected electrical components is below. For clarity, the ground station has been split into three subsystems – the base, the elevation subsystem, and the azimuth subsystem. The three subsystems can be seen below. To better show the more important details, all figures of the CAD model have the box base and antenna suppressed.

ITEM NO.	PART NUMBER	QTY.
1	2" x 4" for base	2
2	2" x 4" for base short	2
3	2" x 8" Base Center	1
4	2" x 8" Base Side	2
5	2" x 4" Support	4
6	2" x 8" Top Center	1
7	3"x 3" Tube, 1/4" thick	1
8	Angle Bracket	12



Base Subassembly

Figure 17: The base subsystem

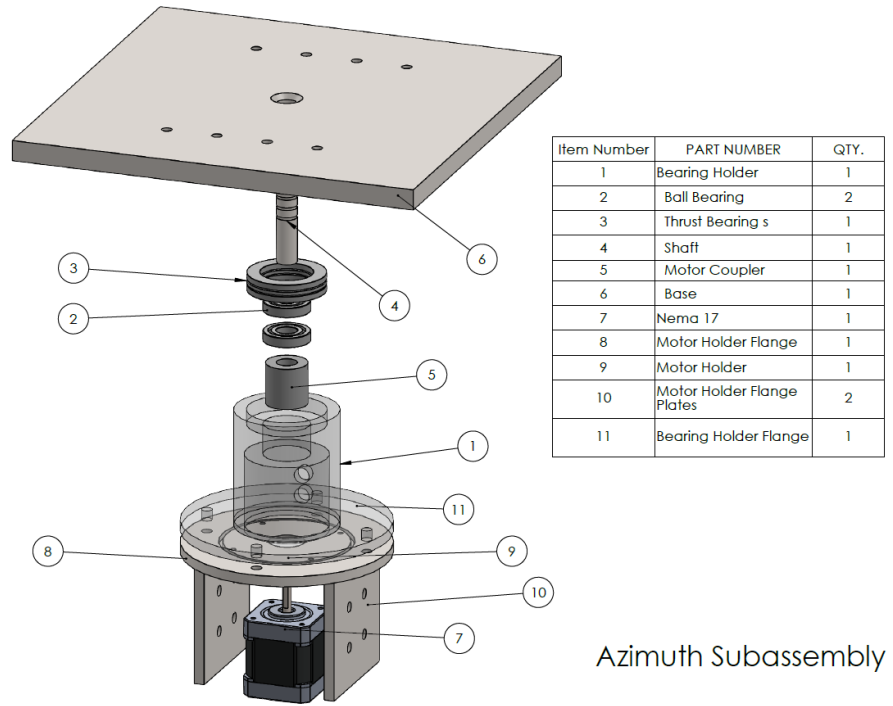


Figure 18: Azimuth subsystem

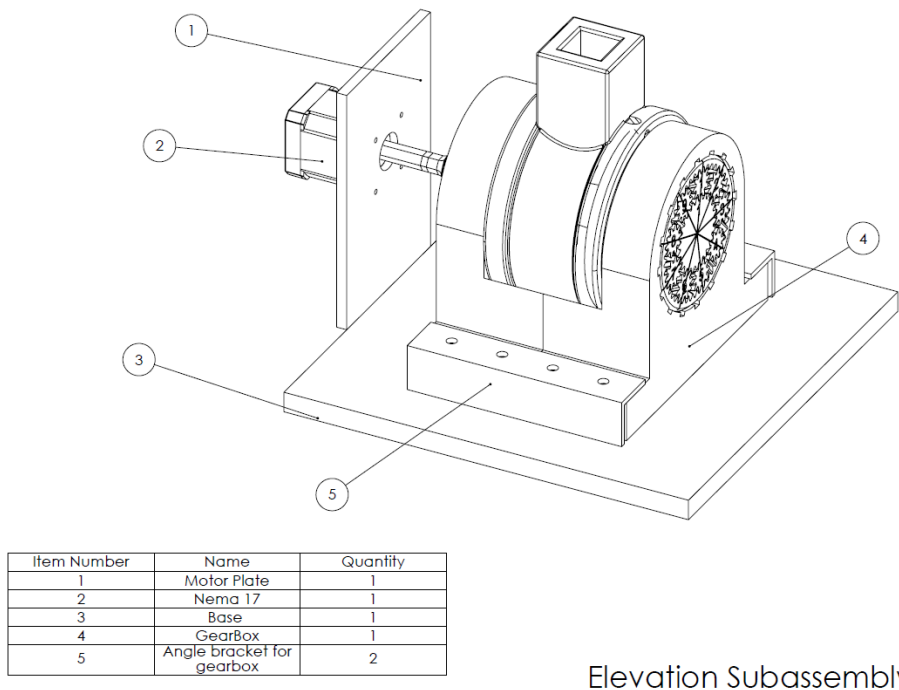


Figure 19: Elevation subsystem

Detailed design documentation for each component of the ground station can be found in Appendix 2.

## Software Design:

### ***System Architecture:***

In our software design, the core architecture is based on the Robotic Operating System (ROS), an existing robotics middleware. ROS provides the services from an operating system, including low-level device control, implementation of commonly-used functionality, and package management. ROS is language-neutral and can be programmed in various languages. The kinetic version of ROS is installed on the Raspberry Pi (RPI), which can fit the Linux system Raspbian Sketch. There are three main parts in the system architecture: the control of devices through the Arduino board, CubeSat orbit prediction using Simplified General Perturbations models (SGP4 Python 1.4), and CubeSat location. As seen in Figure 20 below, the three parts work together as an individual node – the core ROS Master node.

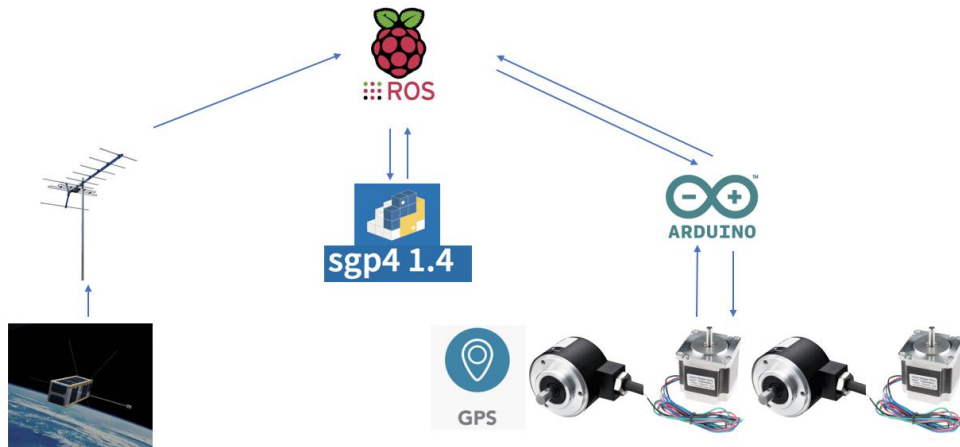


Figure 20: System architecture diagram

In the first part, the antenna works as a publisher. After the CubeSat is located, the initial position data sends a message to the RPI. Using the two-line element (TLE) data, the angle of the antenna can be calculated and set. Next, the SGP4 1.4 Python package receives the initial position data from the first node and calculates the next overhead time and position of CubeSat. When the RPI receives the next overhead position of CubeSat, the program will calculate the intersection angle between the ground station and CubeSat. In the final part, the GPS module will get the current position of the ground station and send this information back to ROS master. Then, the Arduino board will control the stepper motors, which will utilize ROS topics to send goal messages to the server. While the antenna is moving to the goal position, the 'percent\_complete' message periodically transmits feedback values showing the progress in the form of the percentage of the goal point reached. Rosserial needs to be installed on the RPI, which will provide a ROS communication protocol that works over the Arduino's Universal Asynchronous Receiver/Transmitter. In this project, the electronic devices connect

to the Arduino board instead of the RPI, because the Arduino board is a microcontroller motherboard that can simply run one program at a time, over and over again, and only one RPI board cannot support sufficient general-purpose input/output (GPIO) pins to connect these devices. In addition, the Raspberry Pi 3B+ has four USB 2.0 ports; therefore, it can expand communication with up to four Arduino boards.

#### ***User Interface:***

The user interface will enable the user to have simple control and be able to set tasks for the ground station. A convenient method to get remote access to the RPI is through Secure Shell (SSH). With this method, users can access the Linux control tools including the Raspbian desktop system and Linux console. There are two choices of the telnet clients, PuTTY and REALVNC, and the SSH connection can be through Ethernet or mobile Wi-Fi. The RPI is set as fix IP address 192.168.137.214 for Ethernet connection, and 192.168.137.245 for the WIFI connection. The user interface is illustrated in Figure 21 below.

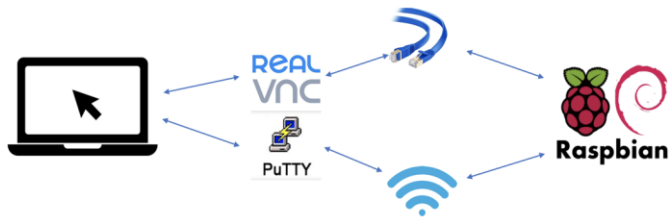


Figure 21: User interface diagram

#### ***Data Flow:***

The primary design for data flow is based on ROS. There are six nodes created for six different tasks, which can be seen in Figure 22 below.

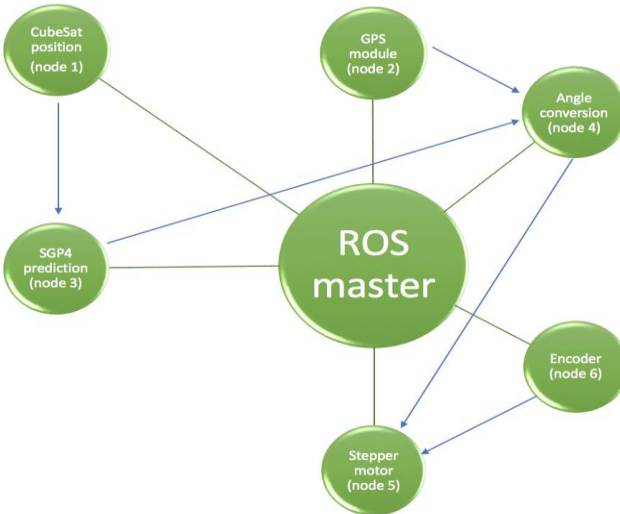


Figure 22: Data flow diagram

The ROS Master provides naming and registration services to the rest of the nodes in the ROS system. It tracks publishers and subscribers to topics as well as services. The role of the Master is to enable individual ROS nodes to locate one another. Once these nodes have located each other they communicate with each other peer-to-peer [24]. The GPS module (node 2) publishes the position of the ground station and sends this message to Angle conversion (node 4) as a subscriber. CubeSat position (node 1) sends the CubeSat position and speed to the SGP4 prediction model (node 3). After calculations are complete, node 3 publishes the next overhead position to node 4, which will convert the position of CubeSat to the Earth-based coordinate system and publish the rotation angles for each of the stepper motors. The stepper motors (node 5) will rotate to their desired angles. The encoder (node 6) publishes the angle value to node 5, to correct the error.

#### ***Stepper Motor Control Simulation:***

Simulations were run to mimic the control of the stepper motor. The RPI sends a message to the topic “stspeed” (stepper motor speed), and the Arduino program uses this to control the speed of the motor. The simulation set up requires the RPI to have the Raspbian Sketch system installed, which is highly optimized for the RPI line’s low performance Advanced RISC Machines CPUs. ROS kinetic and Rosserial Arduino are both installed on this RPI. The RPI was controlled through SSH using the REALVNC client. The result of this simulation was very successful in mimicking the ground station system. The RPI work was successfully monitored through SSH and run on ROS to communicate with the Arduino to control a stepper motor. These simulations were first run on very small stepper motors with weak specifications. Once received, the same simulation was run on the actual selected motors. The simulation was extremely easy to transfer and yielded equally successful results.

## **Prototype Development**

### **Prototype Description:**

For the prototype of the ground station, a functional tracking system will be fabricated and built to demonstrate the intended use of the system. Given that certain key elements that would be incorporated into the ground station (such as antennae, data relay systems, and user interfaces), are at the discretion of other subsystems in the CubeSat, the ground station will replicate the desired tracking motion as if it were following a celestial body. This will be completed using the available two-line elemental data for either the moon or the International Space Station. The motors should move so that the connector piece where the antenna would be mounted would move to track the body in orbit. This will be verified by comparing the location it is pointed to with the actual location of the object in orbit.

The fabricated prototype will be a valid representation of the final product because it will be able to validate many of the key design choices and calculations that were made to ensure proper function as the scale will be 1:1. The base, for instance, will be made to the same size as specified in the earlier sections, and thus will be able to validate that the system will not tip when a high lateral force is applied to the top of the mast. Adding weight to the top of the mast to simulate an antenna can also be done to show that the minimum speed/torque requirements were met, ensuring that the ground station functions well under a load. Finally, since all the hardware and software will be completed, the functional demonstration will show the operation of the program and data handling, which will verify that the choices to use the microcontroller, power supply, systems architecture, etc. were well thought out and selected.

### **Prototype Construction:**

The following steps were followed/will be followed in order to complete the fabrication of the ground station.

#### **Base Subassembly:**

- Cut the lumber down to the required sizes using a table saw.
- Drill pilot holes in the 2" x 8" Base Center and Top Center. Then, with the use of a jigsaw, cut the out the square profile of the 3 inch x 3 inch square tube.
- Join the following pieces by first drilling pocket holes. Then apply wood glue liberally on the surfaces that need to be joined. Finally, screw the wood screws into the pocket holes.
  - 2" x 4" for base x 2.

- 2" x 4" for base short x 2.
  - 2" x 8" base side x 2.
  - 2" x 8" Base Center x 1.
    - Note: The 2" x 4" pieces only require 2 pocket holes while the 2" x 8" connection require 4 pocket holes.
- Ensure that the 2" x 4" support pieces line up with the 2" x 8" top piece before proceeding with the next step. Also ensure that the square holes are lined up with each other and that the square tube can fit inside these holes.
- Connect the 2" x 4" support pieces to the base with the use of wood screws and wood glue.
- Connect the 2" x 8" Top center to the 2" x 4" support pieces with the use of wood screws and wood glue.
- Make 12 angle brackets by cutting an angle bracket to size and drilling the holes.
- Drill the holes in the 3"x3" center tube with the use of a milling machine or a drill press and use a tap to thread the required holes.
- Attach the square tube to the wood base with the use of the angle brackets. Use nuts to attach the angle brackets to the square tube and self-drilling screws to attach the brackets to the wood.

### **Azimuth Subassembly:**

- Machining the parts:
  - Bearing Holder: Machine the bearing holder on the lathe to achieve the right geometry with the right tolerances. Use a drill press or a milling machine to cut the holes on the side.
  - Shaft: Cut a 0.5" diameter round stock to size and machine the grooves and create the chamfer on the top.
  - Motor Coupler: Machine the holes for the motor shaft and shaft using a lathe. Use a milling machine or drill press to drill the holes on the side of the part and use a tap to thread these holes.

- Base: Use a milling machine to drill the holes in the base plate and create the blind hole on the bottom of the plate. The milling machine is required for this step as misalignment of the holes could lead to a misalignment between the elevation motor and the gearbox.
- Motor Holder Flange, Motor Holder, Bearing Holder Flange Plates: Use the lathe to machine round stock to the required size and geometry. Use a milling machine to drill the through holes in the parts for proper alignment.
- Motor Holder Flange Plates: Use a drill press or a milling machine to drill the holes.
- Assembly:
  - Weld the motor holder flange plates to the motor holder flange, the bearing holder to the bearing holder flange plate, and the shaft to the base plate.
  - Attach the ball bearings to the shaft with the use of the retaining rings.
  - Put the thrust bearing onto the bearing holder. Press fit the ball bearings into the bearing holder.
  - Attach the motor coupler to the shaft with the use of grub screws.
  - Attach the motor holder flange to the square tube with the use of nuts and bolts.
  - Screw motor into the motor holder and screw the motor holder into the motor holder flange.
  - Nut and bolt the motor holder flange to the bearing holder flange.

### **Elevation subassembly**

3D print the components in the orientations mentioned above with the following settings:

- 5 mm walls with 50% infill and 0.2 mm layer height with a 0.4 mm nozzle.
- Keep the extruder as hot as possible to maximize layer adhesion without drooping.

- Print at 75% of regular speed. This ensures the least amount of print artifacts on the gears and allows proper mating of the gear teeth.
- Press 8mm diameter linear rods into the planetary gears.
- Assemble the gearbox by aligning the planetary gears with the lines on the sun gears and zip tying them together. Then, starting with the first ring gear, flex the ring gear outward and align the lines again and release over the planetary gears. Lubricate the gears with 3 in 1 oil.
- Slide the output ring gear holder onto the middle sun gear. Then, slide the two stationary ring gear holders onto either side of the gearbox. Fill the hole in between the output ring gear holder and the stationary ring gear holders with 4.5 mm plastic bb's used in bb guns.
- Cut 1 inch angle brackets to size and drill the required holes in them.
- Using a milling machine for precision, drill the holes required to make the elevation motor plate. Attach the motor to this.
- Attach the motor plate to the base with the use of dowels to locate the plate and nuts to hold it into place.
- Secure the gearbox to the base with the use of bolts, washers, and nuts, using the angle bracket to disperse the force evenly.

The final prototype can be seen in Figure 23 below.

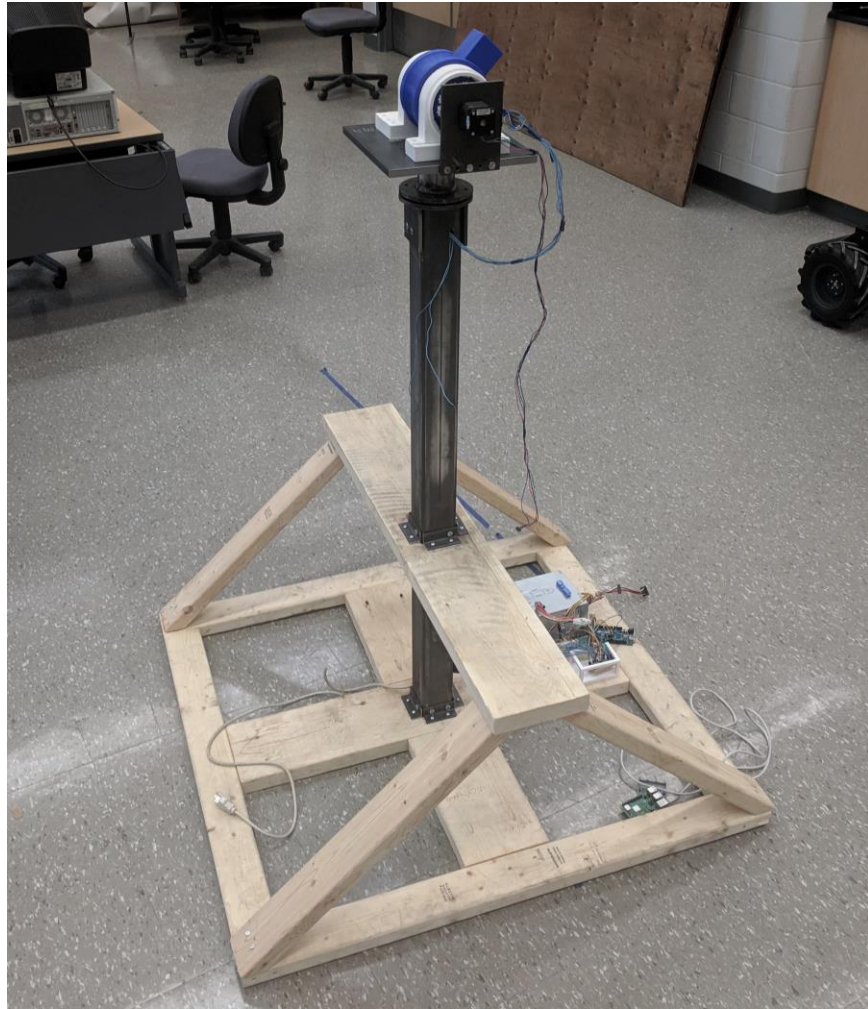


Figure 23: Final prototype

### **Prototype Cost:**

Not including the costs of labor, the final cost of all materials and services was \$1062.89. The budget provided by our supervisors was \$1,000, along with another \$300 from the provided MSE4499 Capstone budget. The only expense not incurred due to the purchase of materials was the welding done by the UMS. Although the welds were not complex, there was no one in the group with the required welding skill in order to perform these welds. Therefore, the welding work had to be outsourced to the UMS. The detailed breakdown of prototype cost can be seen in the following tables, split up into the different places parts were ordered from. Table 18 provides details on the cost of engineering time and software licenses that the project would have cost.

Table 18: Costs of materials from electronics shop

Item	Quantity	Cost/Unit	Shipping Cost	Total Cost
Rotary Encoder	2	\$76.19	\$0.00	\$152.38
GPS Module	1	\$20.99	\$9.81	\$30.80
Raspberry Pi 3B+	1	\$94.95	\$13.95	\$108.90
Nema 17 Motors	3	\$7.33	\$24.64	\$46.63
Stepper Motor Drivers	2	\$15.56	\$0.00	\$31.12
EVGA Power Supply	1	\$79.99	\$0.00	\$79.99
			Subtotal	\$449.82
			Tax	13%
			<b>Final Total</b>	<b>\$508.30</b>

Table 19: Costs of materials from University Machine Services

Item	Quantity	Cost per Unit	Total Cost
2" x 8" x 12' Wood	1	Exact breakdown unknown	
2" x 4" x 8' Wood	4		
4' x 8' Wood Weather Treated	2		
<b>UMS Wood Materials Cost</b>			
3" x 3" x 4' (1/4" thick) Square Metal Tube	1	Exact breakdown unknown	
1" Steel Angle, 1/8" thick x 60"	1		
1" diameter, 1" long Metal Rod	1		
1/2" diameter, 4" length Shaft	1		
1" x 1" x 1", 12" long Z Bracket	1		
6" x 4", 1/4" Thick Steel Plate	1		
Low-Carbon Steel Disc 1/2" Long, 5" Diameter	2		
4.5" long, 2.5" diameter Steel Rod	1		
10" x 10" x 1/2" Steel Plate	1		
1/2" long, 3" diameter Low-Carbon Steel Disc	1		
<b>UMS Metals Estimate</b>			<b>\$87.86</b>
Thrust Ball Bearing	1	\$22.25	\$22.25
Ball Bearings	2	\$11.12	\$22.25
		<b>Final Total (incl. Tax)</b>	<b>\$251.75</b>

Table 20: Costs of materials from miscellaneous shops

Item	Store	Quantity	Cost/Unit	Total Cost
3DP Filament	Amazon	2	\$30.00	\$60.00
Wood Glue	Home Depot	1	\$20.00	\$20.00
Nuts (assorted)	Home Depot	1	\$40.00	\$40.00
Bolts (assorted)	Home Depot	1	\$50.00	\$50.00
Dowels	Home Depot	1	\$2.00	\$2.00
Linear Rods for Gearbox	Home Depot	3	\$12.00	\$12.00
Welding	UMS	1 hour	\$60.00	\$60.00
			Subtotal	\$268
			Tax	13%
			<b>Final Total</b>	<b>\$302.84</b>

Table 21: Costs of general project resources

Resource	Rate	Estimated Cost
Engineering Time	880 hours at \$50/hour	\$44,000
SolidWorks <sup>12</sup>	Standard license for each member 4x\$8000	\$32,000
MATLAB & Simulink <sup>13</sup>	Standard license for each member 4x\$(2850+4300)	\$28,600
Microsoft Office <sup>14</sup>	Standard license for each member 4x\$200	\$800

### **Validation Protocols and Results:**

A test plan was created to validate that the prototype works as intended in the original design. The first phase in validation was ensuring that the mechanical and electrical components worked successfully. The table below provides a summary of the results of testing.

Table 22: Validation for each mechanical/electrical component

Test	Result
Rotating platform spins freely on thrust bearing	Pass
The azimuth motor moves forwards by the correct amount based on input signal in full step mode	Pass
The azimuth motor moves forwards by the correct amount based on input signal in micro step mode	Pass
The azimuth motor moves backwards by the correct amount based on input signal in full step mode	Pass
The azimuth motor moves backwards by the correct amount based on input signal in micro step mode	Pass
The azimuth motor stops when a pause signal is received	Pass
The azimuth encoder reports correct position information	Pass
The elevation motor moves forwards by the correct amount based on input signal in full step mode	Pass
The elevation motor moves forwards by the correct amount based on input signal in micro step mode	Pass
The elevation motor moves backwards by the correct amount based on input signal in full step mode	Pass
The elevation motor moves backwards by the correct amount based on input signal in micro step mode	Pass
The elevation motor stops when a pause signal is received	Pass
The elevation motor reports correct positional information	Pass

It can be seen that all the tests of the individual components were passed. Afterwards, the integration of these components within their respective subsystems was tested in a similar manner.

Table 23: Validation for integration of mechanical/electrical components

Test	Result
Elevation motor moves the connected elevation subsystem platform in full step mode	Pass
Elevation motor moves the connected elevation subsystem platform in micro step mode	Pass
Azimuth motor shaft turns the central gear in the gearbox in full step mode	Fail
Azimuth motor shaft turns the central gear in the gearbox in micro step mode	Pass

The azimuth motor was unable to turn the central gear in the gearbox in full step mode without slipping, due to tolerance issues within the gearbox. However, the motors will both always be run in micro step mode, so this will not be an issue moving forward.

There were a variety of software tests completed as well. They are as follows:

1. ROS communication test to ensure all components are wired correctly and communicating with each other:

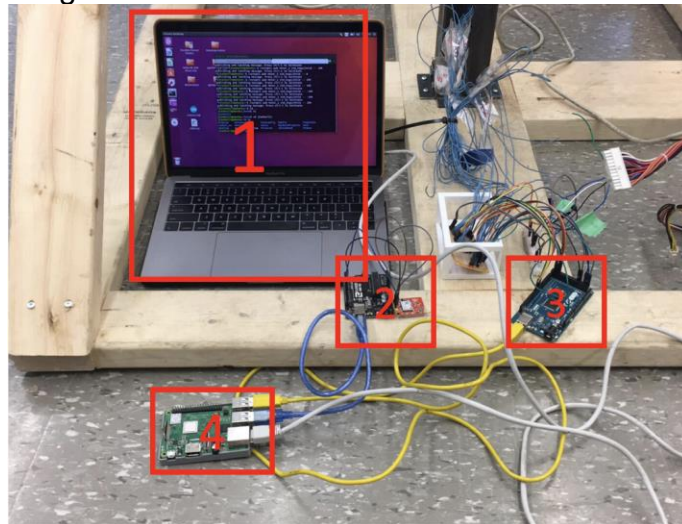


Figure 24: Software communication set up

In Figure 24, 1 is the monitor, 2 is the first Arduino board and GPS module, 3 is the second Arduino board, and 4 is the Raspberry Pi.

2. ROS test to see if the Raspberry Pi publishes data for the two stepper motors (Figure 25), if the Raspberry Pi gets GPS coordinate data from the Arduino board (Figure 26), and use rqt\_graph command to monitor node communication (Figure 27).

```
jianhuli@ubuntu:~/catkin_ws/src/beginner_tutorials/scripts$ rosrun beginner_tutorials moonros.py
[INFO] [1554911117.884777]: azal49.0 140.0
[INFO] [1554911119.887322]: azal49.0 140.0
[INFO] [1554911121.864944]: azal49.0 140.0
[INFO] [1554911123.868652]: azal49.0 140.0
[INFO] [1554911125.868774]: azal49.0 140.0
[INFO] [1554911127.868334]: azal49.0 140.0
[INFO] [1554911129.869127]: azal49.0 140.0
[INFO] [1554911131.866399]: azal49.0 140.0
[INFO] [1554911133.869312]: azal49.0 140.0
[INFO] [1554911135.869219]: azal49.0 140.0
[INFO] [1554911137.869647]: azal49.0 140.0
[INFO] [1554911139.868946]: azal49.0 140.0
[INFO] [1554911141.868989]: azal49.0 140.0
```

Figure 25: Data for two stepper motors

```
[INFO] [1554911851.533216]: /sunros_5046_1554911117738I heard x: 43.0082015991
y: -81.2730026245
z: 0.0
[INFO] [1554911851.533699]: /sunros_5046_1554911117738I heard x: 43.0082015991
y: -81.2730026245
z: 0.0
[INFO] [1554911851.534189]: /sunros_5046_1554911117738I heard x: 43.0082015991
y: -81.2730026245
z: 0.0
[INFO] [1554911851.534590]: /sunros_5046_1554911117738I heard x: 43.0082015991
y: -81.2730026245
z: 0.0
[INFO] [1554911851.535095]: /sunros_5046_1554911117738I heard x: 43.0082015991
y: -81.2730026245
z: 0.0
[INFO] [1554911851.535458]: /sunros_5046_1554911117738I heard x: 43.0082015991
y: -81.2730026245
z: 0.0
[INFO] [1554911851.535907]: /sunros_5046_1554911117738I heard x: 43.0082015991
y: -81.2730026245
z: 0.0
```

Figure 26: GPS coordinate data

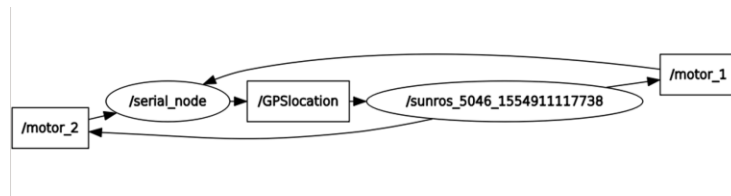


Figure 27: Node communication

The communication between each node was successful. The Arduino board received the angle set for both stepper motors and successfully published the GPS location back to the Raspberry Pi board.

3. GPS test to ensure the module is functioning properly. The result can be seen in Figure 28 below.

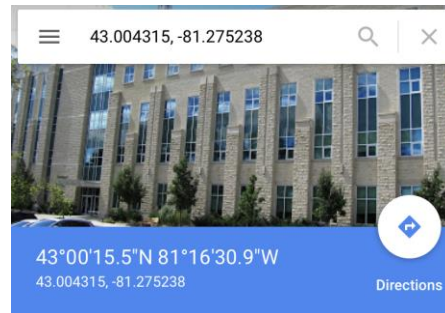


Figure 28: Result from GPS module compared to Google Map coordinates

Compared to the Google Map coordinates, the result from the GPS module has an error within 0.005%. The GPS was set to update the data twice per second.

4. Moon tracking test to compare our results for calculated elevation and azimuth angles (Figure 29) to available online data (Figure 30).

```
/Users/jianhuili/PycharmProjects/SGPtest/ver
2019-04-10 16:21:07.899778
19.866000 80.197000
3178 80
```

Figure 29: Results from moon tracking code

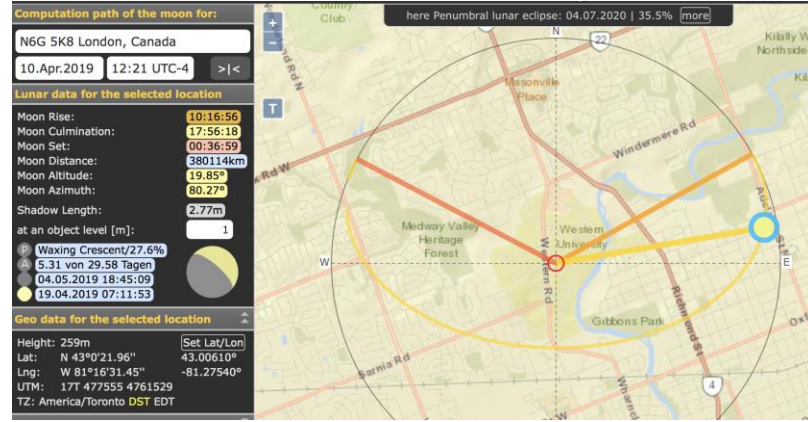


Figure 30: Online moon data [25]

The calculated moon elevation angle was 19.866 degrees and azimuth angle was 80.197 degrees. The differences in both are less than 1.5%, which can be attributed to the atmospheric refraction effect. As well, our code to calculate the moon position is based on the theoretical moon orbit.

- ISS tracking test to compare our results for calculated latitude and longitude of the ISS (Figure 31) to available online data (Figure 32).

```
/Users/jianhuili/PycharmProjects/SGPtest/venv/bin/python /Users/jianhuili/Py
2019-04-10 16:14:40.657303
-51.477250961450636 173.18636536263688 427.4642343386276
137.7510087174042 -17.830462161092814
```

Figure 31: Results from ISS prediction code

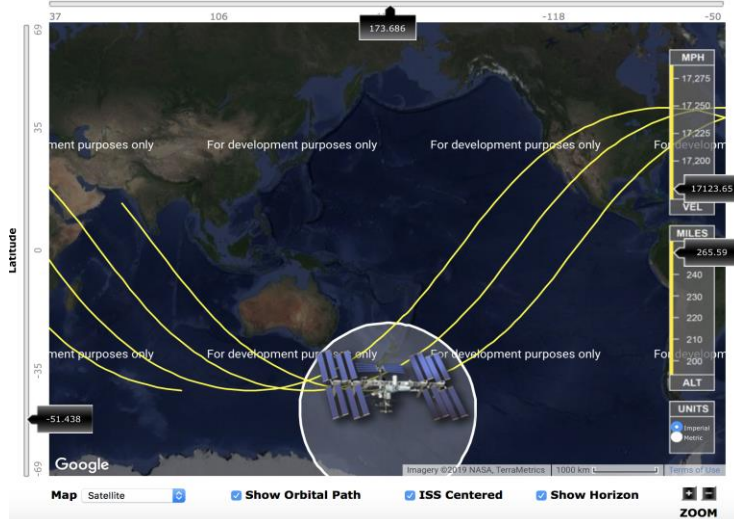


Figure 32: Actual ISS location [26]

Looking at the figures above, the prediction code returned the location of the ISS as a latitude of -51.477 and longitude of 173.186. The real location of the ISS was a latitude of -51.438 and longitude of 173.686. The difference is within 0.288%; therefore, our prediction code is within high accuracy. The second line in Figure 30 calculated an azimuth angle of 137.75 degrees and an elevation angle of -17.830 degrees.

All software code can be found in Appendix 3. Lastly, the entire system was tested to ensure all components were properly integrated and that the requirements were being met. Since the satellite has yet to be launched, testing was completed using available data for the moon, the sun, and the International Space Station. Since there are specific days and times when these objects are more visible (especially with the moon's changing phases), testing was completed over the course of multiple dates and times. It is important to note that this testing was completed at locations with close proximity to the Thompson Engineering Building, so the field of range is significantly smaller than it would actually be. However, enough data was obtained to prove the validity of the ground station. The results for a number of these tests can be seen in the tables below.

Table 24: Validation for entire system tracking the Moon on Sunday, March 31<sup>st</sup> at 10 am

Test	Result
Determines location of ground station	Pass
Determines location of Moon in orbit	Pass
Calculates the angle between ground station and orbiting object	Pass
Azimuth motor (alone) moves to calculated angle	Pass
Elevation motor (alone) moves to calculated angle	Pass
Azimuth and Elevation controlled simultaneously	Pass
Azimuth motor updates position based on orbit	Pass
Elevation motor updates position based on orbit	Pass

Elevation motor rotates gearbox to desired angle	Fail
Azimuth motor rotates platform to desired angle	Pass
Encoders provide accurate feedback of motor angle	Pass
Antenna connector points in direction of orbiting object	Fail
Antenna connector moves with direction of orbiting object	Pass
Moon remains in center of image frame	Fail

Table 25: Validation for entire system tracking the Moon on Sunday, March 31<sup>st</sup> at 12 pm

Test	Result
Determines location of ground station	Pass
Determines location of Moon in orbit	Pass
Calculates the angle between ground station and orbiting object	Pass
Azimuth motor (alone) moves to calculated angle	Pass
Elevation motor (alone) moves to calculated angle	Pass
Azimuth and Elevation controlled simultaneously	Pass
Azimuth motor updates position based on orbit	Pass
Elevation motor updates position based on orbit	Pass
Elevation motor rotates gearbox to desired angle	Pass
Azimuth motor rotates platform to desired angle	Fail
Encoders provide accurate feedback of motor angle	Fail
Antenna connector points in direction of orbiting object	Pass
Antenna connector moves with direction of orbiting object	Fail
Moon remains in center of image frame	Fail

Table 26: Validation for entire system tracking the Sun on Sunday, March 31<sup>st</sup> at 3 pm

Test	Result
Determines location of ground station	Pass
Determines location of Sun in orbit	Pass
Calculates the angle between ground station and orbiting object	Pass
Azimuth motor (alone) moves to calculated angle	Pass
Elevation motor (alone) moves to calculated angle	Pass
Azimuth and Elevation controlled simultaneously	Pass
Azimuth motor updates position based on orbit	Pass
Elevation motor updates position based on orbit	Pass
Elevation motor rotates gearbox to desired angle	Fail
Azimuth motor rotates platform to desired angle	Fail
Encoders provide accurate feedback of motor angle	Fail
Antenna connector points in direction of orbiting object	Fail
Antenna connector moves with direction of orbiting object	Fail
Sun remains in center of image frame	Fail

Table 27: Validation for entire system tracking the ISS on Monday, April 1<sup>st</sup> at 1:30 pm

Test	Result
Determines location of ground station	Pass
Determines location of ISS in orbit	Pass
Calculates the angle between ground station and orbiting object	Pass
Azimuth motor (alone) moves to calculated angle	Pass
Elevation motor (alone) moves to calculated angle	Pass
Azimuth and Elevation controlled simultaneously	Pass
Azimuth motor updates position based on orbit	Pass
Elevation motor updates position based on orbit	Pass
Elevation motor rotates gearbox to desired angle	Fail
Azimuth motor rotates platform to desired angle	Fail
Encoders provide accurate feedback of motor angle	Fail
Antenna connector points in direction of orbiting object	Fail
Antenna connector moves with direction of orbiting object	Fail
ISS remains in center of image frame	N/A

Table 28: Validation for entire system tracking the Sun on Monday, April 8<sup>th</sup> at 2:00 pm

Test	Result
Determines location of ground station	Pass
Determines location of ISS in orbit	Pass
Calculates the angle between ground station and orbiting object	Pass
Azimuth motor (alone) moves to calculated angle	Fail
Elevation motor (alone) moves to calculated angle	Fail
Azimuth and Elevation controlled simultaneously	Fail
Azimuth motor updates position based on orbit	Fail
Elevation motor updates position based on orbit	Fail
Elevation motor rotates gearbox to desired angle	Fail
Azimuth motor rotates platform to desired angle	Fail
Encoders provide accurate feedback of motor angle	Fail
Antenna connector points in direction of orbiting object	Fail
Antenna connector moves with direction of orbiting object	Fail
Sun remains in center of image frame	Fail

For testing the accuracy of the system, a web-camera was placed in the interface that would hold the antenna, since the “field-of-view” of an antenna is comparable to that of a camera. An image processing approach was applied that looks at the image (which ideally would be the moon or sun) finds circular objects in the frame using the Hough Transform in the OpenCV library [27]. The program returns the location of the center of the largest circle as well as its radius. Since a perfect pointing accuracy would imply that the satellite is right in the center of the field-of-view, by comparing the center of the largest circle (sun or moon) to center of the frame, the accuracy can be illustrated. The following figures show the algorithm applied to still frames of the moon.



Figure 33: Off-center crescent moon



Figure 34: Off-center full moon

From the above tests, the system is effective at various capacities in each situation, which shows that the system is mostly functional until complete integration occurs. This is a large oversight that was only discovered during the testing period of the project, which was far too late for many major corrections to occur; however, given the marginal capacity of each system's performance individually, the prototype is effective. In future iterations, taking into consideration various shortfalls, a better approach would be to test various subsystems together before committing to a complete build at once.

In the first test sequence of the tracking, most of the validation tests were passed, except for the elevation motor controlling the gearbox to the correct angle. This was later found to be a logical programming error, as a pre-scale value that was being used to convert the angle to accommodate for the gearbox's reduction was improperly declared. In the second run, believing that the issue was resolved, fixtures were tightened, and the ground station was relocated to test again, however, the combination of these caused two problems. Firstly, the new location was slightly uneven, which caused the rotating platform to be slightly off angle since it simply sits on the thrust bearing. This introduced rubbing between the rotating platforms recess and the shaft on which the bearing sat, and this friction was too much for the azimuth motor to overcome, so azimuth control was lost. Additionally, testing the rotatability of the azimuth platform also caused the encoder wires to become frayed. Since the encoders were already affixed hard to access, future tests were reliant on the open loop controllability of the stepper motors. In the sun and ISS tracking test, it appeared as though the motor's performance began to degrade, which was unexpected as the previous functional elevation motor began to skip steps, though it would operate with no load, meaning the motor did not burn out. In the final test, the drivers overheated and this resulted in the system no longer working, apart from the separate software.

## Conclusions

The prototype created was able to test the important components of the design, as it was manufactured to be as close to the final design as possible. Looking at the original product design specifications, the prototype was successful in being a compact size compared to existing ground stations and manufactured from many off the shelf components, with the exception of expensive items that were 3D printed or custom manufactured in the metal shop. As well, the software was able to accurately track orbiting objects such as the Sun, Moon, and ISS with extremely high accuracy. From the design verification and results, it was determined that the ground station works well when the individual components are tested; however, there is a large gap in the integration of the complete system. In future renditions of the design, it would be beneficial to attempt systems integration much sooner so that any issues, such as the misalignment of the bearings or the motor degradation could be discovered and addressed sooner. Recommendations to further improve the system are summarized in the following section.

## **Future Work and Recommendations**

### **Mechanical Recommendations:**

1. Heat temper the motor flange that is welded to the two side plates to alleviate stress in the part that is causing the misalignment of the motor.
2. Replace the 3D printed component used to hold the gearbox in place as the fit between the gearbox and the housing is too tight, causing additional friction in the gears.
3. Perform quality control to ensure that wood is not warped.
4. Build a box base with already obtained weatherproofed wood.
5. Waterproof the elevation subassembly by enclosing the subassembly everywhere except the output shaft and coating the outside of the output shaft with clear coat spray-on paint to prevent seepage through the 3D printed layer lines.
6. Buy and attach a holder to the base for all of the electronics that is IP67 rated.

### **Electrical Recommendations:**

1. Make a power distribution board for all of the electronics so they have a constant power supplied throughout their operation and there are no shorts that can trip the power supply unit.
2. Create a shield for the Arduino board so that all the electronics can be easily attached to one physical interface with dedicated connectors that will hold the wires.
3. Use ribbon cables and connectors to make wire management easier and less prone to tangling/breakage and increase the ease of setup since they will be bunched together in a specific order.

### **Software Recommendations:**

1. Test on an already launched CubeSat.
2. Use machine learning to predict future location of an orbiting object that does not have widely available data.
3. Add in priority lists for multiple CubeSat tracking when ours is not visible.

## References

- 1 What is a CubeSat. (2018, November 27). Retrieved from <http://www.asc-csa.gc.ca/eng/satellites/cubesat/what-is-a-cubesat.asp>
- 2 Cakaj, S., Kamo, B., Lala, A., & Rakipi, A. (2014). The Coverage Analysis for Low Earth Orbiting Satellites at Low Elevation. (*IJACSA*) International Journal of Advanced Computer Science and Applications, 5(6). doi:[http://thesai.org/Downloads/Volume5No6/Paper\\_2-The\\_Coverage\\_Analysis\\_for\\_Low\\_Earth\\_Orbiting\\_Satellites\\_at\\_Low\\_Elevation.pdf](http://thesai.org/Downloads/Volume5No6/Paper_2-The_Coverage_Analysis_for_Low_Earth_Orbiting_Satellites_at_Low_Elevation.pdf)
- 3 TS Kelso. (1980). Models for Propagation of NORAD Element Sets. Retrieved from <http://www.celestrak.com/NORAD/documentation/spacetrk.pdf>
- 4 Full Ground Station Kit VHF/UHF/S-band. (n.d.). Retrieved from <https://www.isispace.nl/product/full-ground-station-kit-for-vhfuhfs-band/>
- 5 S-band Ground station antenna for LEO satellites. (n.d.). Retrieved from <https://gomspace.com/shop/subsystems/ground-systems/nanocom-as2000.aspx>
- 6 S. Alcaide. (2014). Mobile CubeSat Command and Control (MC3) 3-Meter Dish Calibration and Capabilities", Naval Postgraduate School, Monterey, California. Retrieved from <http://www.dtic.mil/dtic/tr/fulltext/u2/a607479.pdf>
- 7 A. Hughes and W. Drury, Electric Motors and Drives: Fundamentals, Types and Applications, 4th ed. Newnes, 2013.
- 8 Face-Mount Crossed-Roller Bearing. (n.d.). Retrieved from <https://www.mcmaster.com/2010n12>
- 9 Ball Bearing Open, Trade Number R8, for 1/2" Shaft Diameter. (n.d.). Retrieved from <https://www.mcmaster.com/60355k505>
- 10 Thrust Ball Bearing for 1-1/4" Shaft Diameter, 1-7/8" OD, 0.437" Thick. (n.d.). Retrieved from <https://www.mcmaster.com/6655k24>
- 11 External Retaining Ring for 1/4" OD, Black-Phosphate 1060-1090 Spring Steel. (n.d.). Retrieved from <https://www.mcmaster.com/97633a130>
- 12 AISI 4140 Alloy Steel (UNS G41400). (2019). Retrieved from [https://www\\_azom\\_com/article.aspx?ArticleID=6769](https://www_azom_com/article.aspx?ArticleID=6769).
- 13 Metal Supermarkets. (2016, August 22). 7 Things to Consider When Choosing a Stainless Steel Grade. Retrieved from <https://www.metalsupermarkets.com/7-things-consider-choosing-stainless-steel-grade/>
- 14 Gear Boxes. (n.d.). Retrieved from <https://www.mcmaster.com/gear-boxes>

15 High Torque 160:1 Compound Planetary Gearbox. (2017). Retrieved from <https://www.thingiverse.com/thing:2375916>

16 Polylactic Acid (PLA, Polylactide). (n.d.). Retrieved from <https://www.makeitfrom.com/material-properties/Polylactic-Acid-PLA-Polylactide>

17 .76, 1.0 & 1.2M - C & Ku-Band Receive Only Series 1761, 1111 & 1130 Technical Specifications. (n.d.). Retrieved from <https://gdmissionsystems.com/-/media/General-Dynamics/Satcom/PDF/Antennas/VSAT-Products/Technical-Documentation/Antenna-Specifications-Sheets/1000-006.ashx?la=en&hash=CADD06C82ED49C4D204D4F09EA6A2A4F7E5CED09>

18 The Drag Equation. (n.d.). Retrieved from <https://www.grc.nasa.gov/www/k-12/rocket/drageq.html>

19 AMCI : Advanced Micro Controls Inc: Stepper vs Servo. (2019).Retrieved from <https://www.amci.com/industrial-automation-resources/plc-automation-tutorials/stepper-vs-servo>

20 ROS Documentation. (n.d.). Retrieved from <http://wiki.ros.org/Master>

21 R. Dix, Material Considerations in Fused Filament Fabrication. (2018).

22 S. P. Radzevich, Dudleys handbook of practical gear design and manufacture. Boca Raton: CRC Press, Taylor et Francis Group. (2016).

23 9 J. E. Shigley and C. R. Mischke, Mechanical engineering design. Boston: McGraw-Hill. (2001).

24 ROS Documentation. (n.d.). Retrieved from <http://wiki.ros.org/Master>

25 Retrieved from <https://www.mooncalc.org/#/43.0061,-81.2754,13.39/2019.04.10/12:21/1/3>

26 ISS Tracker. (n.d.). Retrieved from <http://www.isstracker.com>

27 A. Mordvintsev, K. Abid. 2013. Hough Circle Transform. Retrieved from [https://opencv-python-tutroals.readthedocs.io/en/latest/py\\_tutorials/py\\_imgproc/py\\_houghcircles/py\\_houghcircles.html](https://opencv-python-tutroals.readthedocs.io/en/latest/py_tutorials/py_imgproc/py_houghcircles/py_houghcircles.html)

## Appendix 1: Material Property Calculations for FEA on 3D printed objects

$K_{FFF}$  is used to reduce the uniform isotropic material property to the value that 3D printing produces. These values are listed for different properties in Table 29 and were found via testing.  $A_w/A_x$  is the ratio of wall cross sectional area to total cross sectional area.  $A_i/A_x$  is the ratio of infill cross sectional area to total cross sectional area.  $K_{i,\%}$  is a function of the 3D print's infill percentage, and  $K_{i,i}$  is a function of the 3D print's infill shape. These values were also determined via testing and can be found in Table 30 and Table 31.

Table 29:  $K_{FFF}$  Values

	Ultimate tensile strength $S_{ut}$	Yield Strength $S_y$	Young's Modulus, $E$
$K_{FFF}$	0.8330	0.8274	0.5451

Table 30: K% Values

Infill %	Ultimate tensile strength, $S_{ut}$	Yield Strength, $S_y$	Young's Modulus, $E$
10	0.1298	0.1419	0.0871
20	0.1348	0.1517	0.0990
30	0.1817	0.2067	0.1434
40	0.2060	0.2269	0.1603
50	0.2450	0.2778	0.2058
60	0.2722	0.3224	0.2364
70	0.3356	0.3224	0.2878
80	0.4117	0.4822	0.3539
90	0.5746	0.6821	0.5143
100	0.7307	0.8658	0.5408

Table 31:  $K_{\text{infill}}$  Values

	Ultimate tensile strength, $S_{\text{ut}}$	Yield Strength, $S_y$	Young's Modulus, $E$
<b>Grid</b>	1	1	1
<b>Triangle</b>	1.348	1.468	2.258
<b>Cubic</b>	1.904	1.844	1.867

Table 32 shows the values used to 3D print the two components most likely to fail: the output ring gear and the input connector.

Table 32: Print settings

Setting	Ring Gear	Input Connector
Wall Thickness	5 mm	5 mm
Infill Percentage	50%	50%
Infill Type	Cubic	Cubic

Using these values, the values required for the formula were calculated. As the parts had a wall thickness of 5 mm and were not thicker than 10 mm at any given place, there was no infill in either part. Therefore,  $A_i/A_x = 0$  and  $A_w/A_x = 1$ . Using these values, and the values from Table 29, more accurate part properties can be calculated as seen in Table 32. As the physical properties used in the formula of the two parts are the same, the material properties were only calculated once.

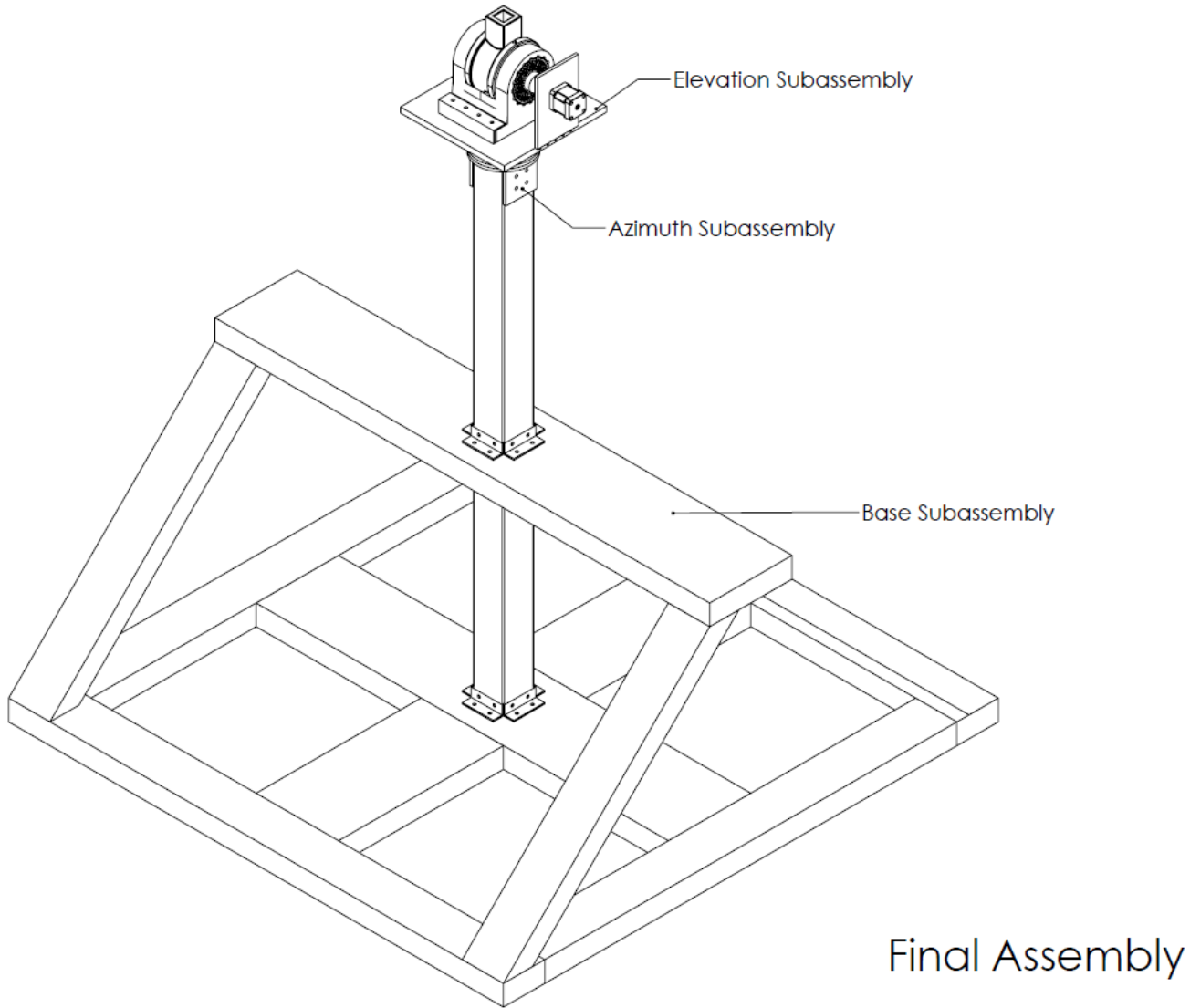
Table 33: Material properties

	Ultimate tensile strength, $S_{\text{ut}}$	Yield Strength, $S_y$	Young's Modulus, $E$
$\frac{A_w}{A_x} + \frac{A_i}{A_x} * K_{i,\%} * K_{i,t}$	1	1	1
$K_{FFF}$	0.8330	0.8274	0.5451
<b>Rated Material</b>	59 MPa	70 MPa	3500 MPa

Properties [13]			
Adjusted Material Properties	49.147 MPa	57.918 MPa	1907.85 MPa

## Appendix 2: Complete Detailed Design Documentation

### Full Model Drawings:



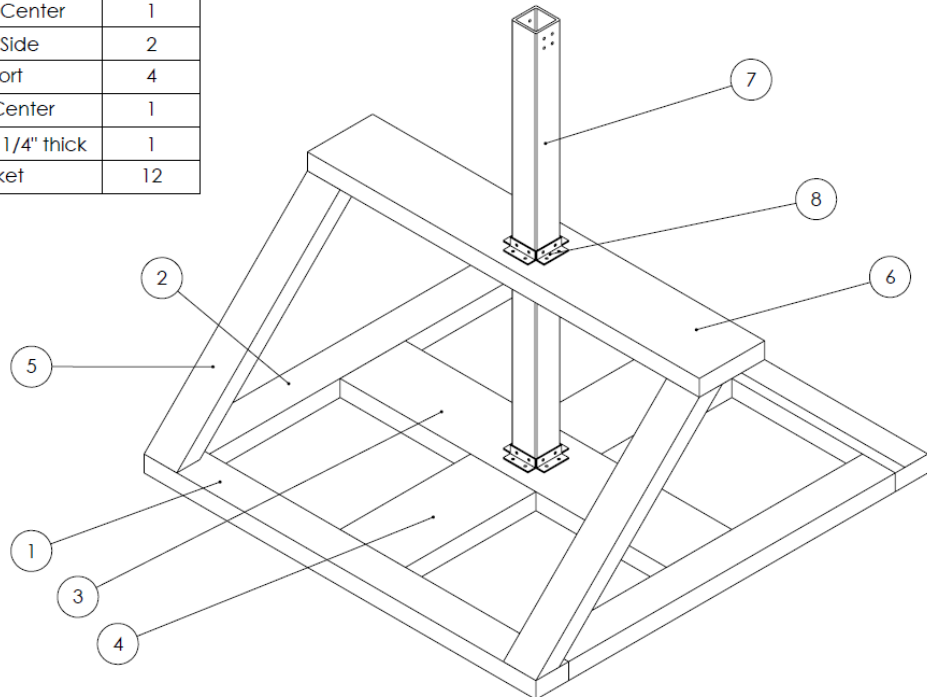
The three main subassemblies are shown above.

Note: Tolerances for all wood components are  $\pm 0.05"$  unless otherwise stated.

Tolerances for all angle brackets are  $\pm 0.05"$  unless otherwise stated.

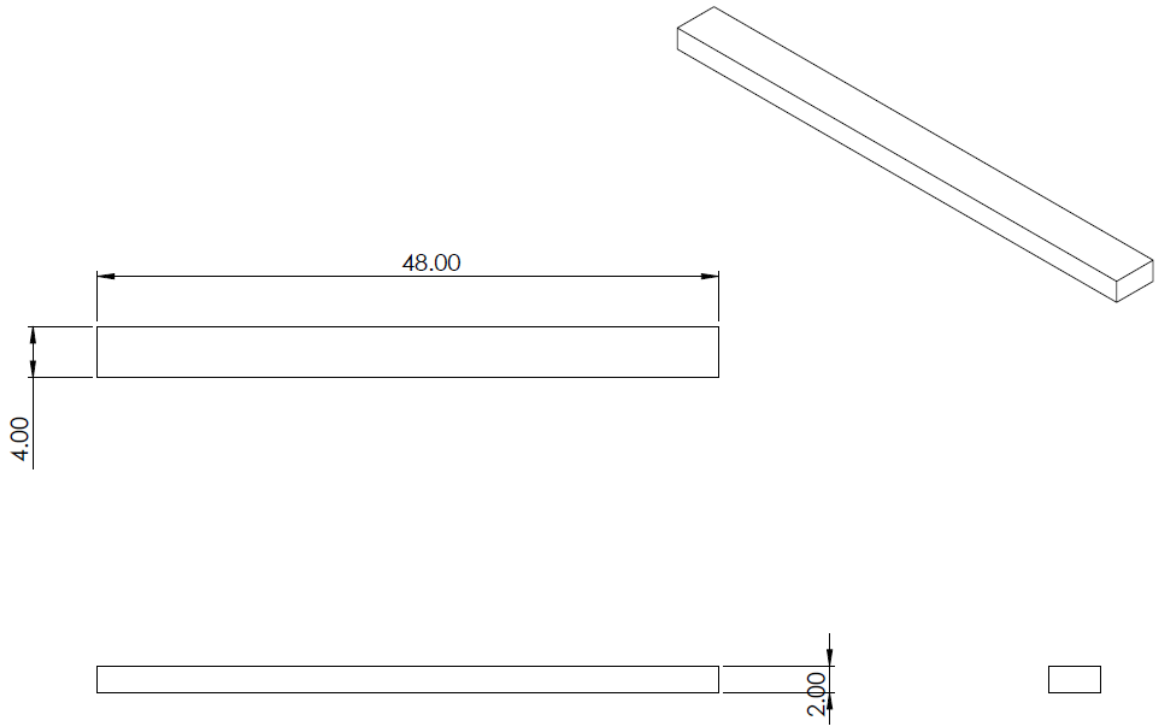
Tolerance for all metal components are  $\pm 0.01"$  unless otherwise stated.

ITEM NO.	PART NUMBER	QTY.
1	2" x 4" for base	2
2	2" x 4" for base short	2
3	2" x 8" Base Center	1
4	2" x 8" Base Side	2
5	2" x 4" Support	4
6	2" x 8" Top Center	1
7	3"x 3" Tube, 1/4" thick	1
8	Angle Bracket	12



Base Subassembly

The base subassembly is made from 2"x4" and 2"x8" pieces of pine lumber along with angle brackets to connect the 3"x3" Square Tube. The following drawings show the dimensions of each of the pieces in the Base Subassembly.

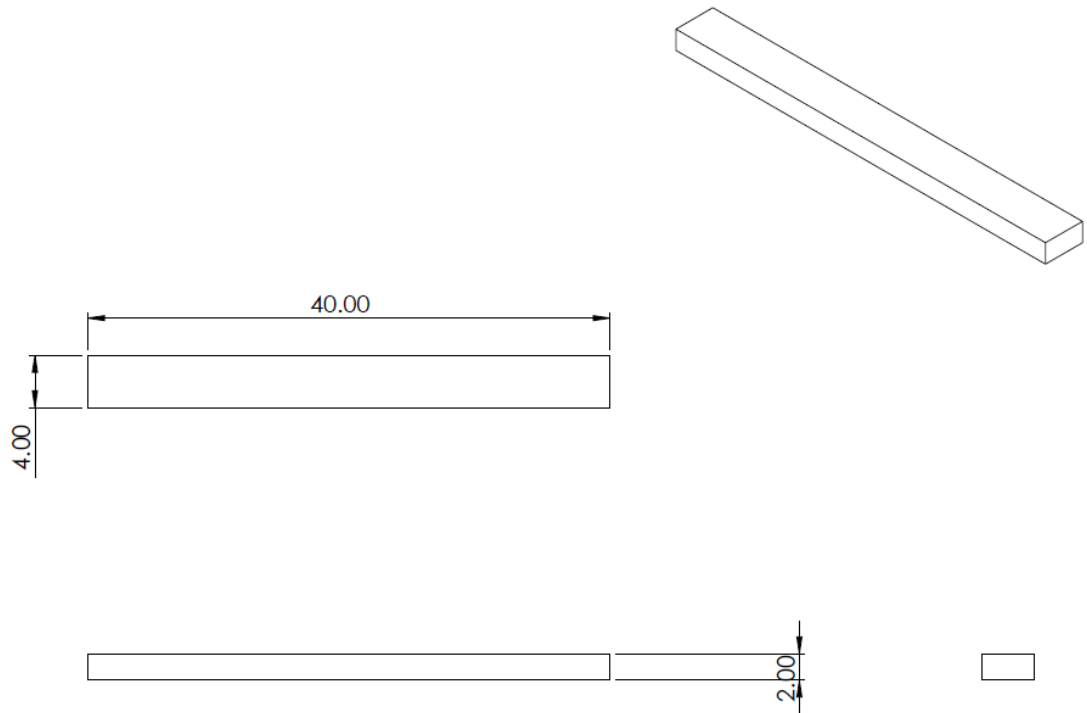


## 2X4 FOR BASE

All Dimensions in INCHES

Quantity: 2

2"x4" piece of lumber. Longest piece of 2"x4" required for this project.

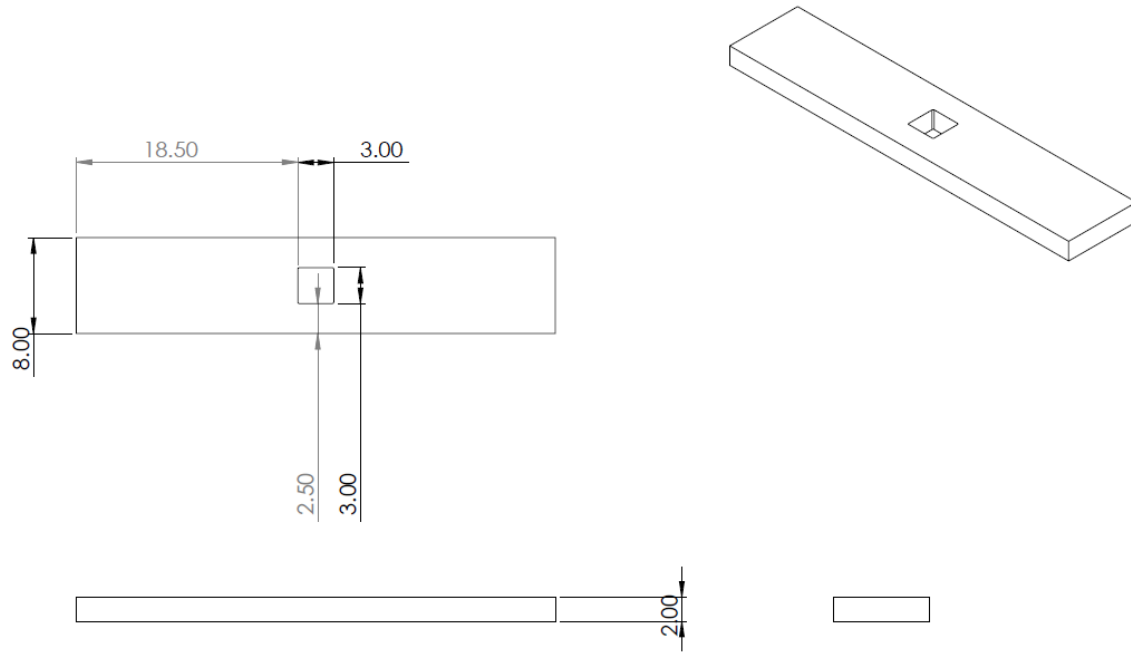


## 2X4 FOR BASE SHORT

All Dimensions in INCHES

Quantity: 2

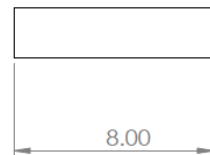
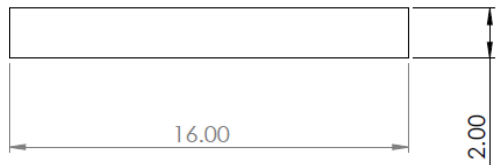
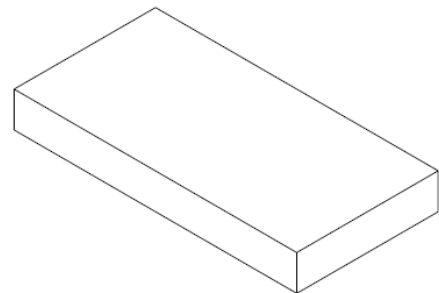
2"x4" piece of lumber. Shorter than the previous piece of 2"x4" in order to form a square box base.



## 2X8 BASE CENTER

All Dimensions in INCHES

2"x 8" piece of lumber. Used to hold the center pole in place with the use of 4 angle brackets that go around the hole and are screwed into the wood using self-drilling screws.

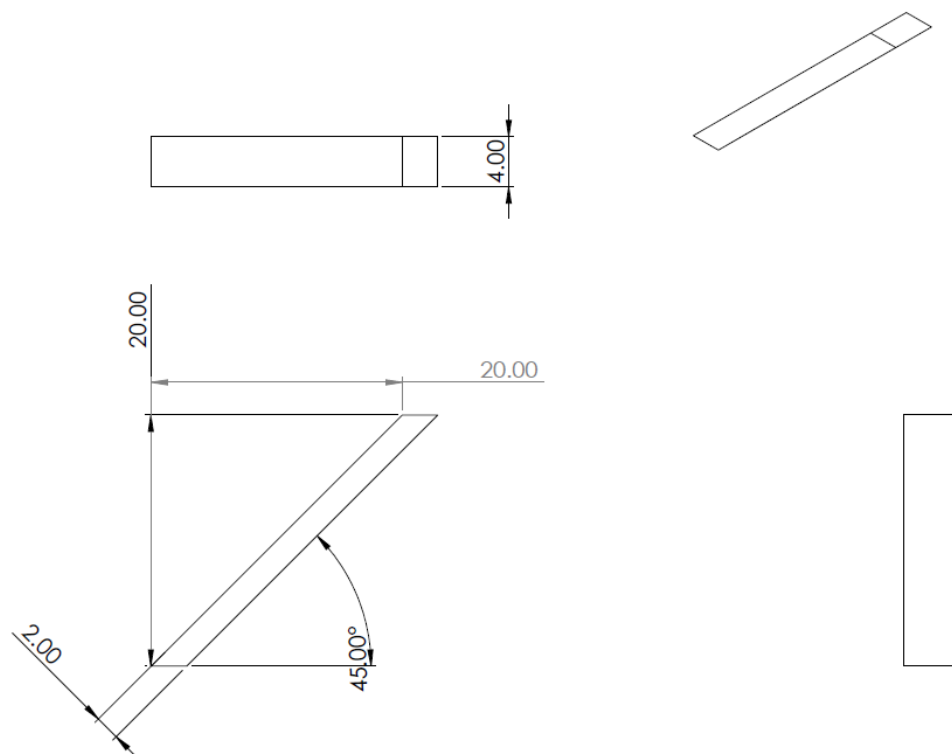


## 2X8 BASE SIDE

All Dimensions in INCHES

Quantity: 2

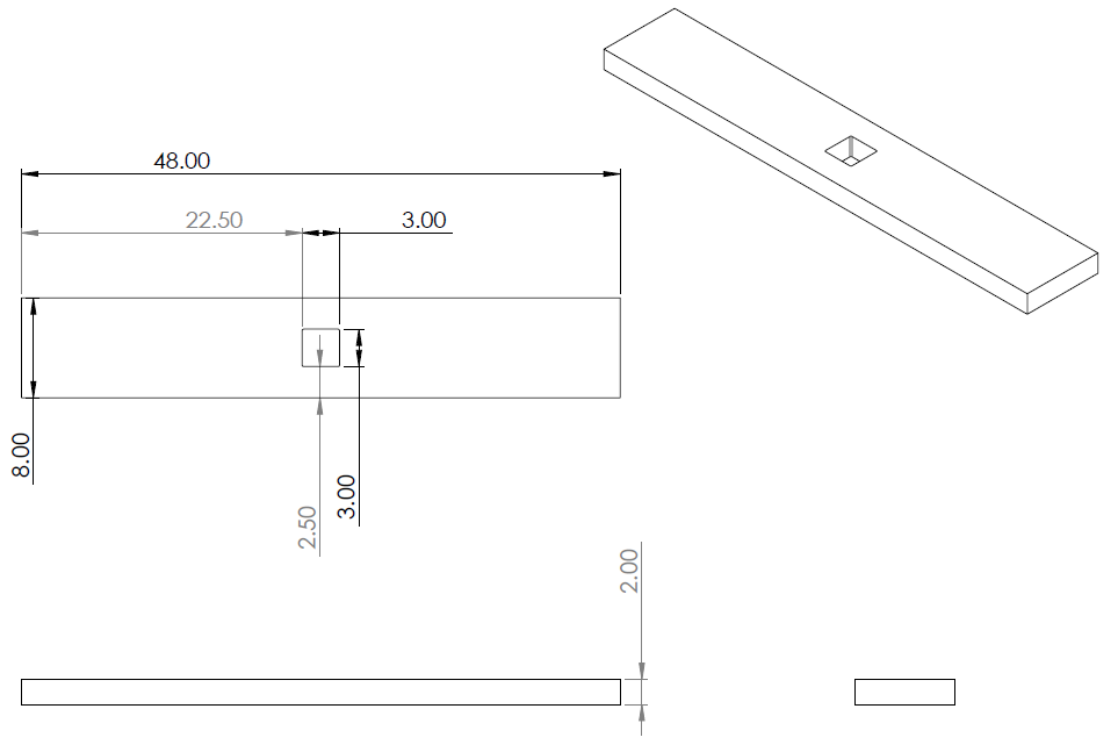
2"x 8" piece of lumber. Two pieces are used on either side of the 2" x 8" Base Center to provide more rigidity to the base.



## 2X4 SUPPORT

All Dimensions in INCHES  
QUANTITY: 4

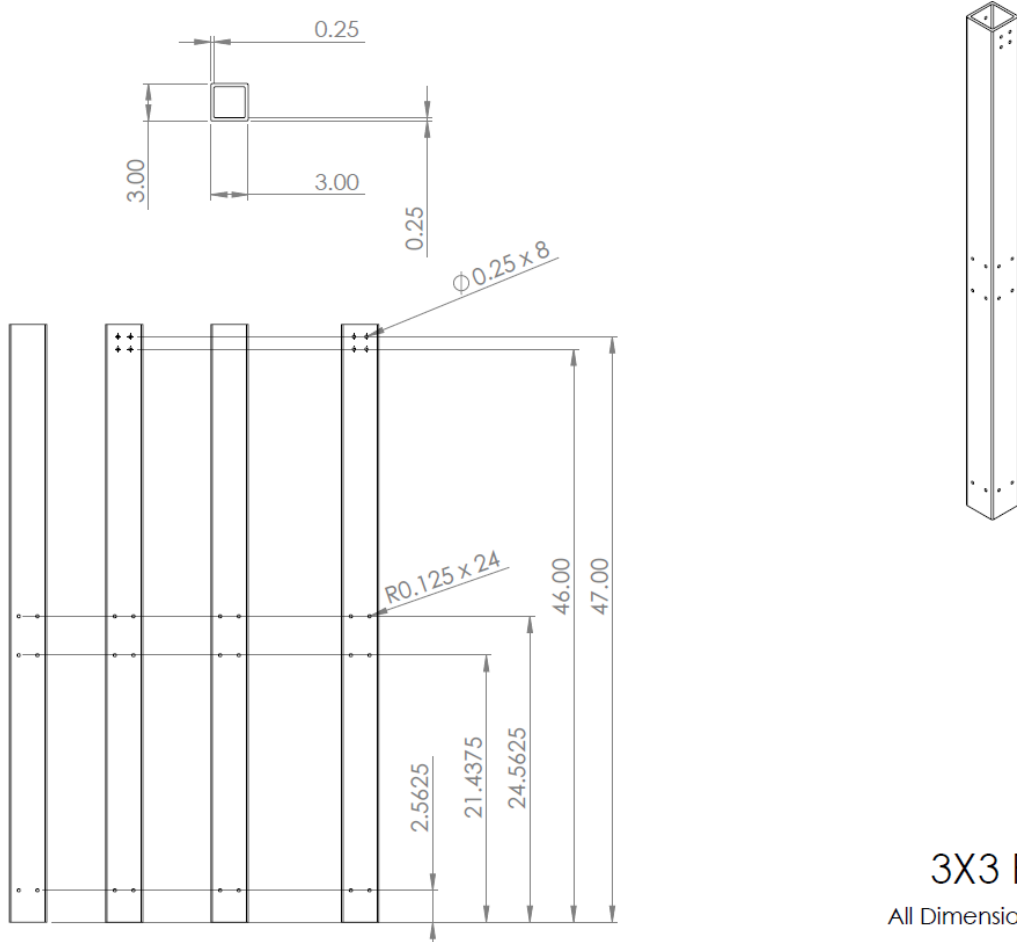
2"x4" piece of lumber used hold the top 2" x 8" Top Center at a height of 20 inches.



## 2X8 TOP CENTER

All Dimensions in INCHES

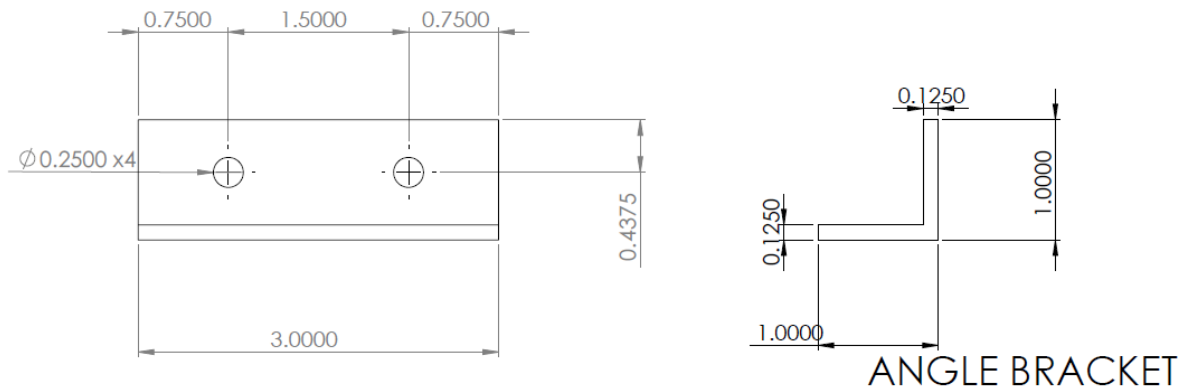
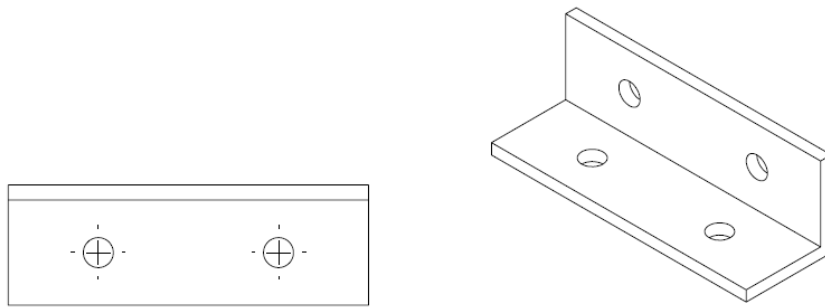
2"x 8" piece of lumber. Like the 2" x 8" base center, this piece is used to hold the center pole in place with the use of 8 angle brackets that go around the hole (4 on the top and 4 on the bottom) and are screwed into the wood using self-drilling screws.



**3X3 POLE**

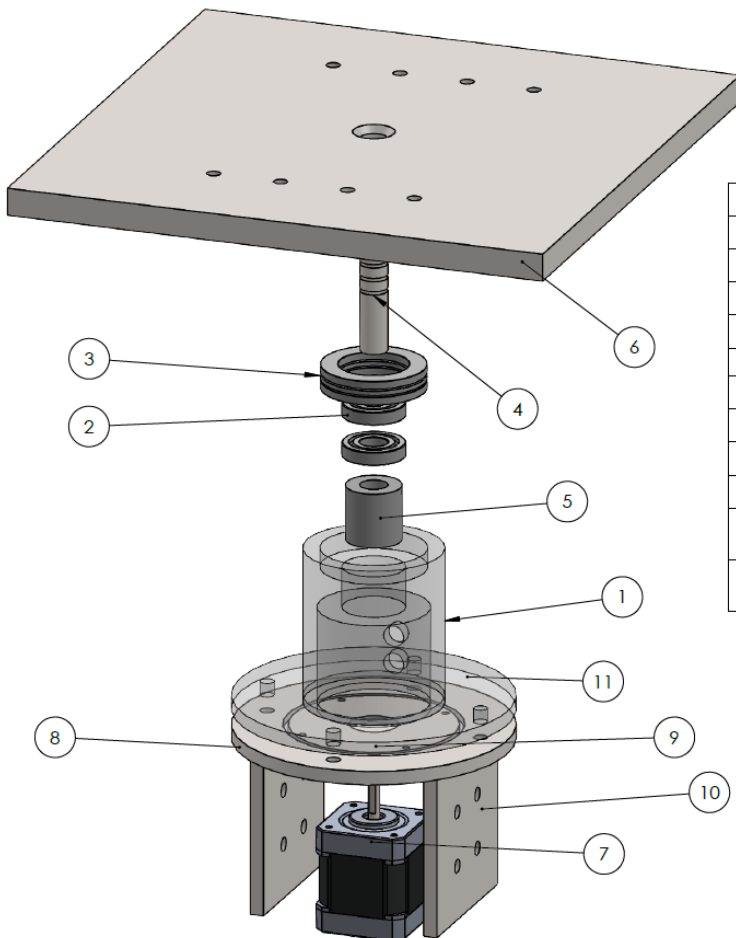
All Dimensions in INCHES

3"x3",  $\frac{1}{4}$ " thick square tube used to connect the base subassembly to the elevation and azimuth subassemblies. The bottom 24  $\frac{1}{4}$ th inch holes are used to attach the angle brackets on the base to the pole. These holes need to be threaded as it is not possible to install nuts in these locations. The 8  $\frac{1}{4}$ th inch holes are used to connect the pole to the azimuth subassembly. These holes do not need to be threaded as it is possible to use nuts for these holes.



All Dimensions in INCHES  
Quantity: 12

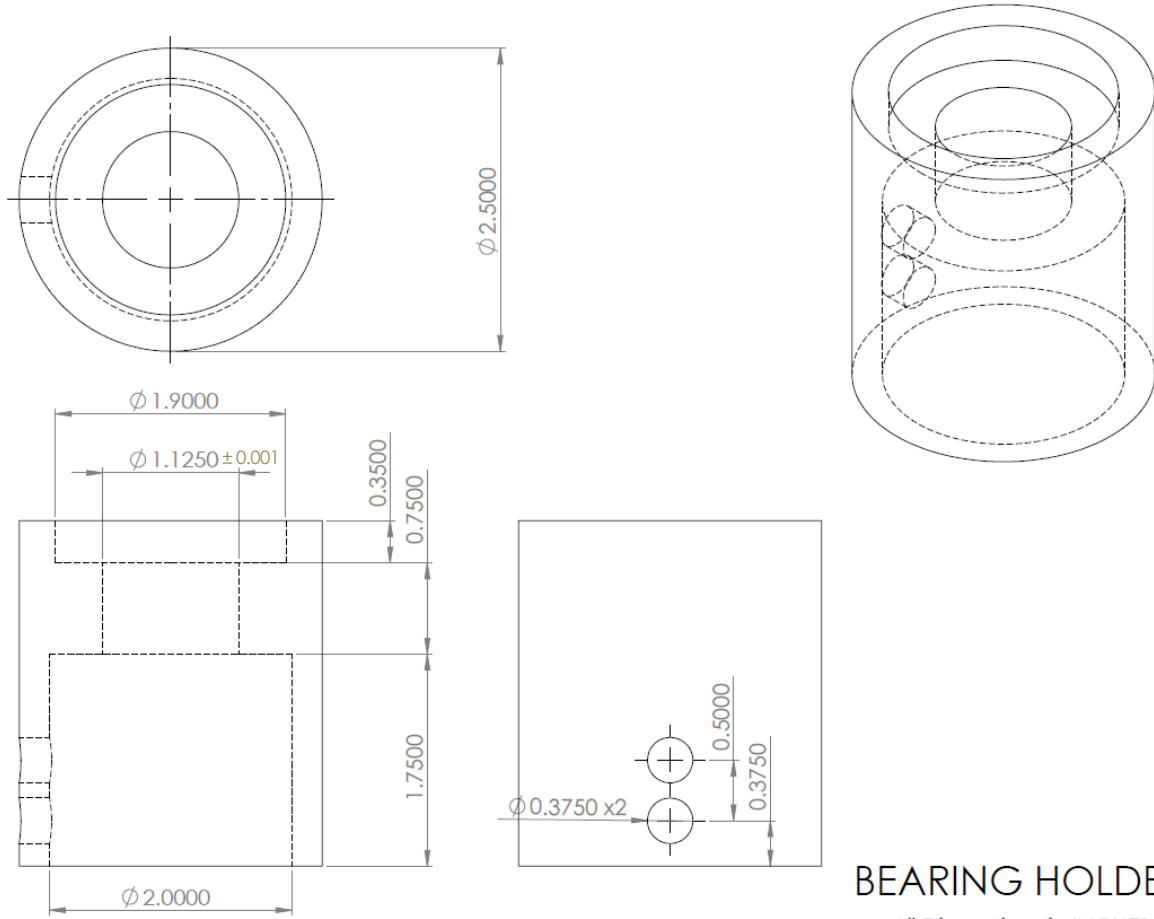
1 inch angle brackets used to connect the base to the pole. 1/4<sup>th</sup> inch nuts are used to connect these to the pole and 1/4<sup>th</sup> inch self-drilling screws are used to connect these to the wood.



Item Number	PART NUMBER	QTY.
1	Bearing Holder	1
2	Ball Bearing	2
3	Thrust Bearing s	1
4	Shaft	1
5	Motor Coupler	1
6	Base	1
7	Nema 17	1
8	Motor Holder Flange	1
9	Motor Holder	1
10	Motor Holder Flange Plates	2
11	Bearing Holder Flange	1

Azimuth Subassembly

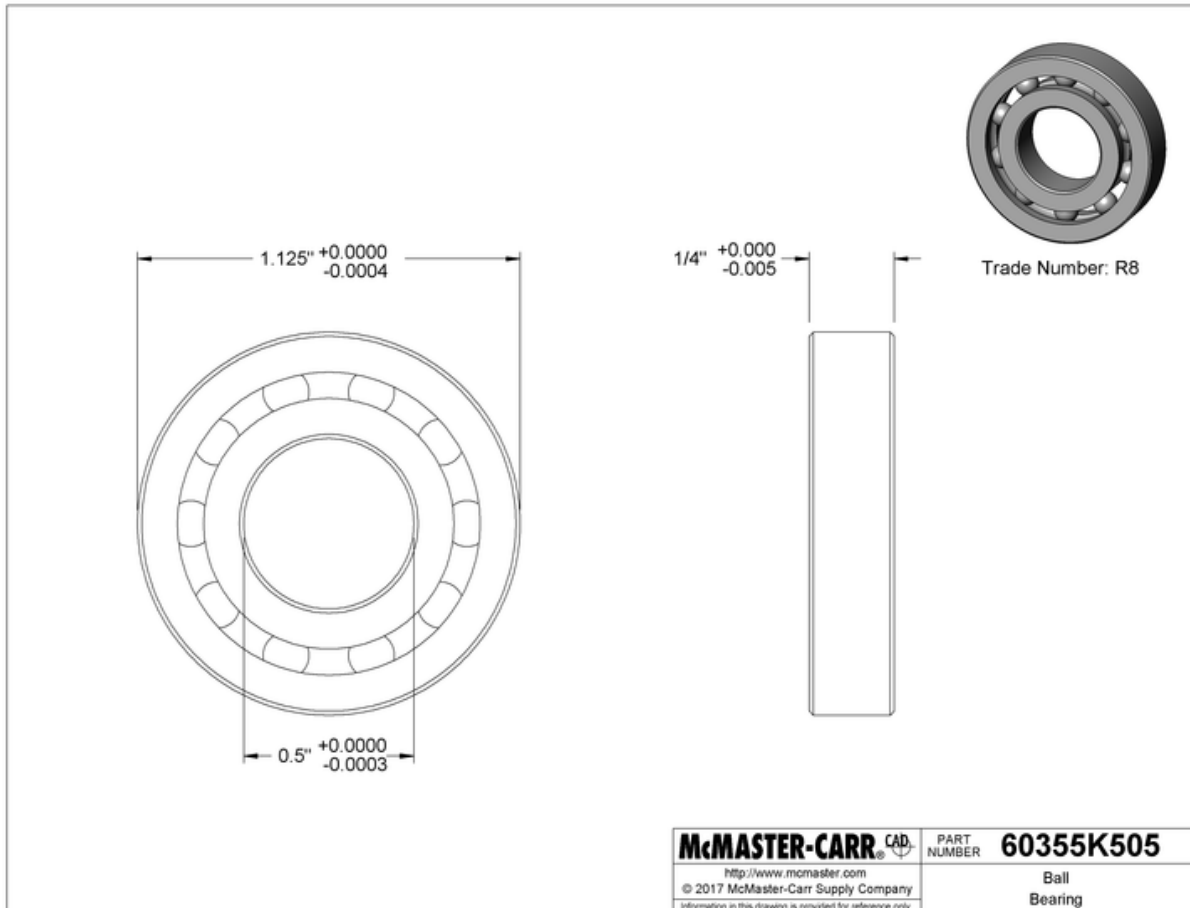
An exploded view of the Azimuth Subassembly along with a Bill of Materials for the subassembly.



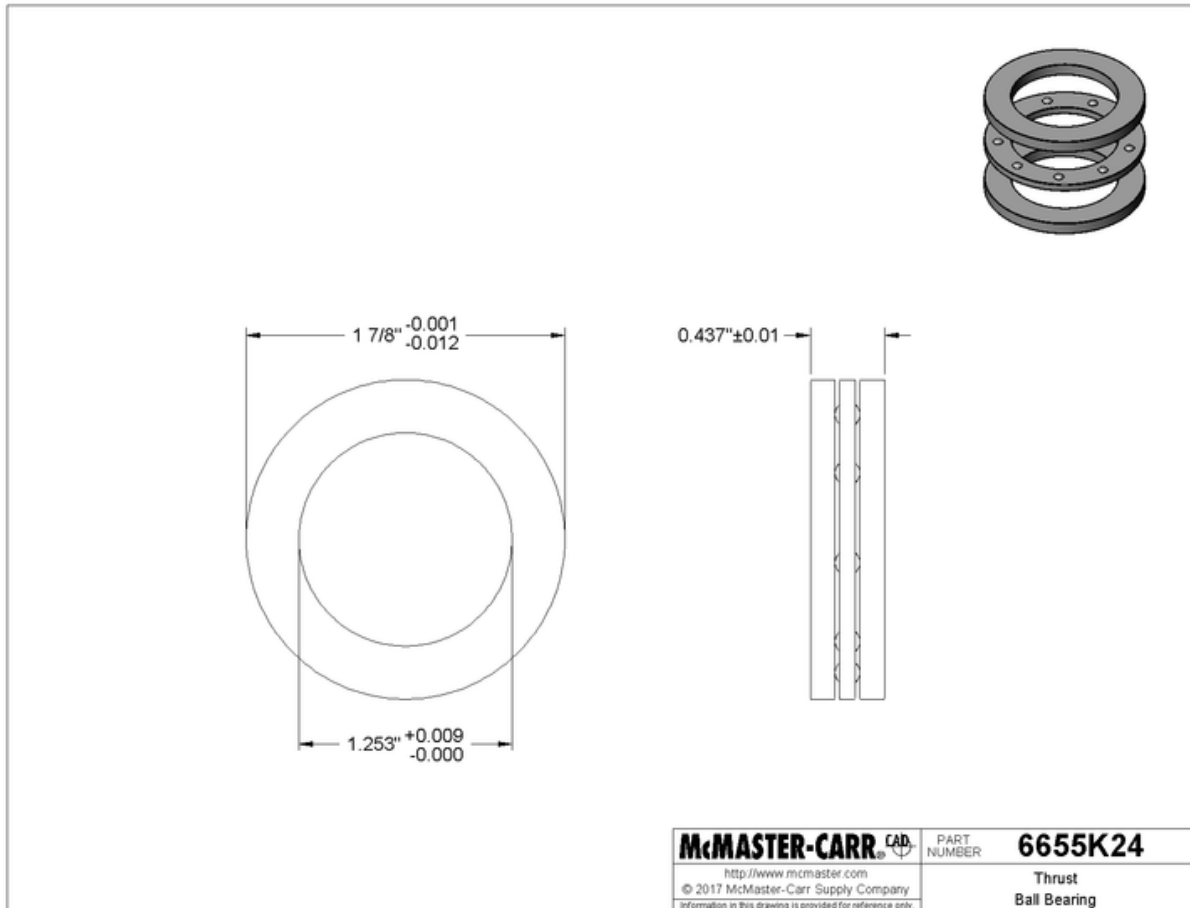
**BEARING HOLDER**

All Dimensions in INCHES

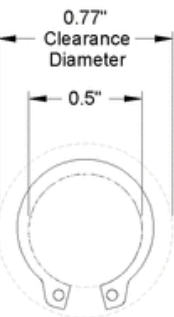
Used to hold the two ball bearings, held in place via press fit on the bearing holder, and the thrust bearing. The holes on the side allow access to the motor coupler for assembly and maintenance.



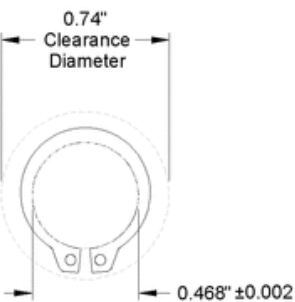
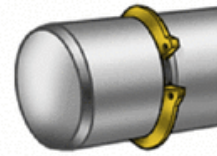
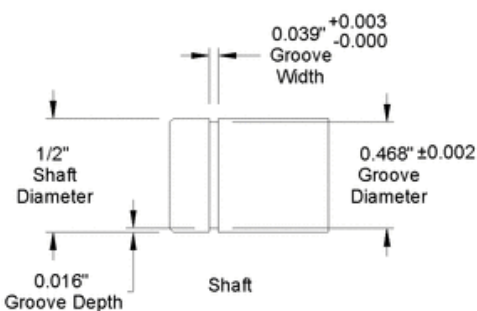
Ball bearing drawing from McMaster Carr (<https://www.mcmaster.com/60355k505>).



Thrust bearing drawing from McMaster Carr. (<https://www.mcmaster.com/6655k24>)

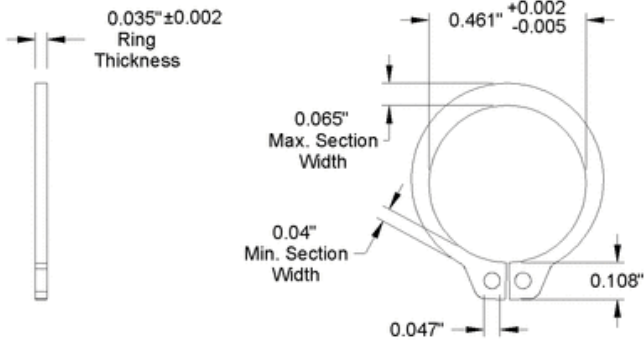


Expanded over Shaft



Released in Groove

Note: Clearance diameter is the diameter of a housing that can pass freely over the ring.



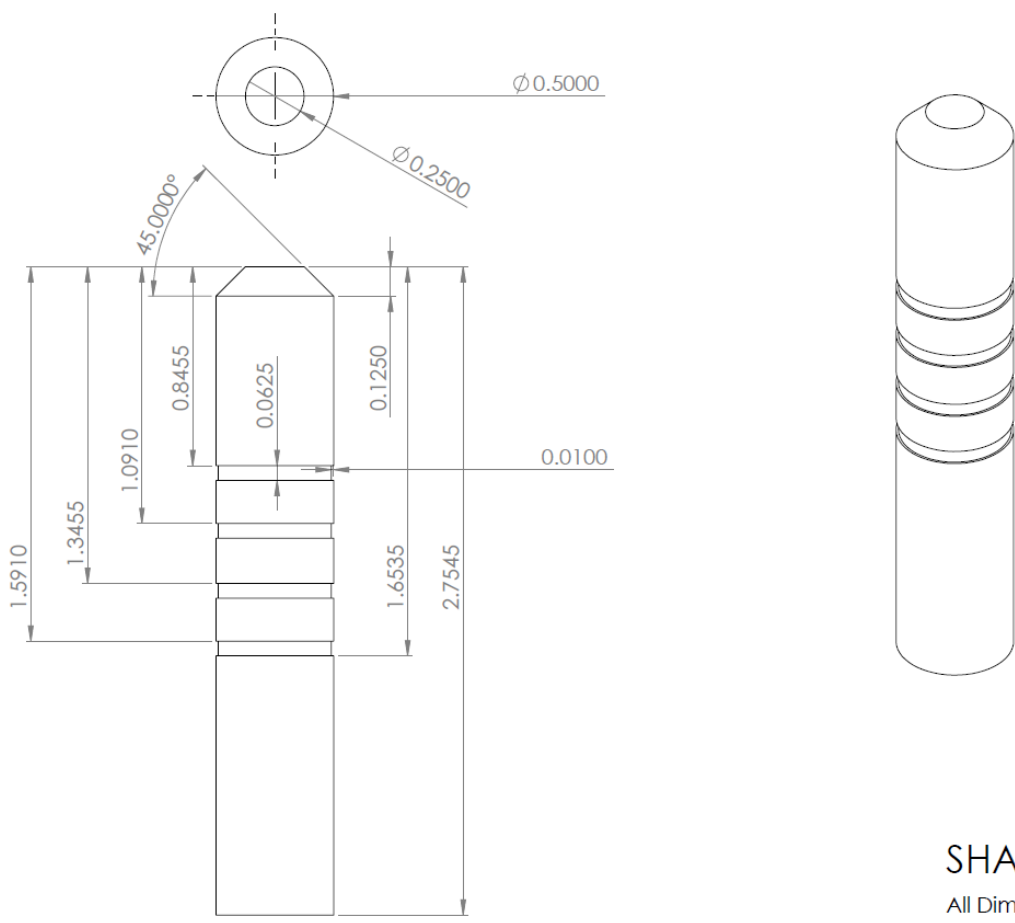
**McMASTER-CARR** CAD

<http://www.mcmaster.com>  
© 2011 McMaster-Carr Supply Company  
Information in this drawing is provided for reference only.

PART NUMBER **97633A200**

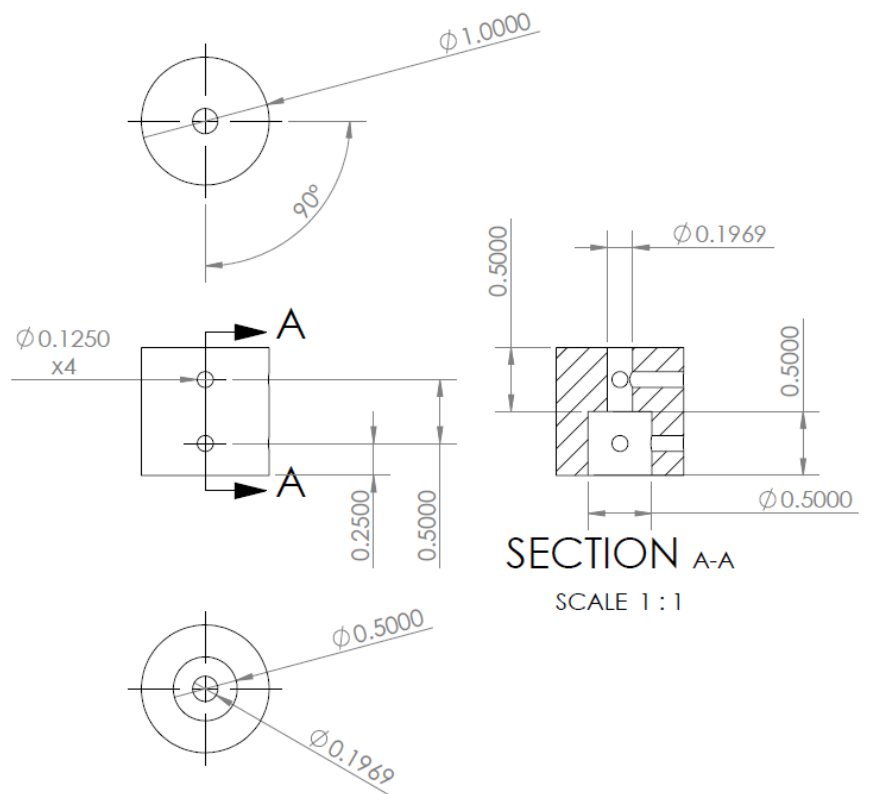
Black-Finish Steel  
External Retaining Ring

Retaining Rings from McMaster-Carr. (<https://www.mcmaster.com/97633a200>)  
Quantity required: 4.

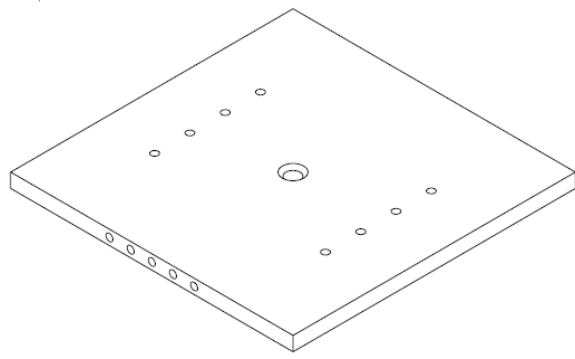
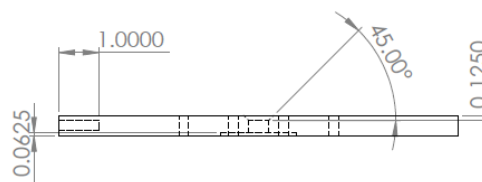
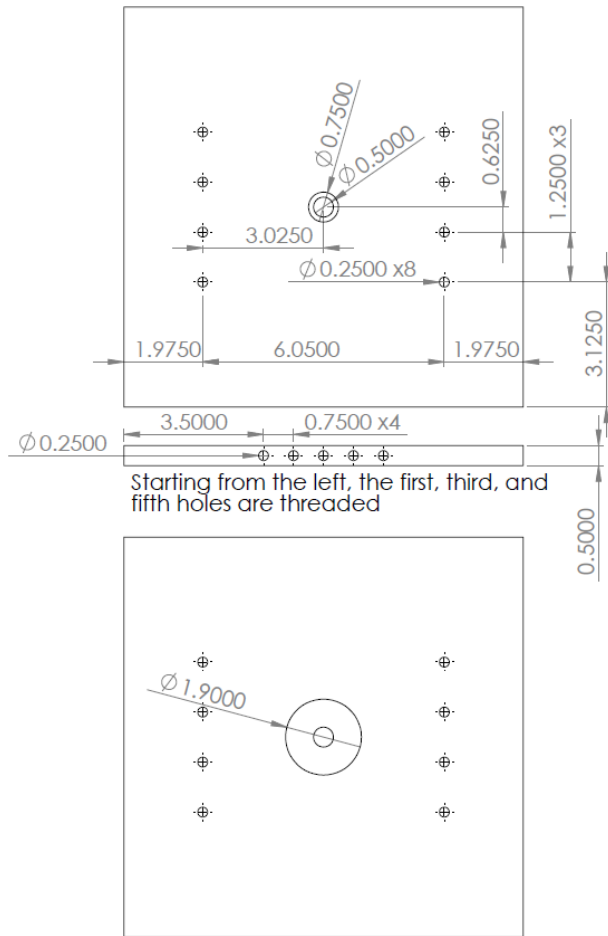


SHAFT

All Dimensions in INCHES

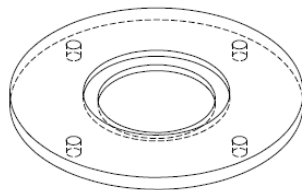
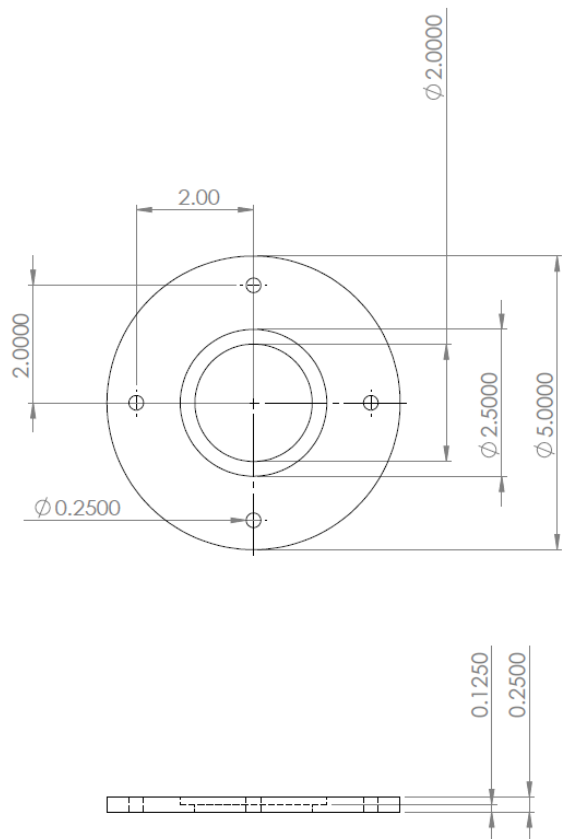


Coupler  
All Dimensions in INCHES

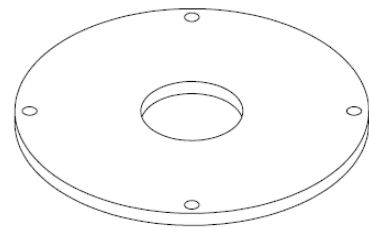
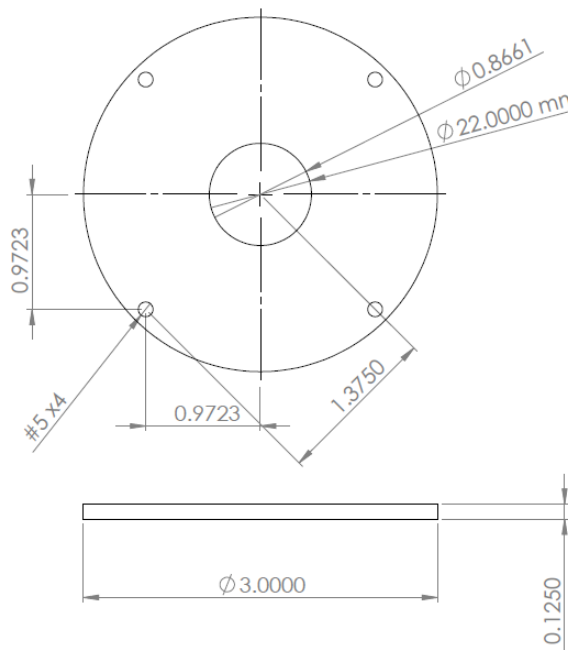


**BASE**

All Dimensions in INCHES

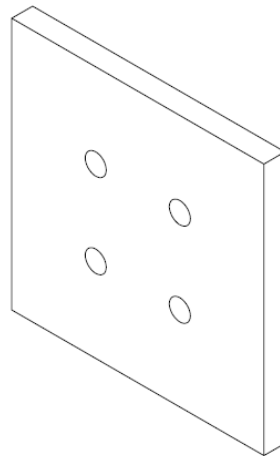
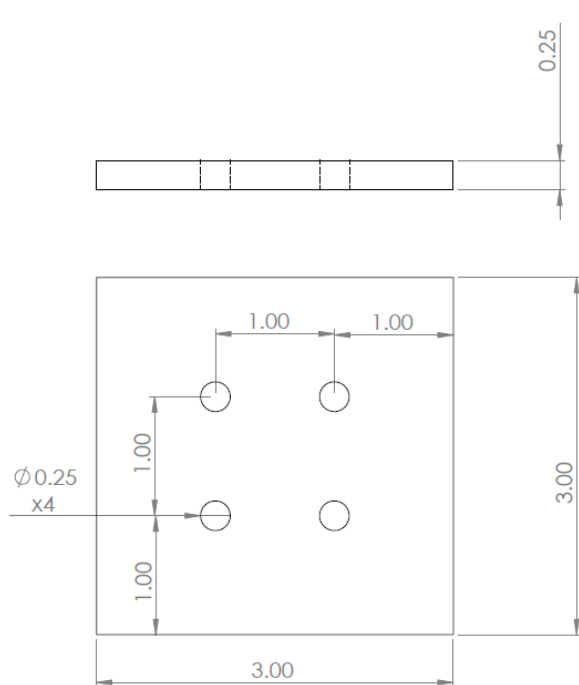


MOTOR HOLDER FLANGE  
All Dimensions in INCHES



## Motor Holder

All Dimensions in INCHES

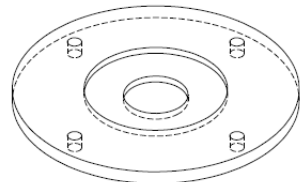
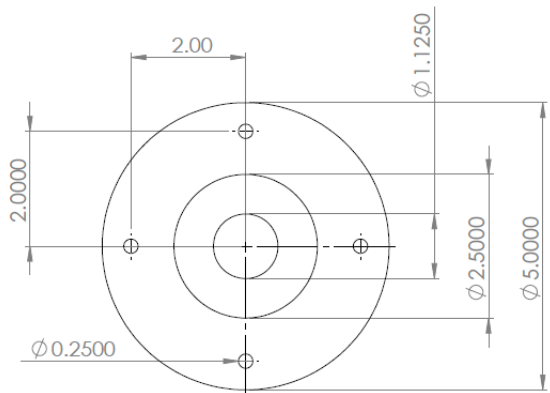


## Motor Holder Flange Plates

All Dimensions in INCHES

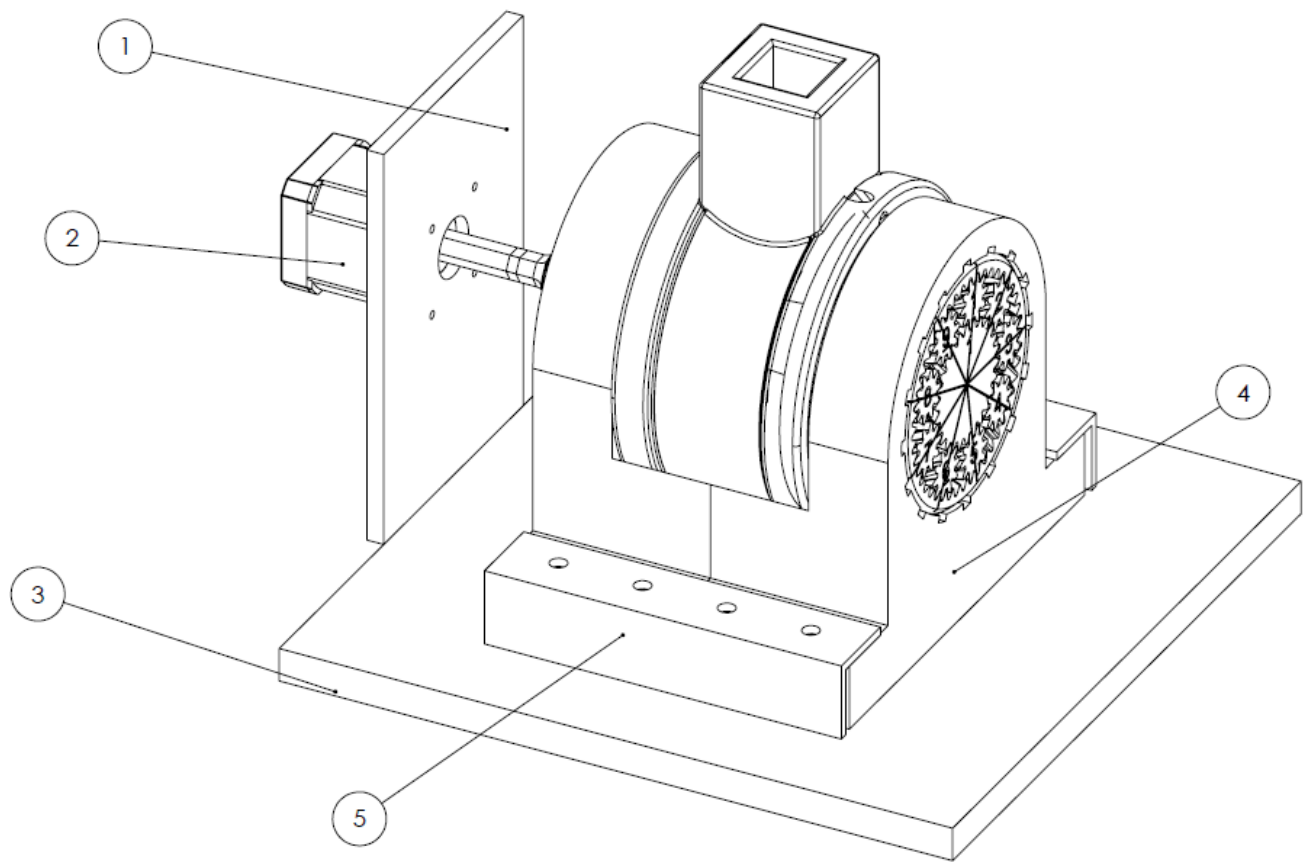
Quantity: 2

©2010 Cengage Learning. All Rights Reserved. May not be copied, scanned, or duplicated, in whole or in part. Due to electronic rights, some third party content may be suppressed from the eBook and/or eChapter(s). Editorial review has determined that any suppressed content does not materially affect the overall learning experience. Cengage Learning reserves the right to remove additional content at any time if subsequent rights restrictions require it.



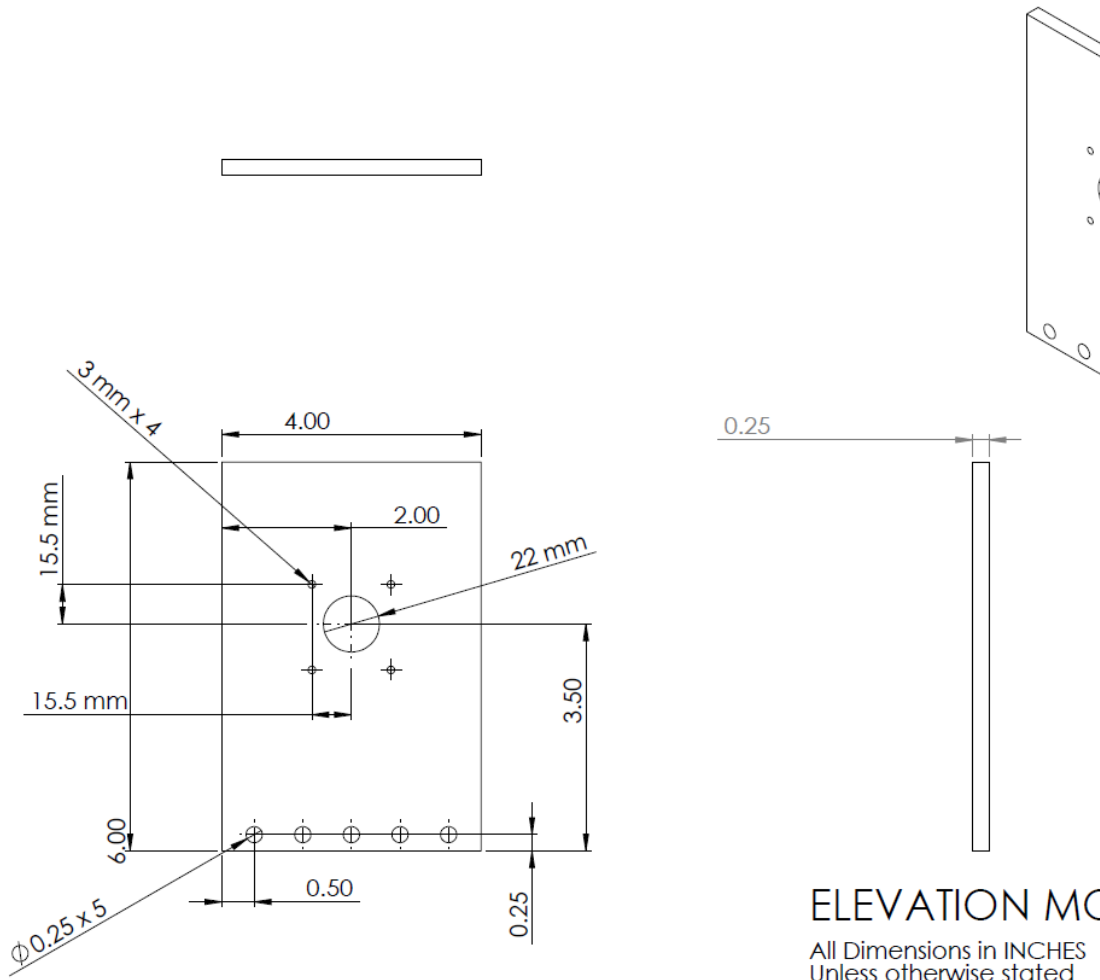
## Bearing Holder Flange

All Dimensions in INCHES



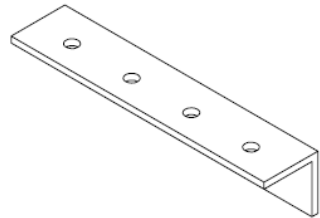
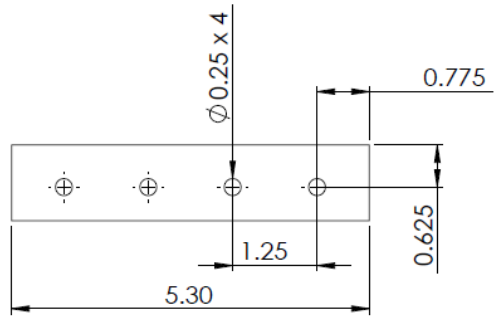
Item Number	Name	Quantity
1	Motor Plate	1
2	Nema 17	1
3	Base	1
4	GearBox	1
5	Angle bracket for gearbox	2

Elevation Subassembly



## ELEVATION MOTOR PLATE

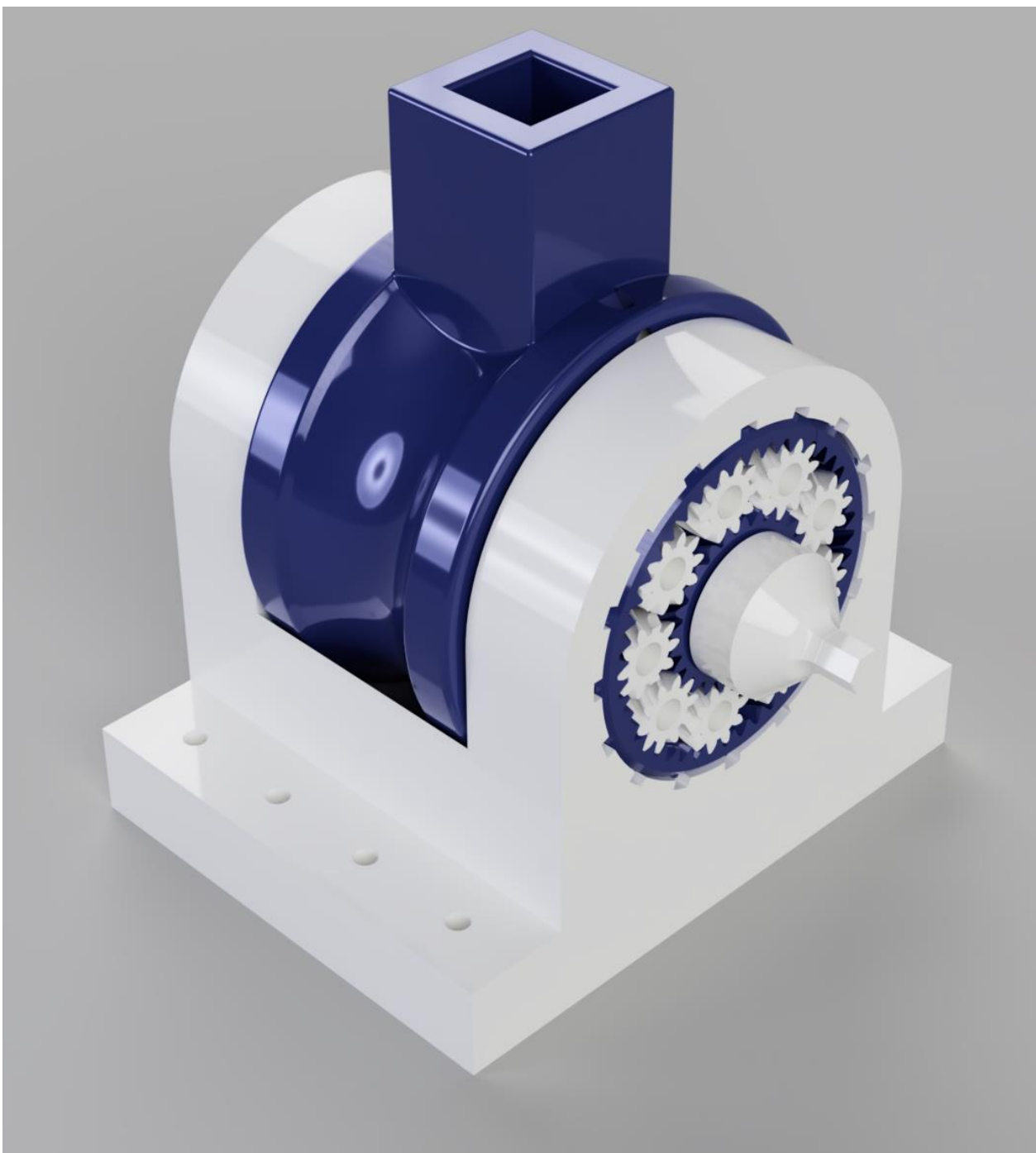
All Dimensions in INCHES  
Unless otherwise stated



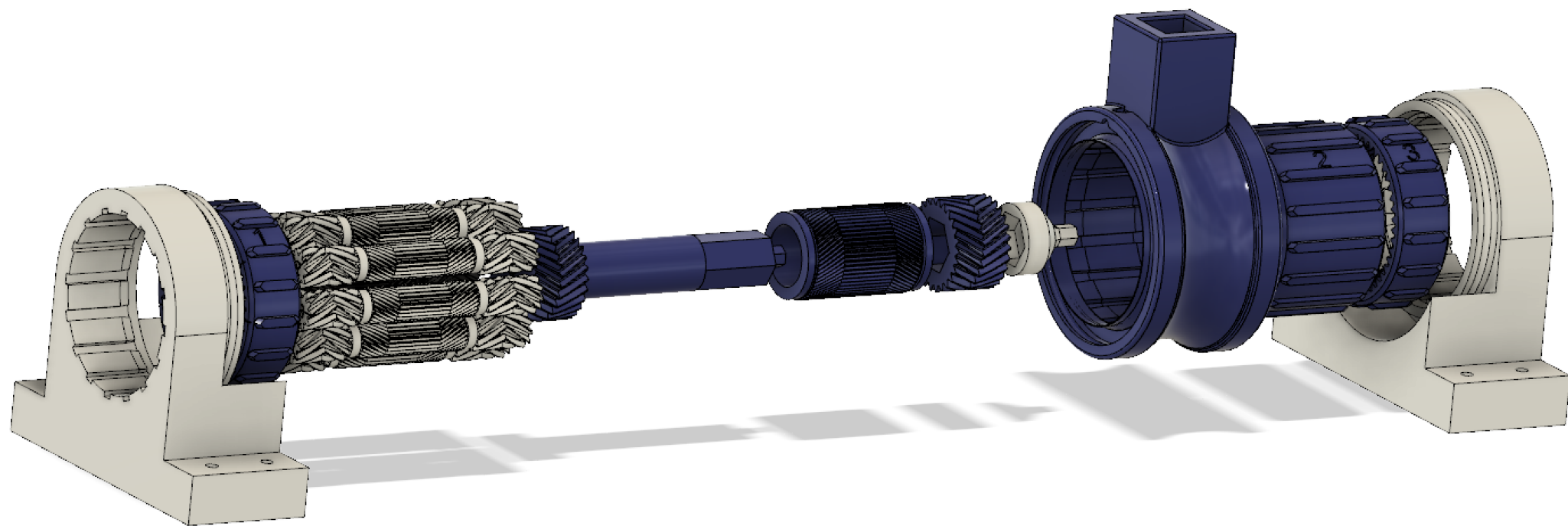
## ANGLE BRACKET FOR GEARBOX

All Dimensions in INCHES

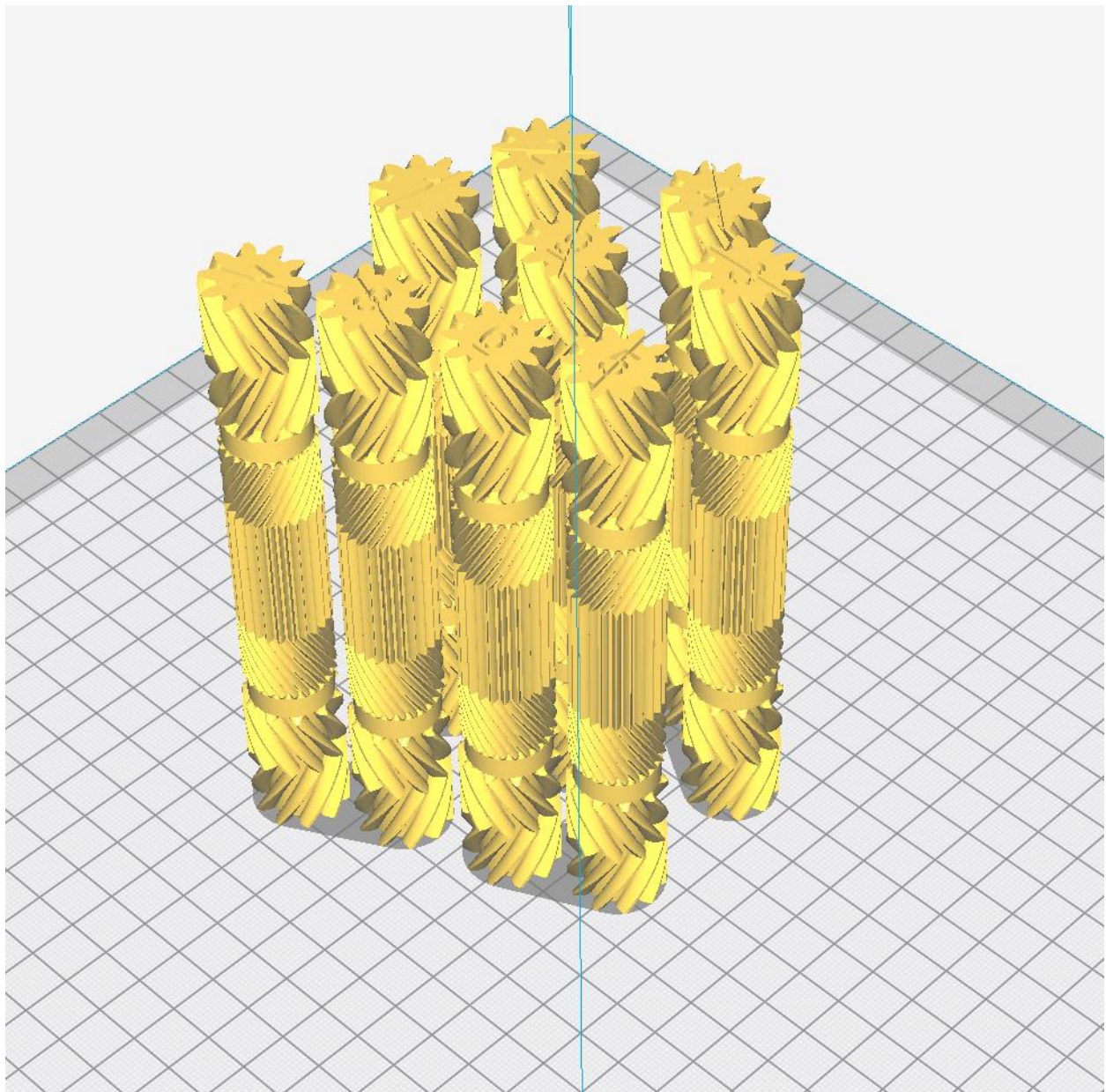
**3D Printed Gear Box:**



Exploded View:

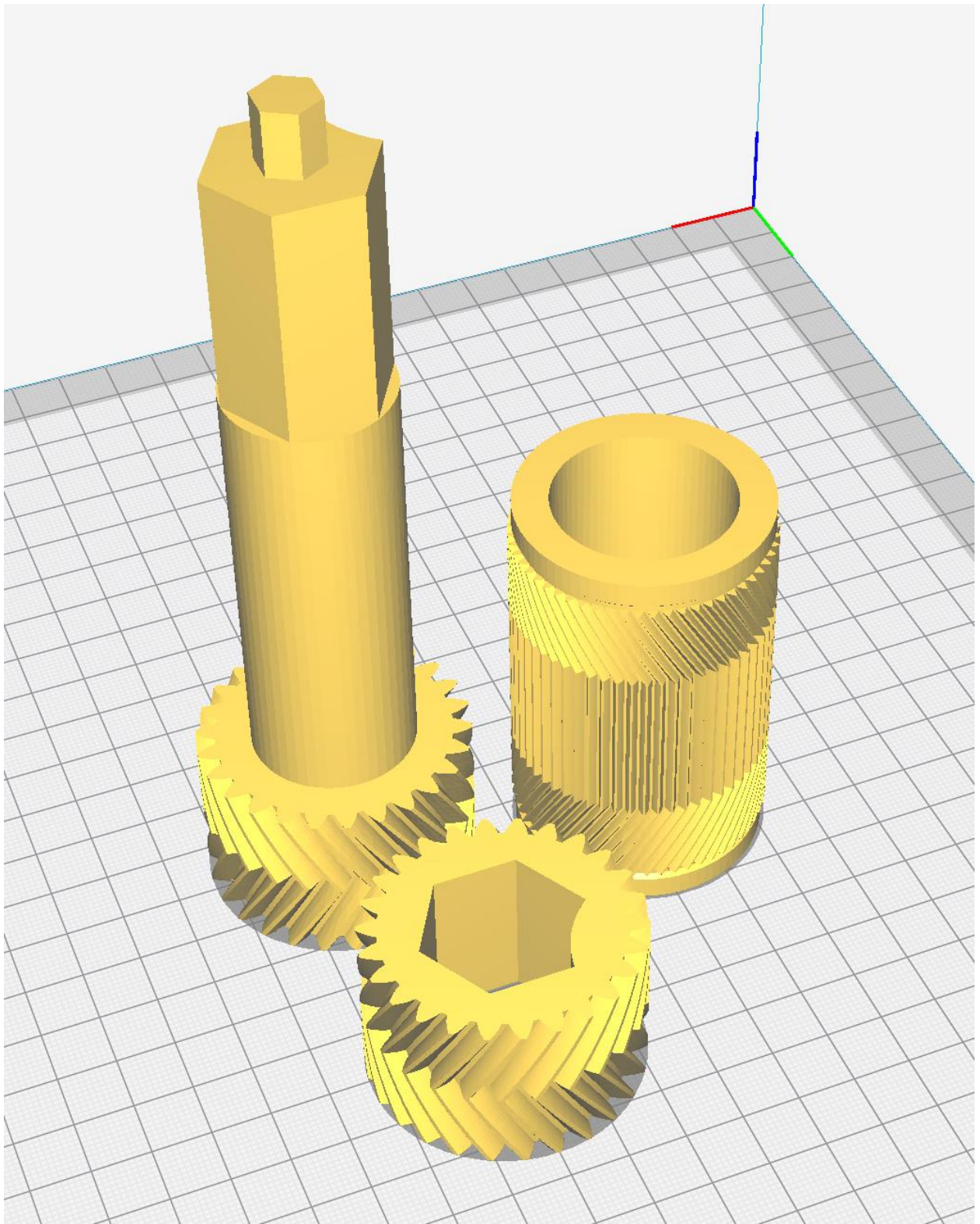


As the printing orientation matters for print strength and surface quality of the gears in the gearbox, the following pictures illustrate the printing orientation for different components of the Gears.



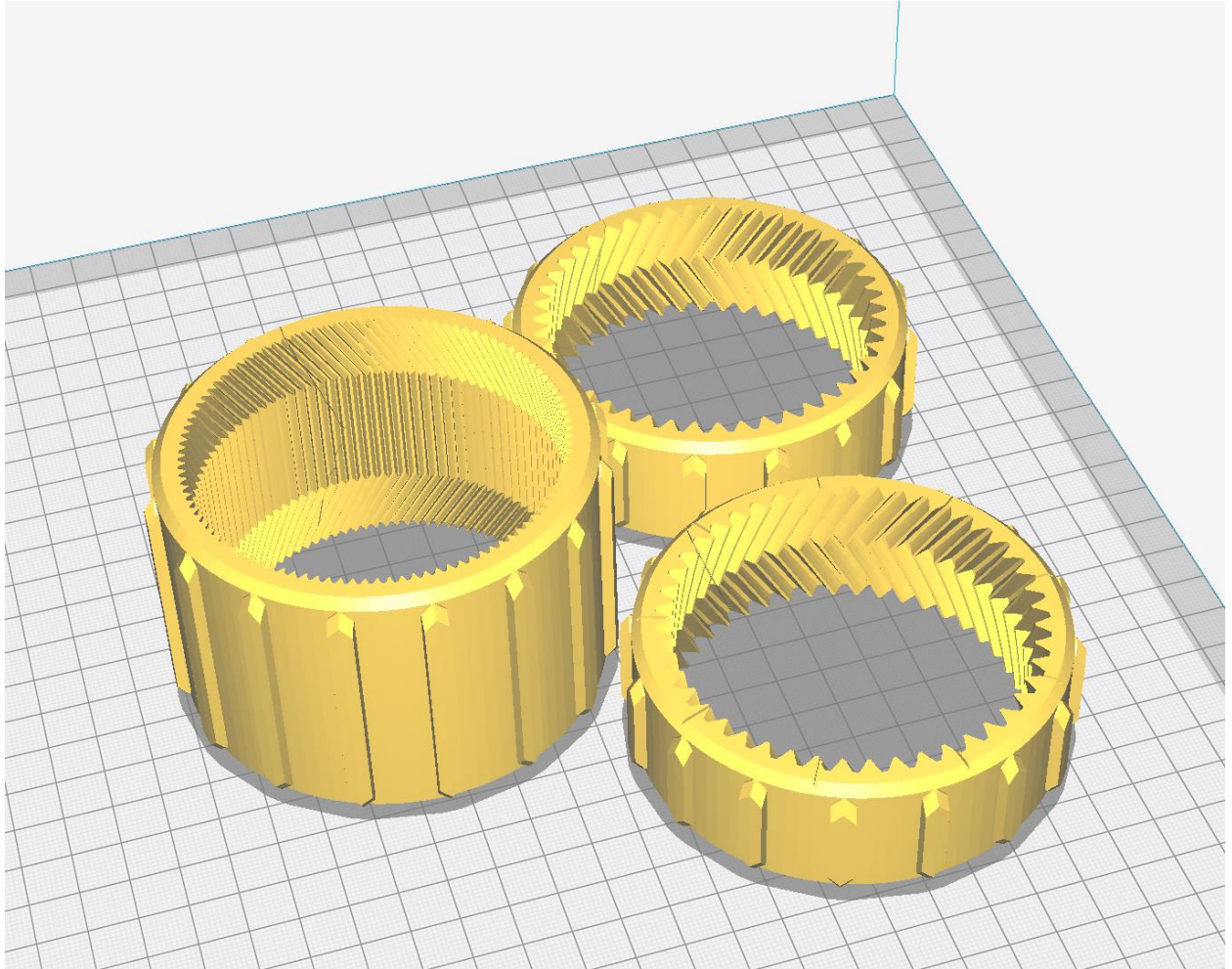
All 9 Planetary Gears, printed upright with the numbers facing up.

Approximate Print Time: 1 day, 12 hours.



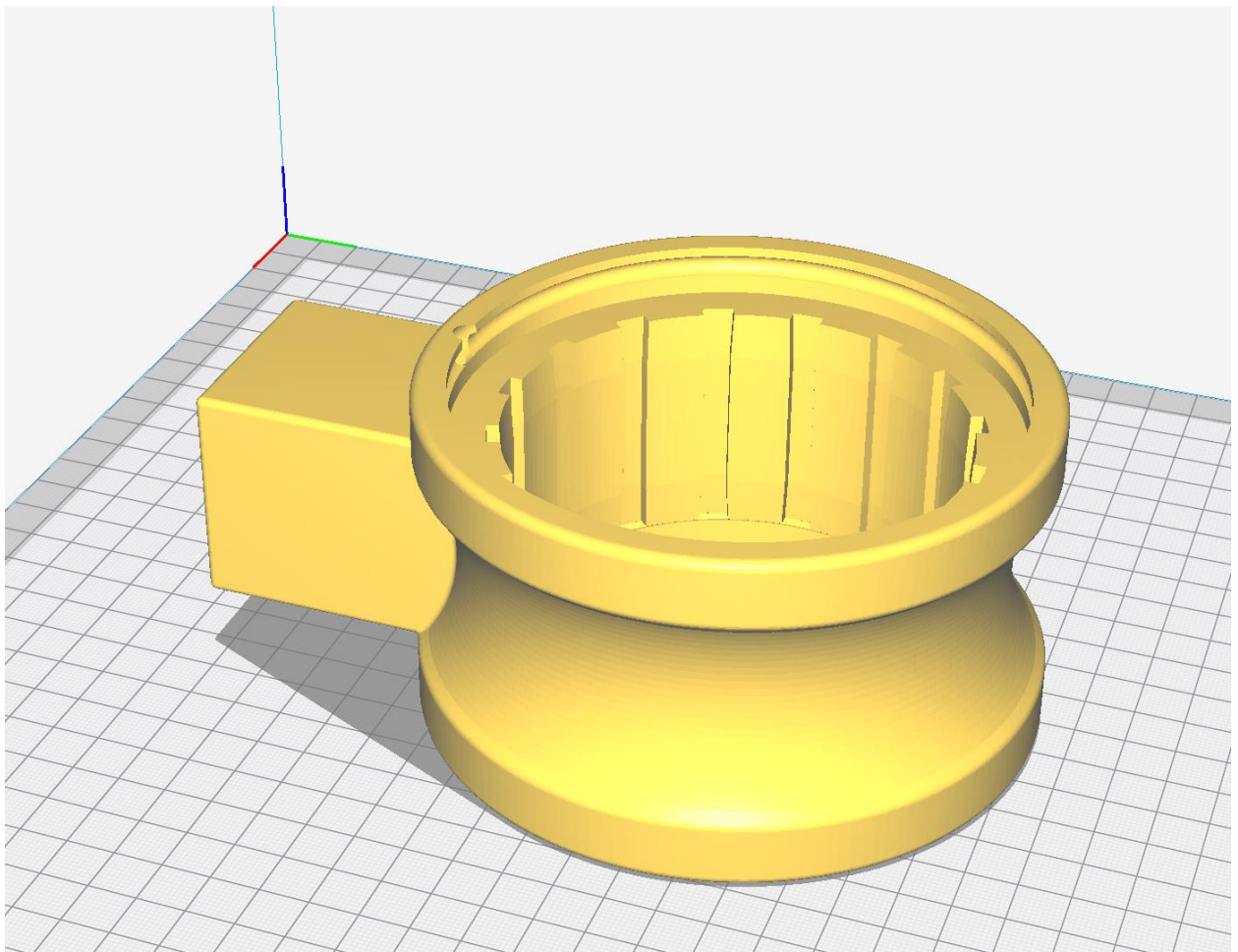
3 Components required for the sun gears.

Approximate print time: 23 hours.



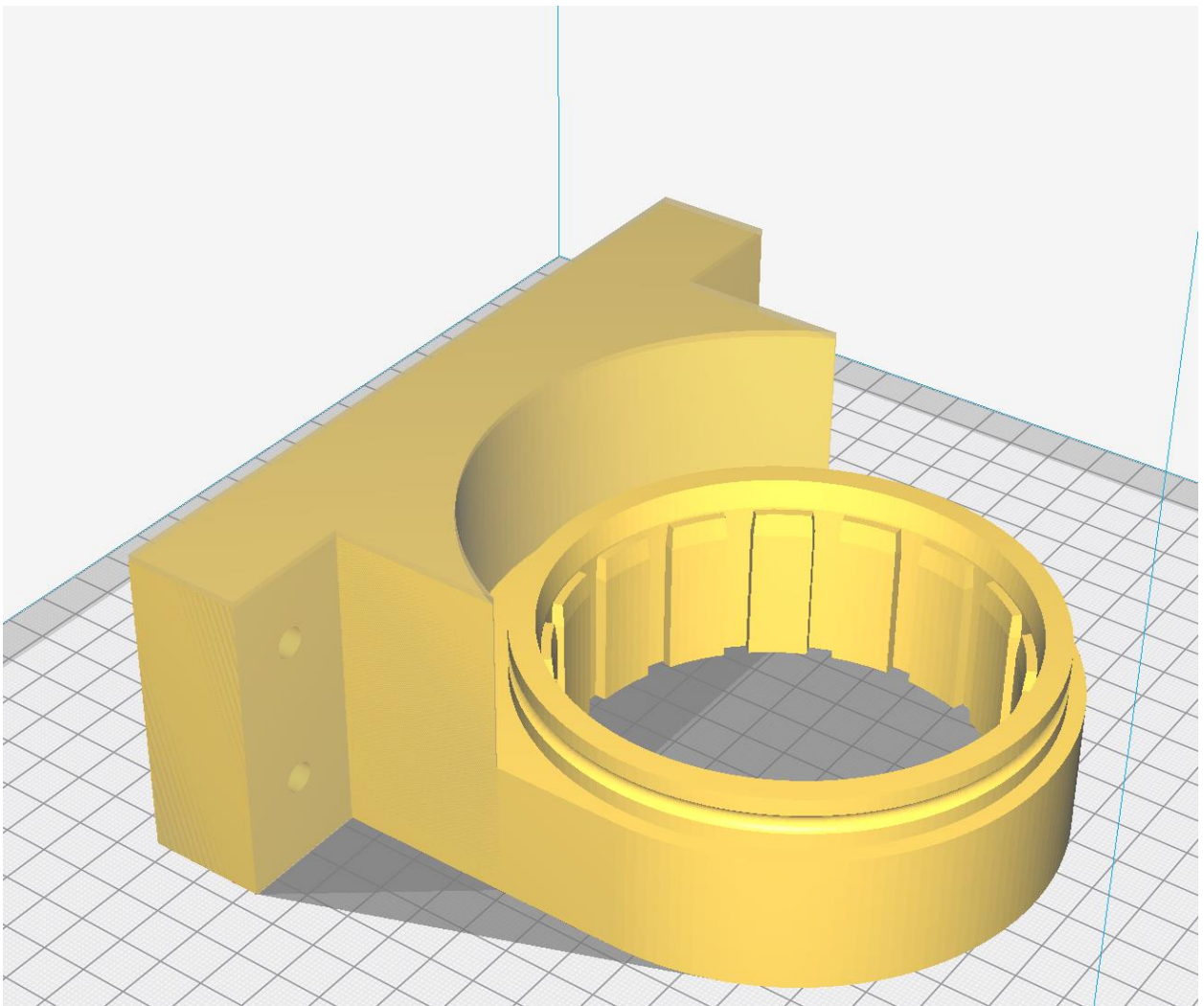
3 Ring gears (tune filament extrusion before printing as tolerances for the gaps are tight)

Approximate Print Time: 1 day, 14 hours.

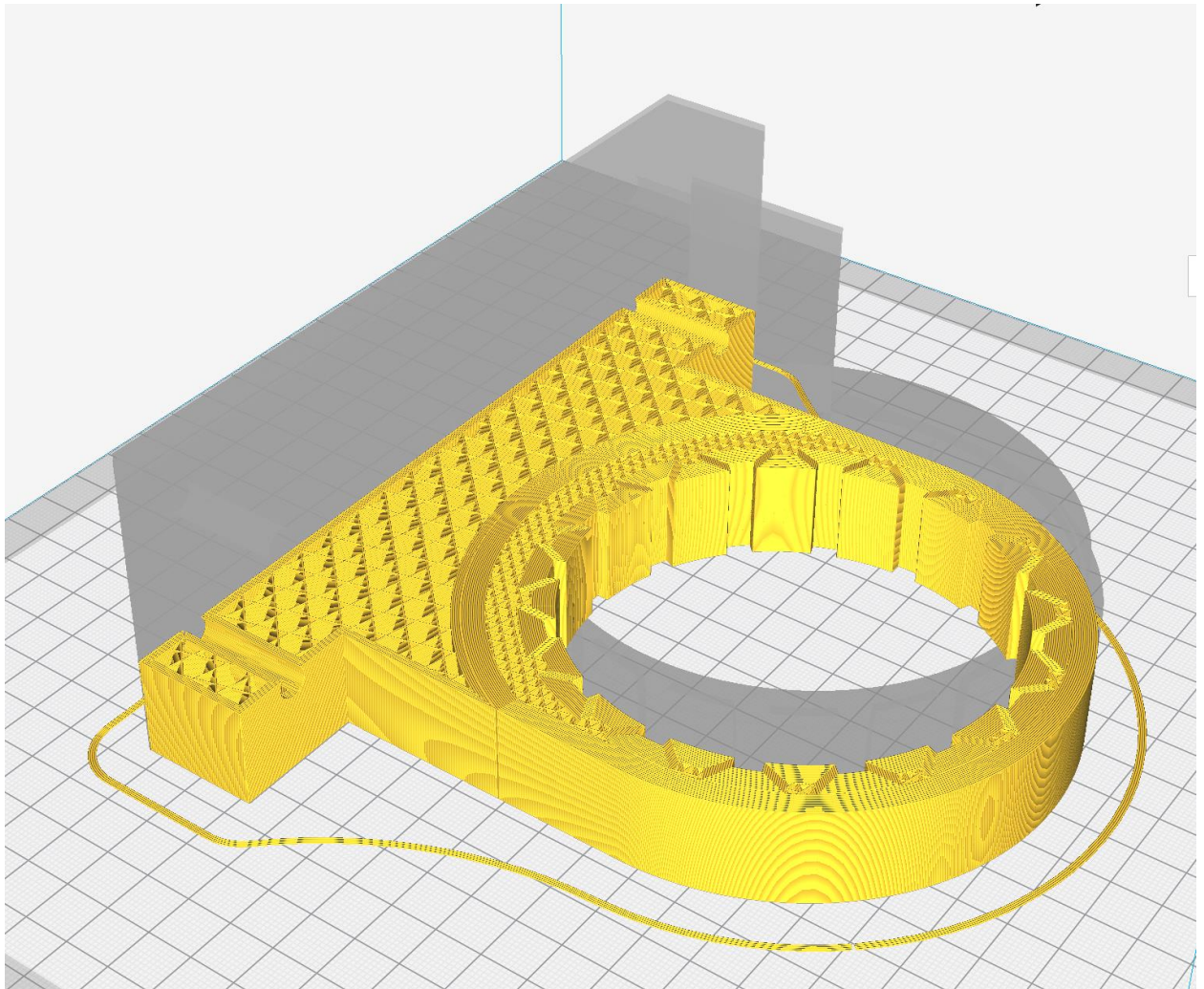


The output shaft is the only component that requires supports. There is support built into the part of the output shaft that houses the ring gear. Custom supports should be added in the slicer to support only the 90° overhangs of the antenna shaft holder.

Approximate print time: 1 day 16 hours.



The stationary ring gear holders require approximately 600 grams of filament if printed with the setting used for the other components. In order to reduce this and the print time, an STL of the bottom part of the holders (the part not in contact with the ring gears) was overlaid onto the regular model. Then, it was used to modify the print settings of only the base part of this model to reduce infill and number of walls in those locations. This can be seen in the image below.



Approximate reduced print time: 1 day, 2 hours. Amount of filament used: 390 grams.

Original print time: 2 days, 1 hour. Amount of filament used: 600 grams.

### **Appendix 3: Software Code**

All software code can be found at <https://github.com/cubesat-project/CubeSat/tree/master/GS>.